



Universitat de Girona

STRUCTURE AND HYDROGEN DYNAMIC BEHAVIOR IN PROTON SPONGE CATIONS AND ORGANOMETALLIC COMPLEXES

Yevhen HORBATENKO

Dipòsit legal: Gi. 123-2014

<http://hdl.handle.net/10803/128511>

ADVERTIMENT. L'accés als continguts d'aquesta tesi doctoral i la seva utilització ha de respectar els drets de la persona autora. Pot ser utilitzada per a consulta o estudi personal, així com en activitats o materials d'investigació i docència en els termes establerts a l'art. 32 del Text Refós de la Llei de Propietat Intel·lectual (RDL 1/1996). Per altres utilitzacions es requereix l'autorització prèvia i expressa de la persona autora. En qualsevol cas, en la utilització dels seus continguts caldrà indicar de forma clara el nom i cognoms de la persona autora i el títol de la tesi doctoral. No s'autoritza la seva reproducció o altres formes d'explotació efectuades amb finalitats de lucre ni la seva comunicació pública des d'un lloc aliè al servei TDX. Tampoc s'autoritza la presentació del seu contingut en una finestra o marc aliè a TDX (framing). Aquesta reserva de drets afecta tant als continguts de la tesi com als seus resums i índexs.

ADVERTENCIA. El acceso a los contenidos de esta tesis doctoral y su utilización debe respetar los derechos de la persona autora. Puede ser utilizada para consulta o estudio personal, así como en actividades o materiales de investigación y docencia en los términos establecidos en el art. 32 del Texto Refundido de la Ley de Propiedad Intelectual (RDL 1/1996). Para otros usos se requiere la autorización previa y expresa de la persona autora. En cualquier caso, en la utilización de sus contenidos se deberá indicar de forma clara el nombre y apellidos de la persona autora y el título de la tesis doctoral. No se autoriza su reproducción u otras formas de explotación efectuadas con fines lucrativos ni su comunicación pública desde un sitio ajeno al servicio TDR. Tampoco se autoriza la presentación de su contenido en una ventana o marco ajeno a TDR (framing). Esta reserva de derechos afecta tanto al contenido de la tesis como a sus resúmenes e índices.

WARNING. Access to the contents of this doctoral thesis and its use must respect the rights of the author. It can be used for reference or private study, as well as research and learning activities or materials in the terms established by the 32nd article of the Spanish Consolidated Copyright Act (RDL 1/1996). Express and previous authorization of the author is required for any other uses. In any case, when using its content, full name of the author and title of the thesis must be clearly indicated. Reproduction or other forms of for profit use or public communication from outside TDX service is not allowed. Presentation of its content in a window or frame external to TDX (framing) is not authorized either. These rights affect both the content of the thesis and its abstracts and indexes.



DOCTORAL THESIS:

Structure and Hydrogen Dynamic Behavior in
Proton Sponge Cations and Organometallic
Complexes

Yevhen Horbatenko
2013

Doctorat en Ciències Experimentals i Sostenibilitat

supervisor:
Dr. Sergei F. Vyboishchikov

Memòria presentada per optar al títol de Doctor per la Universitat
de Girona



El Dr. Sergei F. Vyboishchikov, professor agregat del departament de Química de la Universitat de Girona,

CERTIFICO:

Que aquest treball, titulat “**Structure and Hydrogen Dynamic Behavior in Proton Sponge Cations and Organometallic Complexes**”, que presenta en Yevhen Horbatenko per a l’obtenció del títol de Doctor, ha estat realitzat sota la meva direcció.

Signatura

Girona, 21 de Octubre de 2013

千里之行，始于足下

*“A journey of a thousand miles
begins with a single step”*

Lao Zi

Contents

List of Tables	xi
List of Figures	xiii
List of Abbreviations	xv
List of Publications	xvii
Acknowledgements	xix
Summary	xxi
Resumen	xxiii
Resum	xxvii
1 Introduction	1
1.1 Proton sponges	2
1.1.1 Asymmetric proton sponges	8
1.1.2 Symmetric proton sponges	11
1.1.3 Description of hydrogen bonds	12

1.2	Organometallic complexes	16
1.2.1	σ -Complexes	21
1.2.2	Interligand hypervalent interactions	23
1.2.3	Complexes with additional Si \cdots H interactions	30
1.2.4	Potential energy surface in organometallic complexes with two silyl and one hydride ligands	35
1.3	Organocobalt(V) complexes	36
2	Methods	39
2.1	Potential energy surface representation	40
2.1.1	Model potential for one-dimensional hydrogen transfer	40
2.1.2	Model potential for two-dimensional hydrogen transfer	41
2.1.3	Model potential for N -dimensional hydrogen transfer	43
2.2	Vibrational SCF	47
2.3	Vibrational MP2	50
2.4	Vibrational Coupled Clusters	52
2.5	Numerov method	54
2.6	Distributed Gaussian functions method	58
3	Objectives	61
4	Results and discussion	63
4.1	Jacobi coordinates for triatomic system	63
4.2	One-dimensional Hamiltonian matrix elements	66
4.3	Three-dimensional Hamiltonian matrix elements	69
4.4	Three-dimensional linear-least squares method	74
4.5	Hydrogen motion in proton sponge cations: A theoretical study	76
4.5.1	Three-dimensional vibrational frequencies	78

4.5.2	Three-dimensional vibrational wavefunctions . . .	79
4.6	Dynamic behavior of hydrogen in transition metal bis(silyl)hydride complexes	86
4.6.1	Three-dimensional vibrational frequencies . . .	87
4.6.2	Three-dimensional vibrational wavefunctions . .	88
4.6.3	$J(\text{Si-H})$ coupling constants	93
4.7	$\text{Si}\cdots\text{H}$ interligand interactions in cobalt(V) and iridium(V) bis(silyl)bis(hydride) complexes	95
4.7.1	Wiberg bond indices and spin-spin coupling constants	96
5	Conclusions	101
Appendix A Hydrogen motion in proton sponge cations:		
	A theoretical study	107
Appendix B Dynamic behavior of hydrogen in transition metal bis(silyl)hydride complexes		
		121
Appendix C $\text{Si}\cdots\text{H}$ interligand interactions in cobalt(V) and iridium(V) bis(silyl)bis(hydride) complexes		
		135
	Bibliography	145

List of Tables

1.1	Asymmetric proton sponges	10
1.2	Symmetric proton sponges	11
4.1	3D vibrational frequencies for proton sponges	80
4.2	3D vibrational frequencies for rhodium complexes	89
4.3	Averaged spin-spin coupling constants $\langle J \rangle$	94
4.4	Si–H WBI and spin-spin coupling constants $J(\text{Si–H})$ for cobalt complexes	97
4.5	Si–H WBI and spin-spin coupling constants $J(\text{Si–H})$ for iridium complexes	99

List of Figures

1.1	Prototypical proton sponge	3
1.2	Protonated sponges with the shortest and the longest N–N distances	4
1.3	Asymmetric derivatives of DMAN studied by NMR	6
1.4	Proton sponges with sterically compressed NHN ⁺ intramolecular hydrogen bond	9
1.5	Proton motion PES dependence on various O–O distances	14
1.6	Various types of symmetric potentials for proton motion	15
1.7	First transition metal complex with silicon ligand	16
1.8	Transition metals that give isolable silyl-metal compounds	17
1.9	Classical and non-classical interactions in complexes containing silicon ligands	18
1.10	Variety of structures in transition metal complexes with silicon ligands	18
1.11	Dewar–Chatt–Duncanson model for interactions metal- η^2 -silane	19
1.12	The σ -complex $\text{Re}_2(\text{Ph}_2\text{SiH}_2)(\text{CO})_8$	21
1.13	σ -Complexes isolated as individual compounds	23
1.14	The first complex with IHI	24
1.15	Orbital interaction diagram for IHI	26
1.16	Niobium and titanium complexes with IHI	28

1.17	The first complex with simultaneous Si–H and IHI . . .	29
1.18	The first complexes with simultaneous H···Si···H interactions	31
1.19	The structure of tungsten complex	32
1.20	The structure of ruthenium complexes	33
1.21	Iron complexes with suggested simultaneous Si···H···Si interactions	34
1.22	Hydrogen fluxionality in rhodium a hydrido-bis(silyl) complexes	35
1.23	Bonding patterns in transition metal complexes with two silyl and one hydride ligands	36
1.24	Organocobalt(V) complexes	38
4.1	Three-atomic coordinate system used to build Jacobi coordinates	64
4.2	Proton sponges analyzed for possible vibrational patterns	77
4.3	The PES and probability density contour plots for proton sponge cations	84
4.4	The PES and probability density contour plots for proton sponge cation PS6pbe	85
4.5	Cp bis(silyl)hydride complexes analyzed for possible vibrational patterns	86
4.6	Tp bis(silyl)hydride complexes analyzed for possible vibrational patterns	87
4.7	The PES and probability density contour plots for rhodium complexes	92
4.8	Cobalt and iridium candidates for Si–H interactions . .	96

List of Abbreviations

Cp	cyclopentadienyl
Cp [*]	1,2,3,4,5-pentamethylcyclopentadienyl
Cy	cyclohexyl
DFT	density-functional theory
DMAN	1,8-bis(dimethylamino)naphthalene
Et	ethyl
HF	Hartree-Fock
ⁱ Bu	iso-butyl
IHI	interligand hypervalent interactions
ⁱ Pr	iso-propyl
IR	infrared
L	ligand
LLSM	linear least-squares method
M	transition metal
MBO	Mayer bond order
Me	methyl
MEP	minimum energy path
MWF	maximum wavefunction path
MO	molecular orbital
NMR	nuclear magnetic resonance
PES	potential energy surface
Ph	phenyl

PS	proton sponge
Pyl	pyrrolyl
QFF	quartic force field
^t Bu	tert-butyl
TMC	transition metal complex
TP	trispyrazolylborate
TS	transition state
VSCF	vibrational SCF
VMP2	vibrational MP2
VCC	vibrational CC
WBI	Wiberg bond index

List of Publications

This thesis is based on the following articles:

1. Y. Horbatenko, S. F. Vyboishchikov “Hydrogen Motion in Proton Sponge Cations: A Theoretical Study”, *Chem. Phys. Chem.* **2011**, *12*, 1118–1129.
2. Y. Horbatenko, S. F. Vyboishchikov “Dynamic Behavior of Hydrogen in Transition Metal Bis(silyl) Hydride Complexes”, *Organometallics* **2013**, *32*, 514–426.
3. Y. Horbatenko, S. F. Vyboishchikov “Si···H interligand interactions in cobalt(V) and iridium(V) bis(silyl)bis(hydride) complexes”, *ChemPlusChem (Special Issue dedicated to the memory of Dr. D. Schröder)* **2013**, *78*, 1073–1081.

Acknowledgements

“*A journey of a thousand miles begins with a single step*”. This phrase begins my thesis, since having written these lines I have realized that to reach this point it was really a journey, sometimes difficult, sometimes unpredictable, but mostly interesting and joyful. Of course this journey would be impossible without people who supported and cheered me up all these years.

First of all, I would like to thank my supervisor Dr. Sergei Vyboishchikov for his patience, help and support. I have learned many things from him. It was interesting to listen to his explanations that were always clear. Also, I would like to thank his family Yulya, Viktoria, Alex for kindness and understanding which I was treated with.

I am thankful to the former PhD student of Sergei, Samat (and his Suzuki), who was the very first friend I made in Girona, and whom I discussed lots of things while returning home after work late at night with.

Thanks to Emili who was our coordinator of master program. Miquel, thank you for having given me the opportunity to work on Repsol project, and Marcel (El Rey del ADF) for your help with ADF.

I am grateful to all actual and former IQC members: to Quansong, Albert, Jordi, Edu, Pata, Mireia, Juanma, Silvia (who always has cold), to my triathlon team Ferran (odna butilka vodki) and Mark (ola k ase?), to our “rival” (in a good sense) team *Las Perracas Cíclicas*

Pedro, Eloy and Ana Dí, to Sergi, Laia, Vero, to our mexican friends Oscar (compadre), Rafa, Abril, Juan-Pablo, to Majid, to Mikael (más cerveza para la cabeza... y el dolor!), to Alexandra (now we know that all Portuguese people are melancholic because of *saudade*). Moltes gràcies per ensenyar-me la vida nocturna de Girona, pels sopars, lujurias, plateas que vam passar junts. My apologies if I forgot somebody.

I am sincerely saying “thank you” to Carme, our secretary. She is like saving island in the immense ocean of bureaucracy. Without her IQC would sink.

As well I want to thank Yagi-sensei who accepted me for research stay in Japan. It was very nice experience in both senses scientific and cultural. Thanks a lot to his family Takara-sama and Haruka-sama. Without all of them I never could have thought that unknown person can be treated so cordially.

Thanks to Alexander who kindly offered me to go to swim to the sea. After his trainings, now I can swim non-stop about 50 minutes. Speaking about the sea, thanks to Dmitrii who introduced me such amazing kind of sport as windsurf (From beginner to winner!).

My dear parents and dear sister, thank you for all you are doing for me, without your love it would be impossible to reach this point. Also I want to thank my grandparents and other relatives who were worried about me.

I do not want to forget to give thanks to the fellowship of University of Girona and to Repsol for financial support as well.

I am grateful to all of you, because you make me feel happier.

Summary

Superbases such as proton sponges have many important applications in organic synthesis. The corresponding protonated species, with an $\text{N}\cdots\text{H}\cdots\text{N}$ fragment, are characterized by a short strong hydrogen bond. In these systems vibrational motion of hydrogen is highly anharmonic, and, in general, anharmonicity increases with increasing hydrogen bond strength. In some cases the vibrational motion of hydrogen is accompanied by tunnel effect. Thus, the proton dynamics in such systems is interesting to study. It can be described by three cases. In the first case proton can move freely between two nitrogen atoms and the strengthening of one $\text{N}-\text{H}$ bond is accompanied by weakening of the other. In the second case proton can be found between two nitrogen atoms and in the third case the proton can be located closer to one nitrogen atom.

Though quite different chemically, $\text{Si}\cdots\text{H}\cdots\text{Si}$ fragment in bis(silyl)-hydride organometallic complexes, which play an important role in silylation reactions, resembles $\text{N}\cdots\text{H}\cdots\text{N}$ one. In the former systems the hydride can be delocalized between two silicon atoms or can be localized in the vicinity of one of them.

It is important to understand the hydrogen dynamics in these systems. To examine various possible cases of the hydrogen dynamics, and establish criteria between them quantum-chemical calculations have been performed.

There has been considerable interest to transition metals in high oxidation states in organometallic chemistry. Thus, another question addressed in this thesis is about presence of Si...H interactions in bis(silyl)bis(hydride) complexes of cobalt(V) and iridium(V), which can play role as intermediates in various silylation reactions. Although for *3d* transition metals such as cobalt it is not typical to form organometallic complexes in high oxidation states, a few complexes of cobalt(V) were isolated.

The present thesis studies the dynamics of hydrogen in proton sponges and bis(silyl)hydride complexes of rhodium by solving the three-dimensional vibrational Schrödinger equation. Moreover, Si...H interactions in cobalt(V) and iridium(V) bis(silyl)bis(hydride) complexes have been investigated by Wiberg bond indices and NMR spin-spin coupling constant calculations.

To solve the three-dimensional vibrational Schrödinger equation, Jacobi coordinates for a three-particle system have been derived taking into account the symmetry of our system. Three dimensional linear least-squares method has been derived to fit the potential energy surfaces.

Various dynamic patterns for vibrational motion of hydrogen have been found both for N...H...N and Si...H...Si moieties. It has been shown that the dynamic depends crucially on the hydrogen transfer barrier. Moreover, the results indicate substantial tunneling in some of the systems studied. It has been demonstrated that the proton can be described as a particle in a box in proton sponge cations. Also the influence of vibrational motion of hydride on the Si-H spin-spin coupling constants has been indicated in the case of bis(silyl)hydride complexes.

For the bis(silyl)bis(hydride) complexes of cobalt(V), various Si...H interactions have been revealed, including interligand hypervalent interactions, while classical structures have been obtained for the majority of analogous iridium(V) complexes.

Resumen

Las superbases tales como las esponjas de protón tienen muchas aplicaciones importantes en síntesis orgánica. Las correspondientes especies protonadas, presentan un fragmento $N\cdots H\cdots N$ y se caracterizan por un enlace por puente de hidrógeno fuerte y corto. En estos sistemas el movimiento vibracional del hidrógeno es altamente anarmónico, y, en general, la anarmonicidad aumenta con el aumento de la fuerza de enlace por puente de hidrógeno. En algunos casos, el movimiento vibracional del hidrógeno va acompañado de efecto túnel. Por lo tanto, para estos sistemas es interesante el estudio del comportamiento dinámico del protón. Se observan tres patrones de comportamiento diferente. En el primer caso, el protón puede moverse libremente entre los dos átomos de nitrógeno y el fortalecimiento de un enlace $N-H$ está acompañado por el debilitamiento del otro. En el segundo caso, el protón se puede encontrar entre los dos átomos de nitrógeno y en el tercer caso, el protón puede estar situado más cerca de uno de los átomos de nitrógeno.

Aunque son bastante diferentes químicamente, el fragmento $Si\cdots H\cdots Si$ en complejos organometálicos de bis(silil)hidruro, importantes en reacciones de sililación, se asemeja al fragmento $N\cdots H\cdots N$. En el primero el hidruro puede estar deslocalizado entre los dos átomos de silicio o puede estar localizado más cerca de uno de ellos.

En estos sistemas es importante entender la dinámica del hidrógeno.

Para examinar varios casos posibles de la dinámica del hidrógeno y establecer criterios entre ellos se han realizado cálculos químico-cuánticos.

Dentro del campo de la química organometálica ha habido un gran interés en el estudio de metales de transición de alta oxidación. Por lo tanto, otra cuestión tratada en esta tesis es la presencia de interacciones Si...H en complejos de bis(silil)bis(hidruro) de cobalto(V) e iridio(V) que pueden considerarse como intermedios en distintas reacciones de sililación. Aunque para los metales de transición de tipo *3d* como cobalto no es típico formar complejos organometálicos en estados de alta oxidación, se han aislado algunos complejos de cobalto(V).

La tesis presentada estudia la dinámica del hidrógeno en esponjas de protón y en los complejos de bis(silil)hidruro de rodio mediante la resolución de la ecuación de Schrödinger vibracional tridimensional. Además, las interacciones Si...H en complejos de bis(silil)bis(hidruro) de cobalto(V) e iridio(V) se han investigado mediante índices de enlace de Wiberg y constantes de acoplamiento de spin-spin de RMN.

Para resolver la ecuación de Schrödinger vibracional en tres dimensiones, se han deducido coordenadas de Jacobi para un sistema de tres partículas teniendo en cuenta la simetría de nuestro sistema. Para aproximar las superficies de energía potencial se ha deducido un método de mínimos cuadrados lineales en tres dimensiones.

Se han encontrado varios patrones dinámicos para el movimiento vibracional del hidrógeno tanto en el caso del N...H...N como en el caso del Si...H...Si. Se ha visto que la dinámica depende crucialmente de la barrera de transferencia del hidrógeno. Además, los resultados indican un efecto túnel sustancial en algunos sistemas. Se ha demostrado que el protón en las esponjas de protón se puede describir como una partícula en una caja. También se ha indicado que, en el caso de los complejos de bis(silil)hidruro, el movimiento vibracional del hidruro influye en las constantes de acoplamiento de spin-spin de Si-H.

Para los complejos de bis(silil)bis(hidruro) de cobalto(V) se han

revelado interacciones Si–H diversas, incluyendo interacciones de tipo interligando hipervalente, mientras que para los análogos de iridio(V) se han obtenido estructuras clásicas para la mayoría de los complejos.

Resum

Les superbases com ara les esponges de protó tenen moltes aplicacions importants en síntesi orgànica. Les corresponents espècies protonades presenten un fragment $N\cdots H\cdots N$ i es caracteritzen per tenir un enllaç per pont d'hidrogen fort i curt. En aquests sistemes el moviment vibracional de l'hidrogen és altament anharmònic, i, en general, l'anharmonicitat augmenta amb l'augment de la força d'enllaç per pont d'hidrogen. En alguns casos, el moviment vibracional de l'hidrogen va acompanyat per efecte túnel. Per tant, per a aquests sistemes és interessant l'estudi del comportament dinàmic del protó. S'observen tres patrons de comportament diferents. En el primer cas, el protó es pot moure lliurement entre els dos àtoms de nitrogen i l'enfortiment d'un enllaç $N-H$ està acompanyat per l'afebliment de l'altre. En el segon cas, el protó es pot trobar entre els dos àtoms de nitrogen i en el tercer cas, el protó està situat més a prop d'un dels àtoms de nitrogen.

Encara que són bastant diferents químicament, el fragment $Si\cdots H\cdots Si$ en complexos organometàl·lics de bis(silil)hidrur, importants en reaccions d'sililació, s'assembla al fragment $N\cdots H\cdots N$. En el primer, l'hidrur pot deslocalitzar-se entre els dos àtoms de silici o pot estar localitzat més a prop d'un d'ells.

En aquests sistemes és important entendre la dinàmica de l'hidrogen. Per a examinar diversos casos possibles de la dinàmica de l'hidrogen i

establir criteris entre ells s'han realitzat càlculs químic-quàntics.

Dins del camp de la química organometàl·lica hi ha hagut un gran interès en l'estudi de metalls de transició d'alt estat d'oxidació. Per tant, una altra qüestió tractada en aquesta tesi és la presència d'interaccions Si \cdots H en complexos de bis(silil)bis(hidrur) de cobalt(V) i iridi(V). Aquests complexos poden considerar-se com a intermedis en diverses reaccions de sililació. Encara que per als metalls de transició de tipus *3d* com el cobalt no és típic formar complexos organometàl·lics amb estats d'oxidació alt, s'han aïllat uns pocs complexos de cobalt(V).

Aquesta tesi presentada estudia la dinàmica de l'hidrogen en esponges de protó i en els complexos de bis(silil)hidrur de rodi mitjançant la resolució de l'equació de Schrödinger vibracional tridimensional. A més a més, les interaccions Si \cdots H en complexos de bis(silil)bis(hidrur) de cobalt(V) i iridi(V) s'han investigat mitjançant els índexs d'enllaç de Wiberg i constants d'acoblament de spin-spin de RMN.

Per resoldre l'equació de Schrödinger vibracional en tres dimensions, s'han deduït coordenades de Jacobi per a un sistema de tres partícules tenint en compte la simetria del nostre sistema. Per a aproximar les superfícies d'energia potencial s'ha deduït un mètode de mínims quadrats lineals en tres dimensions.

S'han trobat diversos patrons dinàmics pel moviment vibracional de l'hidrogen tant en el cas del N \cdots H \cdots N com en el cas del Si \cdots H \cdots Si. S'ha vist que la dinàmica depèn crucialment de la barrera de la transferència d'hidrogen. A més a més, els resultats indiquen un efecte túnel substancial en alguns sistemes estudiats. S'ha demostrat que el protó a les esponges de protó es pot descriure com a una partícula en una caixa. A més d'això s'ha indicat que, en el cas dels complexos bis(silil)hidrur, el moviment vibracional de l'hidrur influeix en les constants d'acoblament de spin-spin de Si–H.

Per als complexos de bis(silil)bis(hidrur) de cobalt(V) s'han revelat diverses interaccions Si–H, incloent interaccions de tipus interligand hipervalent, mentre que per als anàlegs d'iridi(V) s'han obtingut es-

structures clàssiques per a la majoria dels complexos.

Chapter 1

Introduction

The potential energy surface is a fundamental concept of chemistry. It represents an effective potential in which the motion of nuclei takes place. From chemical viewpoint the most important motion is the vibrational one. In many cases, classical (Newtonian) description of nuclear motion is sufficient, but sometimes quantum-mechanical effects are important. These effects are more pronounced on shallow surfaces, where energy minima are separated from each other by low barriers, leading to tunneling or delocalized phenomena. The hydrogen atom is expected to be more inclined to exhibit non-classical behavior due to its low atomic weight. Therefore, this work will be focused on hydrogen transfer phenomena. A shallow potential with a low barrier favors tunneling and delocalization, whereas a classical situation corresponds to well-separated minima with a high barrier. We will consider two classes of molecules where we expect to find various vibrational patterns for hydrogen transfer. The first class includes proton sponge cations, with an $\text{N}\cdots\text{H}\cdots\text{N}$ moiety, while the second class consists of bis(silyl)hydride organometallic complexes with an $\text{Si}\cdots\text{H}\cdots\text{Si}$ fragment. The hydrogen in proton sponge cations is simultaneously bound to both nitrogen atoms through hydrogen bonds, whereas in

the organometallic complexes the H atom can simultaneously interact with both silicons. In order to distinguish between the localized and delocalized hydrogen behavior, quantum-chemical calculations are necessary.

The study of hydrogen dynamics in proton sponge cations and organometallic complexes will not only help understand behavior of these particular systems, but will also contribute to general knowledge of hydrogen bonding and Si \cdots H interactions in organometallic complexes.

To provide a quantum-chemical description of the hydrogen motion in such type of systems, we numerically solve the vibrational Schrödinger equation. Inasmuch as the hydrogen vibrational motion in a molecule can be coupled with other modes, it will be beneficial to take some of these modes into account.

1.1 Proton sponges

Classical view of acid-base properties was challenged by Alder and co-workers, who discovered in 1968 a very simple organic compound that had an enormous basicity compared to ordinary organic bases. This simple molecule is 1,8-bis(dimethylamino)naphthalene,^{1,2} is a prototypical “proton sponge” (see Figure 1.1). A variety of proton sponges have been created since.³⁻⁶ Presently, proton sponges have a lot of interesting applications. They are of importance in organic synthesis.⁷⁻¹⁴ Their chiral derivatives can be used in asymmetric synthesis.¹⁵⁻¹⁷

A proton sponge usually has two basic nitrogen atoms attached to a relatively rigid organic core. The distance between two nitrogen atoms allows the incoming proton to be coordinated by both nitrogens simultaneously. Thus, the high basicity of the proton sponges is caused by the stabilization of their cationic form due to formation of a short

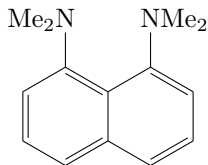


Figure 1.1: Prototypical proton sponge.

strong intramolecular NHN hydrogen bond, which can be either a symmetric $\text{N}\cdots\text{H}\cdots\text{N}$ or an asymmetric $\text{N}-\text{H}\cdots\text{N}$

Many experimental studies have considered the bonding situation in proton sponge cations. The NMR,^{3,18–21} IR spectroscopy,^{22–27} X-ray diffraction^{3,21–29} and, in few cases, neutron diffraction^{30–32} are typical methods for examination of such systems. Nevertheless, it is very difficult to draw conclusions regarding the hydrogen dynamic behavior from purely experimental data, and quantum chemical calculations provide a valuable complement to the experiment. One should also keep in mind that the X-ray diffraction is often unable to locate the hydrogen position with sufficient accuracy. Thus, the characterization of such hydrogen bonds based solely on X-ray data is difficult. Usually, one relies on the N–N distance as the most characteristic of an NHN bond

The typical N–N distance is less than 2.75 Å. The shortest N–N distances can be observed in two cases. The first case is **PS1** perchlorate²⁷ (see Figure 1.2 (a)) which has N–N distance 2.524 Å according to X-ray analysis. The second case is **PS2** hydrochloride³³ (see Figure 1.2 (b)) with an N–N distance of 2.526 Å according to X-ray data. The longest NHN bridge, where proton still interacts with both nitrogen atoms simultaneously, was found for **PS3** hemiperchlorate³² (see Figure 1.2 (c)) where the N–N distance is 2.635 Å according to a neutron diffraction study. In the case of larger distances one out of two $\text{N}\cdots\text{H}$ interactions becomes significantly weaker or disappears.

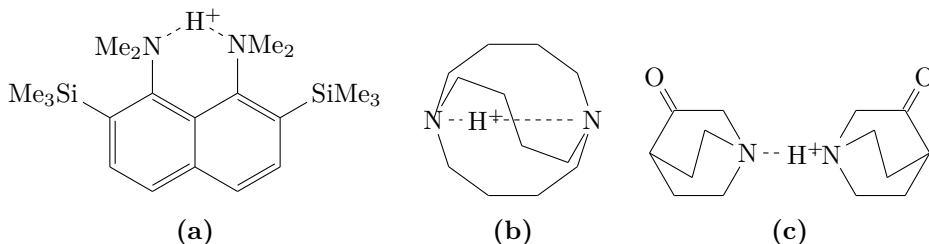


Figure 1.2: Protonated sponges with the shortest (a), (b) and the longest (c) N–N distances. (a) Protonated 2,7-bis(trimethylsilyl)-1,8-bis(dimethylamino)naphthalene (**PS1**); (b) protonated 1,6-diazabicyclo[4.4.4]tetradecane (**PS2**); (c) protonated 3-oxo-azabicyclo[2.2.2]octane (**PS3**).

IR spectra provide valuable information about strength of hydrogen bonds as well. According experimental data the evolution of the IR spectra with shortening the N–N distance is as follows. In the case of hydrogen bonds with NN distance about 2.93 Å, a fine $\nu(\text{NH})$ band about 2970 cm^{-1} can be observed.²² If the NN distance is in the range of 2.80–2.85 Å, $\nu(\text{NH})$ absorption band moves to the $2350\text{--}2450\text{ cm}^{-1}$ region.²² Further decrease of the NN distance from $\sim 2.7\text{ Å}$ to $\sim 2.6\text{ Å}$, typical of weak or medium strong hydrogen bonds, leads to appearance of a broad band of $\nu(\text{NHN})$ at about $1700\text{--}2240\text{ cm}^{-1}$ ^{22,34} and of an intense low-frequency absorption in the region of $400\text{--}900\text{ cm}^{-1}$. In some cases the region can be $1700\text{--}2700\text{ cm}^{-1}$ with a maximum at about 2200 cm^{-1} . Moreover, in some spectra an intense continuous absorption in the region $400\text{--}3000\text{ cm}^{-1}$ can be observed, indicating that proton tunneling takes place in the intramolecular hydrogen bond.^{35–39} The lack of continuous absorption means there is no tunneling and the proton is localized near one out of two nitrogens.^{40,41} Finally, for short distances of about 2.55 Å, typical of a short strong hydrogen bonds, absorption in the high-frequency region almost disappears and only

the 400–700 cm^{-1} region remains.^{22,34,42} The $\nu(\text{NHN})$ vibrations characterized not only by low frequencies but also by unusual or positive spectroscopic isotope effect $\text{ISR}=\nu(\text{NHN})/\nu(\text{NDN})> \sqrt{2}$ and corresponds to the reversed anharmonicity, i.e. the energy difference between the n th and the $(n + 1)$ st vibrational states increases with increasing quantum number n . This is opposite to systems with $\text{ISR} < \sqrt{2}$ which corresponds to the normal anharmonicity, i.e. energy levels are contracted with increasing n .^{24–27,43}

Another widely used tool for studying bonding situation in protonated proton sponge cations is ^1H , ^{13}C , and ^{15}N NMR spectroscopy. According to the experimental data, for various substituted proton sponges, the range of the $J(^{15}\text{N}-^1\text{H})$ coupling constants is from -50 Hz to -17 Hz.^{19,44} The negative sign of J is due to a negative gyromagnetic ratio of nitrogen atom. ^{15}N NMR was used also to study asymmetric derivatives of DMAN^{45–47} (see Figure 1.3 (b), (c) **PS8**, (d) **PS10**). In few cases the $J(^{15}\text{N}-^{15}\text{N})$ coupling constants were obtained from experiment. The largest value obtained so far is 16.7 Hz in a related anionic system with an NHN^- bridge¹⁸ (see Figure 1.3 (a)), although for the systems with NHN^+ bridges, i.e. DMAN and its substituted derivatives (see Figure 1.3 (b) **PS4**, **PS5**, (c), (d)), this value is in the range 8.7–9.8 Hz^{19,44} with the largest value being 9.87 Hz.¹⁹ There is a study of the coupling between ^{15}N atoms of various 1,8-diaminonaphthalenes (see Figure 1.3 (e), (f)) and 1,6-diazacyclodecane. For the 1,8-diaminonaphthalenes authors report coupling constants in the range 1.5–8.8 Hz⁴⁸ while the largest one is of 10.56 Hz in the case of 1,6-diazacyclodecane.⁴⁸

NMR chemical shifts can be used to estimate primary isotope effect $\Delta\delta(\text{H/D})$.⁴³ One can correlate it with spectroscopic isotope effect or, in other words, with the anharmonicity of the potential.⁴³ The general tendency is that while the NHN bridge shortens, $\nu(\text{NHN})$ increases, and if the NHN becomes short enough for the hydrogen motion barrier to disappear ISR reaches unity and $\Delta\delta(\text{H/D})$ reaches zero.

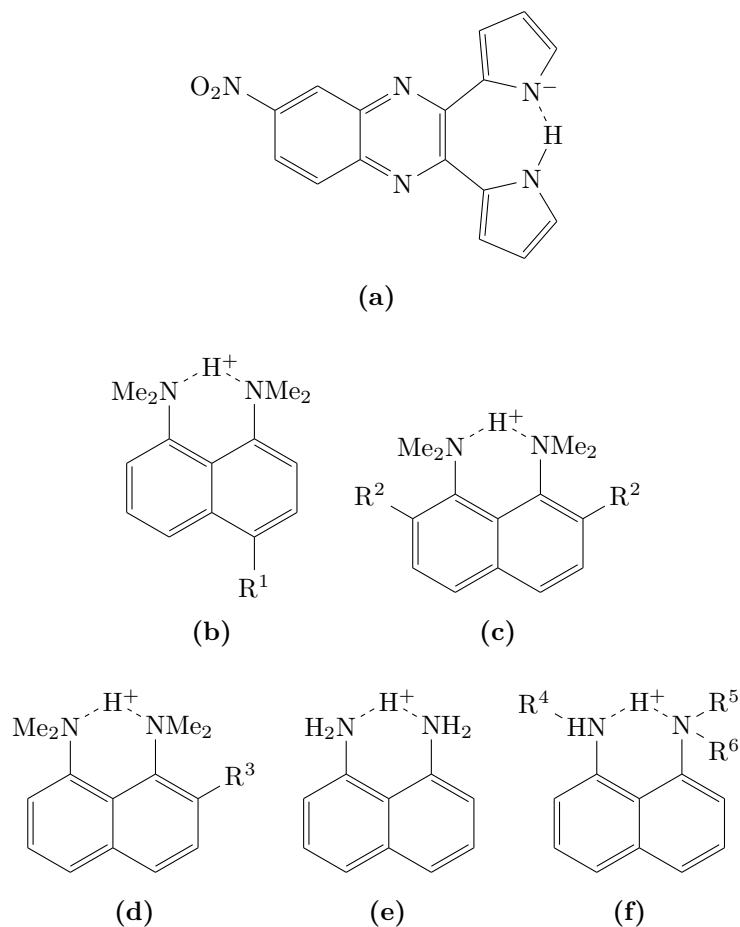


Figure 1.3: Asymmetric derivatives of DMAN studied by NMR. (a) (**Chelate**); (b) $R^1 = 2,4,6$ -trinitrophenyl (**PS4**); NO_2 (**PS5**); Br (**PS6**); (c) $R^2 = \text{H}$ (**PS7**); Cl (**PS8**); Br (**PS9**); (d) $R^3 = \text{Cl}$ (**PS10**); Br (**PS11**); (e) (**PS12**); (f) $R^4, R^5 = \text{H}, R^6 = \text{Me}$ (**PS13**); $R^4, R^5 = \text{Me}, R^6 = \text{H}$ (**PS14**); $R^4 = \text{H}, R^5, R^6 = \text{Me}$ (**PS15**); $R^4, R^5, R^6 = \text{Me}$ (**PS16**).

An ultrafast proton transfer ($\geq 10^{10} \text{ s}^{-1}$) in the NHN^+ bridge between two minima of the PES for the protonated DMAN species was discovered by NMR relaxation study.⁴⁹ The same behavior was found in NHO bridges for some types of Schiff bases⁵⁰ and in OHO bridges for certain β -diketones.⁵¹

By measuring dipolar coupling constant between ^{15}N and ^1H or between both ^{15}N atoms in the NHN^+ or NHN^- bridges one can calculate $\text{N}-\text{H}$ ^{18,50,52} or $\text{N}-\text{N}$ ^{50,52} distance, respectively. The dipolar coupling constant has inverse cubic dependence on distance between two interacting spins. The information about the symmetry of hydrogen bond can be obtained by isotopic perturbation of equilibrium⁵³⁻⁵⁵ analyzing the $\delta(\text{H})$ and $\delta(\text{D})$ chemical shifts and the $J(^{15}\text{N}-^{15}\text{N})$, $J(^{15}\text{N}-^1\text{H})$ coupling constants. This technique is very powerful if one needs to distinguish a single static structure from pair of tautomers.⁵⁶ It works even if signals from individual tautomers coalesce due to equilibrium. The method is based on measuring of isotope shift between ^{13}C chemical shifts of molecules with protium and deuterium ${}^n\Delta_{obs} = \delta(\text{C}(\text{D})) - \delta(\text{C}(\text{H}))$. This isotope shift includes an intrinsic part ${}^n\Delta_0$, which is due to substitution of hydrogen for deuterium. If hydrogen bond is asymmetric, and if NCH_3 is replaced by NCD_3 , an additional contribution to ${}^n\Delta_{obs}$ appears. Such deuteration perturbs the tautomeric equilibrium, and, as a result, the time-averaged chemical shift is displaced. This effect manifests itself as a perturbation isotope shift ${}^n\Delta_e$.²⁰ The method was used to answer the question about symmetry of NHN hydrogen bonds in solution. The results show that, in studied protonated PS (see Figure 1.3 (a), (c) **PS7**, (f)), hydrogen bonds are asymmetric and a pair of rapidly converting tautomers exists in each case.^{19,20,57}

It is not always sufficient to consider the molecular structure at the energy minimum. Often, potential energy surfaces must be computed to gain a deeper insight into hydrogen bonding. Consequently, the choice of an adequate quantum-chemical method to evaluate the PES

is crucial. Even small changes of the surface may cause substantial differences in the hydrogen bond properties. This situation is typical of low-barrier hydrogen bonds

The most important characteristic of a hydrogen bond PES is the height of the barrier for proton motion. The barrier was shown to depend on the level of the quantum-chemical calculation and to lie in the range of 0 – 4.5 kcal·mol⁻¹.⁵⁸ As an example of this dependence N,N,N,N-tetramethylputrescinium ion can serve.⁵² The potentials for the proton stretching were calculated at various levels of theory and the results varies from a double-well potential with a tiny barrier to a double-well potential with a high barrier. In that work not only different barriers were obtained but also qualitatively different behavior of the vibrational wavefunction, i.e. from single-maxima wavefunction to that with two well separated maxima.

Sterically compressed and symmetric (according to X-ray results) NHN⁺ intramolecular hydrogen bonds (see Figure 1.4) were also studied. One example is **PS1-ClO₄**.²⁷ In spite of its remarkably short NHN⁺ bridge (NN distance is 2.52 Å at room temperature) there is a double-well potential with a barrier of about 0.7 kcal·mol⁻¹ at MP2/6-31+G(d,p) level. Another two examples of sterically hindered systems are **PS17-Br**²⁵ and **PS18-Br**.²⁶ The barrier heights were found to be 0.7 kcal·mol⁻¹ and 1.32 kcal·mol⁻¹ respectively (both at MP2/6-31G(d,p) level). According to the results obtained in these works, the best accuracy for the geometry of proton sponges and for the shape of the potential is provided by MP2.

1.1.1 Asymmetric proton sponges

NMR, IR, X-ray, and neutron diffraction (see Page 3) revealed that the highest likelihood to find the proton in NHN⁺ bridge is when the proton is in asymmetric position, i.e. closer to one of two nitrogens.⁵⁹ Asymmetry depends on various factors, i.e. counterion²⁷ (see Table

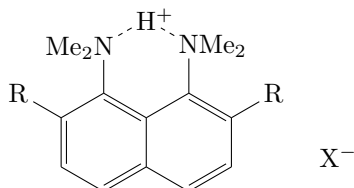


Figure 1.4: Proton sponges with sterically compressed NHN^+ intramolecular hydrogen bond. $\text{R} = \text{SiMe}_3$, $\text{X}^- = \text{ClO}_4^-$ (**PS1-ClO₄**); $\text{R} = \text{Br}$, $\text{X}^- = \text{Br}^-$ (**PS17-Br**); $\text{R} = \text{OMe}$, $\text{X}^- = \text{Br}^-$ (**PS18-Br**).

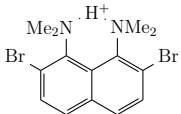
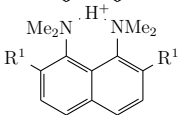
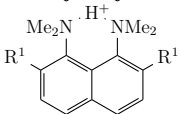
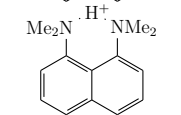
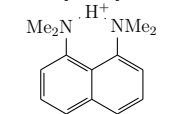
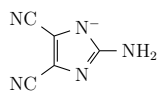
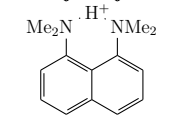
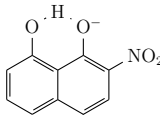
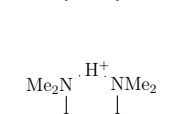
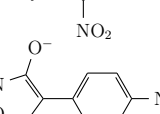
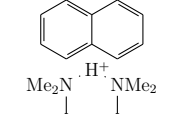
1.1), temperature.^{42,60} Solvent plays a role as well: some ions are symmetric in crystals, but asymmetric in solution.²⁰

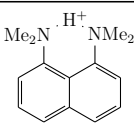
It is only in crystals that symmetric hydrogen bonds were found. Some ions are asymmetric at low temperature, but sometimes appear symmetric in X-ray at room temperature due to averaging over dynamic disorder of hydrogen.^{20,57,61}

In solution the local environment is disordered and two nitrogen atoms have different solvation.^{20,57,61} Hence proton (or charge) localization is favored near one or other nitrogen atom by solvent dipoles which leads to degenerate tautomerism, but if temperature lowers the solvent becomes more ordered which leads to more symmetric hydrogen bond.¹⁹

The most important characteristics of the NHN^+ bridge are the N-H , $\text{H}\cdots\text{N}$, N-N distances and the $\text{N-H}\cdots\text{N}$ angle. There is a direct relationship between the shape of the PES and the position of hydrogen between two nitrogen atoms.

Table 1.1: Asymmetric proton sponges. Intramolecular hydrogen bond geometry determined by X-ray (X) or neutron diffraction (ND) studies. See more in.^{22,59} Distances are given in ångströms. $R^1 = \text{CH}_2\text{OH}$.

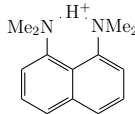
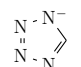
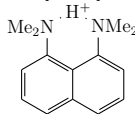
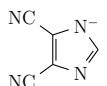
Cation	Anion	N–H	H...N	N–N ^{Ref.}
	Br^-	0.85(5)	1.73(5)	2.547 X ²⁵
	Cl^-	1.16	1.50	2.561 X ²⁷
	SiF_6^{2-}	0.87	1.71	2.556 X ²⁷
	$\text{HOCCl}=\text{CClCOO}^-$	1.106	1.608	2.644 ND ³⁰
		1.16(3)	1.50(3)	2.595 X ⁶²
		1.09(4)	1.52(4)	2.574 X ⁶³
		1.25(2)	1.38(2)	2.586 X ⁶⁴
	$\text{Ni}(\text{O}_2\text{NCHCC}(\text{O})\text{Ph})_3^-$	0.80	1.86	- X ⁶⁵

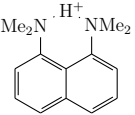
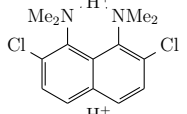
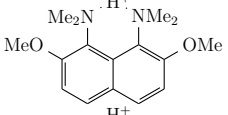
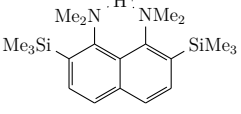
Cation	Anion	N–H	H...N	N–N ^{Ref.}
	<i>nido</i> -7,8-C ₂ B ₉ H ₁₂ ⁻	1.228	1.419	2.599 ND ³¹

1.1.2 Symmetric proton sponges

Although the asymmetric hydrogen bonds are more common, the symmetric ones were also observed in several cases (see Table 1.2). Despite the solvent favors an asymmetric hydrogen bond, calculations, in such systems as formic acid–formic acid anion and maleic acid anion, demonstrated that in the case of a non-polar medium the symmetric hydrogen bond with delocalized charge is more preferred than the asymmetric one with localized charge.^{66–68} It was also shown experimentally that a small counterion, such as CF₃COO⁻, can perturb the symmetry of hydrogen bond, but a large counterion with a delocalized and shielded charge, e.g. B[(C₆H₃(CF₃)₂)₄]⁻, makes it more symmetric.¹⁹

Table 1.2: Symmetric proton sponges. Intramolecular hydrogen bond geometry determined by X-ray (X) or neutron diffraction (ND) studies. See more in.^{22,59} Distances are given in ångströms.

Cation	Anion	N–H	H...N	N–N ^{Ref.}
		1.312	1.312	2.573 X ⁶⁹
		1.321	1.321	2.579 X ⁷⁰

Cation	Anion	N–H	H⋯N	N–N ^{Ref.}
	Br ⁻	1.31(1)	1.31(1)	2.555 X ⁷¹
	Br ⁻	1.29(1)	1.29(1)	2.561 X ²⁴
	Br ⁻	1.30(1)	1.30(1)	2.567 X ²⁶
	ClO ₄ ⁻	1.275	1.275	2.524 X ²⁷

1.1.3 Description of hydrogen bonds

The hydrogen bond A–H⋯B is an attractive interaction between a proton donor A–H and a proton acceptor B, where A and B can be atoms of the same or different type. When B is oxygen or nitrogen the hydrogen bond exists if the A⋯B distance is shorter than 2.5 Å but longer than a covalent N–H or O–H bond length, which is close to 1.0 Å. The hydrogen bond is characterized by a dissociation energy larger than dipole-dipole or dispersion interaction energies. Due to the interaction the A–H bond length slightly increases and the potential energy surface softens, which results in a red shift of the A–H bond stretching vibration. This is the most fascinating effect. Weakening of the A–H bond is accompanied by a strengthening the H⋯B interaction. As bond strength increases, the dynamics of the central proton becomes more complicated compared to a covalently bonded hydrogen described by a simple potential well. For instance for the

O–H···O bond a double-well potential for the proton transfer changes to single-well with decreasing the O–O distance^{72,73} (see Figure 1.5).

The most properties related to the hydrogen bonds vary according to the bond strength. Thus, according to the energy of H···B, one can distinguish three bonding situations, i.e. weak, moderately-strong, and strong hydrogen bonds.

A weak hydrogen bond, in general, has a binding energy no more than 4 kcal·mol⁻¹. The A···B distance can vary between 3.1 Å and 4.3 Å. This weak bond may lead to a double-minimum potential energy surface along the hydrogen transfer reaction coordinate with a high potential barrier (see Figure 1.6b) and the proton transfer can be frozen at low temperature. The proton motion is then *localized* near the minimum positions. However, this barrier is still lower compared to the barrier for dissociation of the A–H covalent bond. In this case tunneling between two wells contributes substantially to hydrogen transfer. The tunnel effect can be observed in fluorescence excitation,^{74,75} infrared,⁷⁶ and microwave^{77,78} spectra. This effect manifests itself in the spectra by tunneling splitting, i.e. by splitting of vibrational energy levels originating from symmetric and antisymmetric combinations of the wavefunctions of each single well. The energy split is defined as a difference between two nearly degenerated states and normally it increases for higher lying states. The maxima of the ground state vibrational wavefunction are located around minima of the PES (see Figure 1.6b). This situation can be treated as two weakly coupled oscillators.

As hydrogen bond strength increases, the barrier on the PES decreases. This leads to an anharmonic potential energy surface along the hydrogen transfer reaction coordinate. In general, anharmonicity increases with increasing the hydrogen bond strength. Moreover, the lower the barrier, the larger tunneling splitting is to be expected.

While the energy for moderate-strong hydrogen bond lies in the interval 4–14 kcal·mol⁻¹ and the A···B distance varies from 2.4 Å to

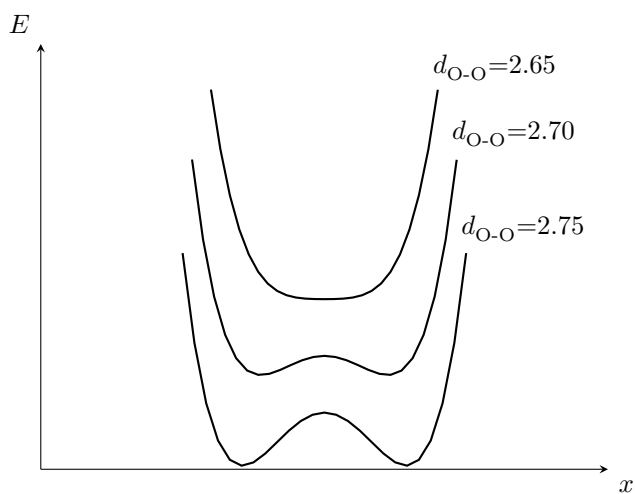


Figure 1.5: After Giese *et al.* [73]. Proton motion PES dependence on various O–O distances. E is the potential energy, x is the proton coordinate. Distance between two oxygen atoms d is given in ångströms. See text for details.

3.3 Å, for the strong one the binding energy is above 14 kcal·mol⁻¹ and the A...B bond distance is less than 2.7 Å. This type of bonds is characterized by a small barrier (see Figure 1.6c), such that the proton moves freely between two minima even at 0 K. In this case the wavefunction still has a single maximum at the central position, although this point is a transition state rather than a minimum on the PES⁷⁹ (see Figure 1.6c). In this situation the proton motion is *delocalized*. In some cases, the barrier disappears leading to a flat potential energy surface (see Figure 1.6a). This phenomenon allows a bound hydrogen to be very mobile.

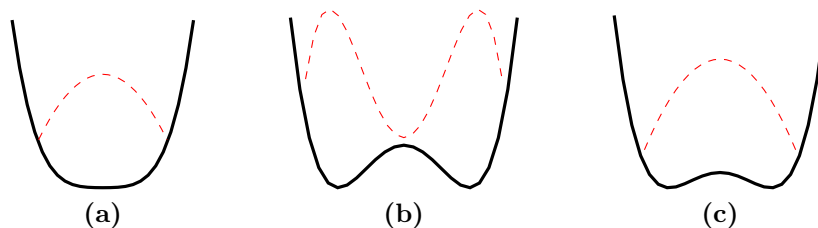


Figure 1.6: Various types of symmetric potentials for proton motion (see text). The solid lines represent PES profiles, and the red dashed lines are the ground-state vibrational wavefunctions.

While these three situations are clear qualitatively, quantum-chemical calculations are necessary in order to distinguish between them. Although the height of the proton transfer barrier is crucial, the vibrational wavefunction obtained by solving the vibrational Schrödinger equation in a given PES is needed to get more insight into the proton dynamics.

All discussed above concerns a one-dimensional picture of the hydrogen transfer, while the hydrogen motion in a polyatomic molecule is obviously coupled with that of other atoms or vibrational modes. According to the nuclear dynamics, two fundamental types of coupling

between proton transfer reaction coordinate and the other motions exists.⁸⁰

The first type is *promoting modes* which modulate the potential along the reaction coordinate leading to a reduction of the barrier. This situation is depicted in Figure 1.5 where the barrier for transfer of proton between two oxygen atoms reduces with reducing the O—O distance.⁷³ A similar situation occurs for the hydrogen transfer along the ammonia chain in 7-hydroxyquinoline·(NH₃)₃ complex, i.e. the distance OH...NH₃ shortens promoting tunneling of hydrogen from OH group.⁸¹ The second type is *reorganization modes* which change the molecular structure, e.g. a rearrangement of single and double bonds as observed in tropolone molecule during the hydrogen transfer between two oxygen atoms.⁸² When tunneling splitting is affected by these two fundamental types of coupling it calls mode-specific tunneling splitting.⁷³

1.2 Organometallic complexes

Transition metal-silyl chemistry originates in 1956 with synthesis of iron complex CpFe(CO)₂SiMe₃ by Wilkinson and co-workers⁸³ (see Figure 1.7).

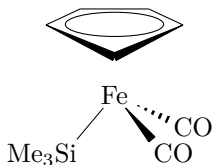


Figure 1.7: First transition metal complex with silicon ligand.

Transition metal silyl complexes play an important role as intermediates in various silylation reactions^{84–86} and even in industrial applications.^{87–89} Various functionalized silyl complexes are valuable reagents

for the synthesis of new silicon-based materials.^{84,90–92} By now, silyl complexes $[L_nM-SiR_3]$ are known for nearly all transition metals^{90,93} (see Figure 1.8).

21 44.956 Sc Scandium	22 47.867 Ti Titanium	23 50.942 V Vanadium	24 51.996 Cr Chromium	25 54.938 Mn Manganese	26 55.845 Fe Iron	27 58.933 Co Cobalt	28 58.693 Ni Nickel	29 63.546 Cu Copper	30 65.39 Zn Zinc
39 88.906 Y Yttrium	40 91.224 Zr Zirconium	41 92.906 Nb Niobium	42 95.94 Mo Molybdenum	43 96 Tc Technetium	44 101.07 Ru Ruthenium	45 102.91 Rh Rhodium	46 106.42 Pd Palladium	47 107.87 Ag Silver	48 112.41 Cd Cadmium
57 138.91 La Lanthanum	72 178.49 Hf Hafnium	73 180.95 Ta Tantalum	74 183.84 W Tungsten	75 186.21 Re Rhenium	76 190.23 Os Osmium	77 192.22 Ir Iridium	78 195.08 Pt Platinum	79 196.97 Au Gold	80 200.59 Hg Mercury

- Observed in matrix studies
- No known examples
- Only complexes containing β -H-Si interactions have been reported

Figure 1.8: Transition metals that give isolable silyl-metal compounds.

One of the most widely used approaches for the synthesis of transition metal-silyl complexes is oxidative addition of silanes.⁹⁰ An oxidative addition of a hydrosilane to a metal center can yield a classical complex with two-center two-electron M–Si and M–H bonds (Figures 1.9a, 1.10a). However, if silane coordination occurs without oxidative addition, the Si–H bond remains intact, leading to a non-classical η^2 -silane σ -complex with a three-center two-electron bond (Figures 1.9b, 1.10e).^{94,95} σ -Complexes play a role as intermediates in oxidative addition reactions.

The variety of possible structures in transition metal complexes with silicon ligands are depicted in Figure 1.10. In an intermediate situation, when the oxidative addition is *incomplete*, the Si–H bond is only partly broken. In σ -complexes (see Figure 1.10a) and those with α -agostic interactions (see Figure 1.10b) the Si–H distance is

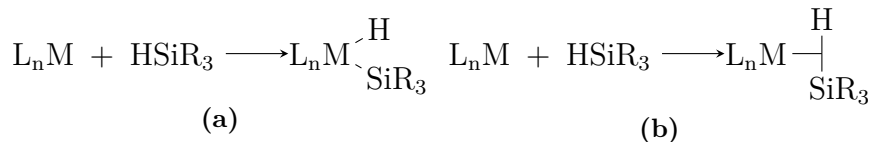


Figure 1.9: Classical (a) and non-classical (b) interactions in complexes containing silicon ligands.

elongated compared to free silane. Further examples of organometallic complexes include interligand hypervalent interactions⁹⁵ (see Figure 1.10c), which usually require the presence of a halogen substituent at silicon and have much larger Si–H distance. In addition to the above-mentioned bonding patterns, silyl complexes may exhibit additional interactions (see Figure 1.10d) leading to a further increase of the Si–H distance. Finally, the longest Si–H distance is observed in pure silyl-hydride complexes (see Figure 1.10e) where there are no interactions at all between silicon and hydrogen. The strength of interactions depends on the degree of oxidative addition.

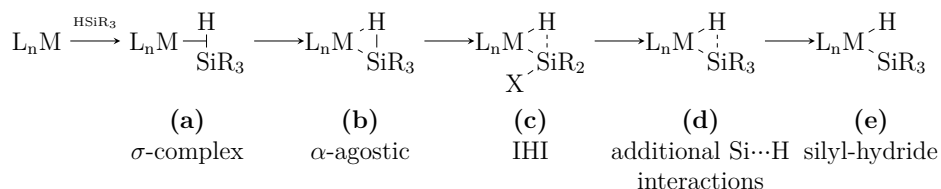


Figure 1.10: Variety of structures in transition metal complexes with silicon ligands: from non-classical to classical.

Theoretical interpretation of Si–H interactions is based on a kind of the Dewar–Chatt–Duncanson model (see Figure 1.11). These interactions involve the donation of the silane Si–H σ -orbital to the metal center. In this situation two electrons from a Si–H bond are

distributed among three centers Si, H, and TM. This type of interactions are referred to as three-center two-electron interactions. The Si–H bond has a much better electron donor ability than H–H and C–H bonds.⁹⁶ On the other hand, due to a lower dissociation energy of the Si–H bond,⁹⁰ the $\sigma^*(\text{Si–H})$ orbital has stronger acceptor properties, thus favoring the $\text{M} \rightarrow \sigma^*(\text{Si–H})$ back-donation. These two effects – the $\sigma(\text{Si–H}) \rightarrow \text{M}$ donation and the $\text{M} \rightarrow \sigma^*(\text{Si–H})$ back-donation – weaken the Si–H bond and eventually give rise to a wide range of structures discussed above, from non-classical to classical silyl-hydride complexes.⁹⁷

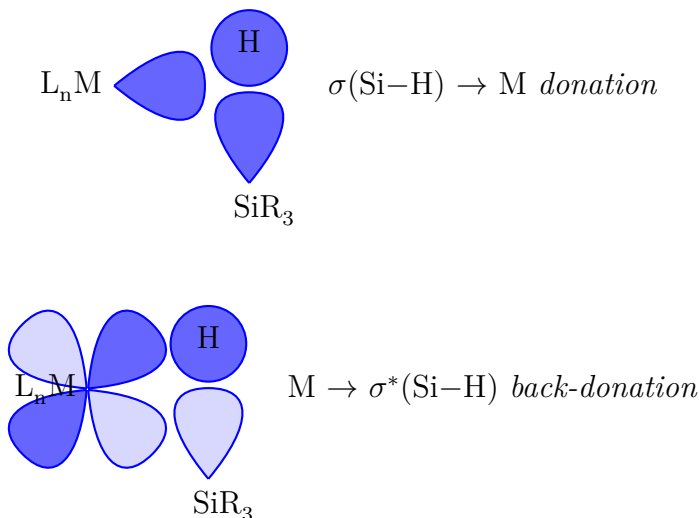


Figure 1.11: After Lin [97]. Dewar–Chatt–Duncanson model for interactions metal- η^2 -silane.

Complexes with non-classical interactions were studied both experimentally and theoretically. The experimental methods employed include the X-ray diffraction,^{94,95,98–103} NMR,^{98–103} IR^{98–100,102,103} and, in few cases, the neutron diffraction.^{104–110} Major differences between σ -

complexes, agostic, and IHI interactions were reviewed by Nikonov.^{98,111} A Si–H distance in the range of 1.7–1.8 Å clearly indicates σ -coordination,^{112,113} while longer Si–H separations are harder to interpret. Nevertheless, for distances up to 2.1 Å there is almost always at least some degree of an Si \cdots H interaction.^{113,114} According to some authors, the interaction can be present for Si \cdots H separations as large as 2.4 Å.^{97,113}

A very valuable tool for assessing non-classical interactions is provided by the NMR, the spin-spin coupling constants $^1J(\text{Si-H})$ being of particular importance. In a free silane, $J(\text{Si-H})$ is about 150–200 Hz,^{90,115} while for classical silyl-hydride complexes it is vanishing or very small (below 20 Hz). In the presence of non-classical interactions $|J(\text{Si-H})|$ is in the range of 20–140 Hz, more typically from 40 to 80 Hz.^{116–119}

It is commonly accepted that $|J(\text{Si-H})| > 20$ Hz corresponds to a direct Si–H interaction,^{90,115} though this criterion is quite arbitrary and the strength of the interaction was shown to not always correlate with $|J(\text{Si-H})|$.¹²⁰ A more unequivocal indication of a direct Si \cdots H interaction is given by the *sign* of $J(\text{Si-H})$. Due to a negative gyromagnetic ratio of the ^{29}Si nucleus, $J(\text{Si-H})$ is negative if the direct Si \cdots H interaction prevails, while through-bond interactions, such as Si–M–H, provide a positive contribution to the total $J(\text{Si-H})$. While in most cases only the absolute value $|J(\text{Si-H})|$ is easily available experimentally, the sign is harder to get, but the sign of *computed* $J(\text{Si-H})$ serves as a valuable indicator of the direct Si–H interaction.^{103,121–123}

Useful data are also supplied by IR spectra. When a non-classical interactions are present, broadening and red shift occur in the Si–H stretching vibrational frequency compared to values of 2100–2200 cm^{-1} typical of a free silane. For σ -complexes, the Si–H vibrations, often coupled with M–H stretching, are observed in the region 1600–1945 cm^{-1} .

1.2.1 σ -Complexes

σ -Complexes in principle can exist in isolated form, but only few examples were obtained and separated as individual compounds.^{124–128} The very first known example of a σ -complex, $\text{Re}_2(\text{Ph}_2\text{SiH}_2)(\text{CO})_8$ (see Figure 1.12), was obtained in 1969 by Hoyano *et al.*¹²⁹ Although the positions of hydrogen atoms were not determined by X-ray spectroscopy, they were placed in the sixth coordination site of each rhenium atom. An evidence for placing them in such coordination sites is provided by the NMR spectrum of an analogous complex $\text{Re}_2(\text{Me}_2\text{SiH}_2)(\text{CO})_8$. Spectroscopic data show that two hydrides are magnetically equivalent. Most probably they are in the symmetrically equivalent positions in the Re–Si–Re plane. If these hydrides are in the Re–Si–Re plane with an Re–H distance of 1.68 Å the Si–H contact is 1.57 Å which is typical of σ -complexes. The Re–Si distances are 2.51 Å and 2.53 Å, respectively. The orbital interaction diagram for silane σ -complexes is shown in Figure 1.11.

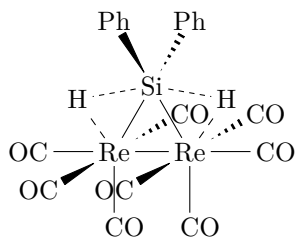


Figure 1.12: The σ -complex $\text{Re}_2(\text{Ph}_2\text{SiH}_2)(\text{CO})_8$. Hydrogen atoms, which are not observed, are shown in the positions suggested by spectroscopic evidence.

Apart from rhenium, σ -complexes are known for Mn,¹²⁴ Mo,^{125,126} and Ru^{127,128} (see Figure 1.13). In the case of the Mn complex¹²⁴ shown in Figure 1.13(a) a bonding interaction between silicon and hydride atoms was shown by X-ray diffraction. Whereas the Mn–Si and

Mn–H distances show regular values of 2.42 Å and 1.55 Å respectively, the Si–H distance is elongated up to 1.76 Å compared to a normal one (1.48 Å). The conclusion about the presence of Si–H interaction is given not only by the X-ray, but also is reflected by NMR. The large value of 64.7 Hz for $J(\text{Si–H})$ coupling constant could point out to non-classical interactions.

Among molybdenum complexes the X-ray diffraction analysis was performed for **Mo1-2**¹²⁵ and **Mo4-1**¹²⁶ complexes (see Figure 1.13(b)) and confirmed the η^2 -coordination of the Si–H bond to the metal center. In **Mo1-2** the molybdenum-bound Si–H bond is elongated (1.77(6) Å) compared to the other two Si–H distances (1.41(6) Å and 1.42(6) Å). NMR also supports the η^2 -silane coordination. In this case the $J(\text{Si–H})$ coupling constant is 39 Hz. The Mo–H distance is 1.70(5) Å, the Mo–Si is 2.501 Å. In the case of the **Mo4-1** complex four hydrogen atoms on silicon were not located due to a positional disorder between $\eta^2\text{-SiH}_4$ and CO ligands. However, the geometry of the MoP_4CSi fragment is similar to that in the **Mo1-2** complex discussed above where the hydrogen positions are known. Thus, together with a $J(\text{Si–H})$ coupling constant of 50 Hz this confirms the η^2 -coordination of the silane molecule in **Mo4-1**. The Mo–Si distance is 2.556 Å. For the other complexes (see Figure 1.13(b)) only NMR data are available. Nevertheless $J(\text{Si–H})$ coupling constants within the range 41–61 Hz indicate that these complexes possess non-classical interactions.^{125,126}

Ruthenium complexes shown in Figure 1.13(c) are the first mononuclear complexes containing two $\text{M}-(\eta^2\text{-SiH})$ bonds. The X-ray data are available for the complexes **Ru2**, **Ru3**, and **Ru5**.¹²⁸ As expected for complexes with η^2 -coordination, both Si–H distances are elongated: 1.84(2) Å and 1.84(2) Å for **Ru2**, 1.73(3) Å and 1.78(4) Å for **Ru3**, 1.77(4) Å and 1.81(3) Å for **Ru5**. It is important to remark that in the case of **Ru2**, and **Ru3** there is no large difference in Ru–H distances for the hydrogens bound to silicon and for those bound to the ruthenium atom only. However, for **Ru5** complex one can ob-

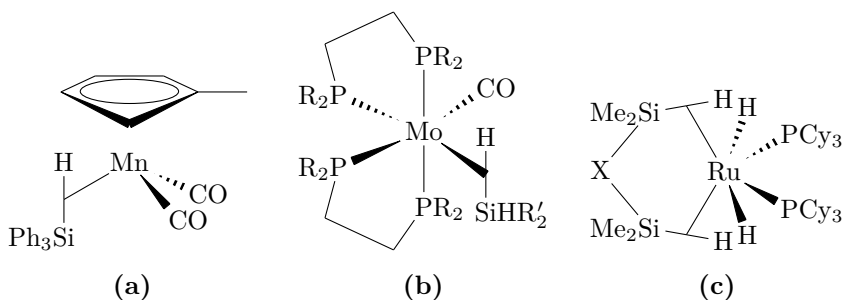


Figure 1.13: σ -Complexes isolated as individual compounds. (b) $\text{PR}_2 = \text{PEt}_2$ (**Mo1**); $\text{P}(\text{CH}_2\text{Ph})_2$ (**Mo2**); PPh_2 (**Mo3**); $\text{P}(\text{}^i\text{Bu})_2$ (**Mo4**); $\text{SiHR}'_2 = \text{SiH}_3$ (**1**); SiH_2Ph (**2**); $\text{SiH}_2(\text{n-C}_6\text{H}_{13})$ (**3**); SiHPh_2 (**4**); (c) $\text{X} = \text{O}$ (**Ru1**); C_6H_4 (**Ru2**); $(\text{CH}_2)_2$ (**Ru3**); $(\text{CH}_2)_3$ (**Ru4**); OSiMe_2O (**Ru5**).

serve a significant difference in the Ru–H distances. If the hydrogen bound to the silicon Ru–H distances are 1.62(4) Å and 1.58(4) Å, if hydrogen is not bound they are 1.55(4) Å and 1.51(3) Å. For all five ruthenium complexes discussed here the $J(\text{Si-H})$ coupling constants are within the range from 22 to 82 Hz, which is in agreement with non-classical nature of these complexes.^{127,128} The NMR spectra for them are temperature-dependent and show the exchange between the $\eta^2\text{-Si-H}$ and Ru–H hydrides.

1.2.2 Interligand hypervalent interactions

The first interligand hypervalent interactions were proposed for the complex $\text{Cp}_2\text{Nb}(\text{SiMe}_2\text{Cl})_2\text{H}$ in 1995 by Nikonov *et al.*⁹⁴ (see Figure 1.14) based on the experimental data. For this complex not only X-ray⁹⁵ but also neutron diffraction data¹⁰⁵ were obtained. According to the neutron diffraction the Nb–Si distance is 2.612 Å lying in the

middle of the typical region for this bond type (2.541–2.685 Å).⁹³ The same distance measured by X-ray is 2.597 Å and is in a good agreement with the previous data. Both distances are substantially shorter than Nb–Si bond in $\text{Cp}_2\text{Nb}(\text{SiMe}_2\text{Ph})_2\text{H}$ ⁹⁵ (2.654 Å) which does not have IHI. The Si–Cl distances obtained by these two methods are also in a good agreement (2.166 Å and 2.163 for neutron diffraction and X-ray correspondingly) and are longer than those for R_3SiCl .⁹⁵ Since X-ray cannot define properly the positions of hydrogens in the vicinity of heavy atoms, there is a difference between Nb–H distances determined by neutron diffraction and X-ray. The Nb–H distance determined by neutron diffraction is larger than that determined by X-ray – 1.816 Å and 1.747 Å respectively, – but both of them are longer than Nb–H in $\text{Cp}_2\text{Nb}(\text{SiMe}_2\text{Ph})_2\text{H}$ (1.672 Å). Despite the difference in Nb–H distances, the Si–H one changes only slightly: 2.076 Å (neutron diffraction) *vs* 2.056 Å (X-ray).

As we have seen, the IHI have several main structural features: The metal-silicon bonds are shorter than normal; the silicon-halogen bonds are longer than in correspondent halosilanes; M–H bond are longer than usual, Si–H contacts are present, in bis(silyl)complexes the Si–M–Si angle is smaller than that in bis(silyl)complexes without IHI.⁹⁵

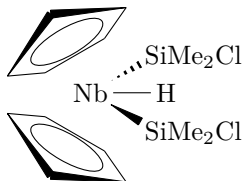


Figure 1.14: The first complex with IHI.

The above mentioned features can be explained by an orbital interaction diagram for the IHI (see Figure 1.15). One needs a halogen

to be in a *trans*-position to the hydrogen for the IHI to occur. Such configuration provides an overlap between the bonding $\sigma(\text{M}-\text{H})$ orbital and the antibonding $\sigma^*(\text{Si}-\text{halogen})$ orbital. The population of $\sigma(\text{M}-\text{H})$ decreases while the population of $\sigma^*(\text{Si}-\text{halogen})$ increases. As a result, elongation of both $\text{M}-\text{H}$ and $\text{Si}-\text{halogen}$ bonds takes place. Simultaneously, the interaction between Si and H increases leading to shortening of the $\text{Si}-\text{H}$ distance. In the bis(silyl) complexes the hydrogen interacts with both silyl groups and the orbital diagram becomes more complicated, since the $\text{M}-\text{H}$ bonding orbital interacts with a symmetrical combinations of the $\text{Si}-\text{halogen}$ bonding and antibonding orbitals. This interaction is supported by mixing with appropriate metal orbitals (see Figure 1.15). Thus, the interactions which occur are 3c-4e in the case of silyl complexes and 5c-6e in the case of bis(silyl) complexes. It is important to note that one has to distinguish this type of interactions from those in σ -complexes. A description of IHI in terms of σ -complexes can be misleading. In σ -complexes a stronger $\text{Si}-\text{H}$ interaction corresponds to a longer $\text{M}-\text{Si}$ distance, whereas the opposite is true for the IHI.⁹⁵

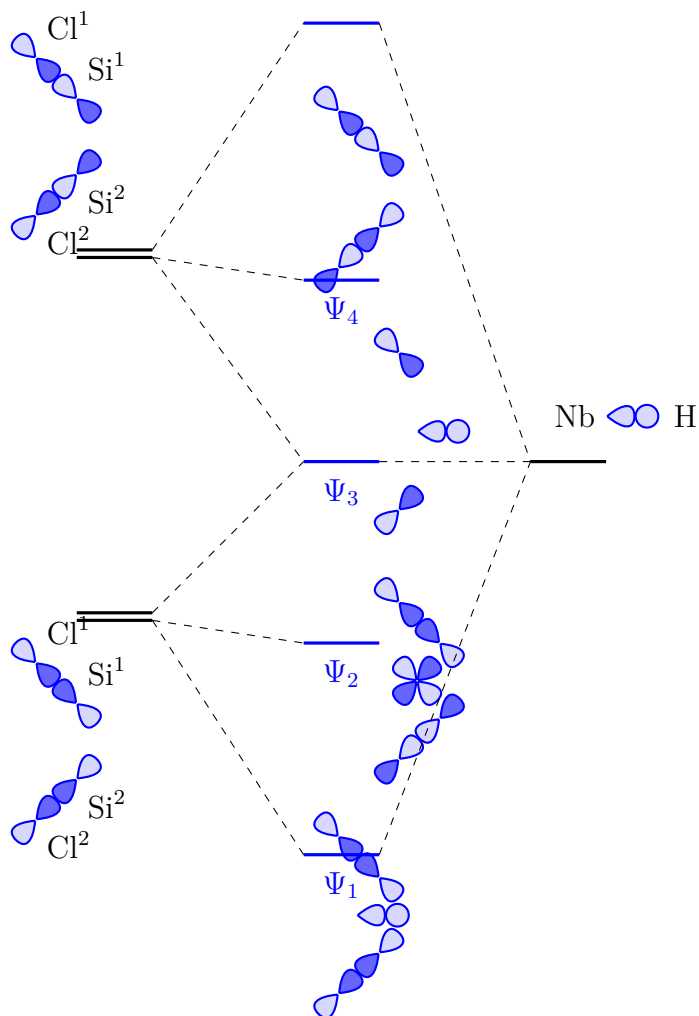


Figure 1.15: Orbital interaction diagram for IHI in $\text{Cp}_2\text{Nb}(\text{SiMe}_2\text{Cl})_2\text{H}$. After Nikonov *et al.* [95].

More examples of IHI complexes with available experimental X-ray data include $\text{Cp}_2\text{Nb}(\text{SiMe}_2\text{Br})_2\text{H}$ and $\text{Cp}_2\text{Nb}(\text{SiMe}_2\text{I})_2\text{H}$ ^{95,130} (see Figure 1.16(a)). They were the first reported examples of complexes with iodosilyl and bromosilyl ligands that had been characterized by X-ray. The Nb–Si distances for these complexes are 2.604 Å and 2.595 Å respectively, short as in $\text{Cp}_2\text{Nb}(\text{SiMe}_2\text{Cl})_2\text{H}$ described above. The Si–Br and Si–I distances are longer than those in R_3SiBr or R_3SiI ¹³⁰ – 2.349 Å and 2.590 Å correspondingly. The Nb–H distances in the Br and I derivatives are longer than in $\text{Cp}_2\text{Nb}(\text{SiMe}_2\text{Ph})_2\text{H}$ and are 1.780 Å and 1.881 Å correspondingly. Si···H contacts are 2.053 Å and 2.070 Å respectively and, as expected, are shorter than in $\text{Cp}_2\text{Nb}(\text{SiMe}_2\text{Ph})_2\text{H}$.

An interesting case is $\text{Cp}_2\text{Nb}(\text{SiMe}_2\text{OMe})_2\text{H}$ ¹³⁰ (shown in Figure 1.16(a)). Two Nb–Si distances (2.624 Å and 2.628 Å) are close to those in a complex without IHI ($\text{Cp}_2\text{Nb}(\text{SiMe}_2\text{Ph})_2\text{H}$), although the Nb–H distance is larger (1.885 Å) in $\text{Cp}_2\text{Nb}(\text{SiMe}_2\text{OMe})_2\text{H}$. The Si–O bonds are elongated (1.696 Å and 1.691 Å) in comparison with those in iron and iridium complexes.^{131,132} There could be various origins of this elongation, e.g. due to a stronger electron donation ability of the Cp_2Nb fragment, due to a weak O–Si···H interactions or both. Thus, this complex can be considered as an intermediate case between non-classical halogen-substituted complexes and classical alkyl-substituted ones.¹³⁰

Another interesting case is the complex $\text{Cp}_2\text{Nb}(\text{SiCl}_3)_2\text{H}$ ¹³³ (see Figure 1.16(b)). Although this complex has three chlorine substituents at each silicon, the IHI are significantly reduced as suggested by ¹H NMR data and by X-ray. Remarkably, there is no significant difference between Si–Cl distances, i.e. they do not depend on whether the chlorine atoms lie in the *trans*-position to the hydrogen or not. These Si–Cl bonds are elongated and lie in the range 2.084–2.099 Å. According to the X-ray data, the Nb–Si bonds are very short (2.560 Å and 2.578 Å). The angle Si–Nb–Si is close to those observed in classi-

cal bis(silyl)systems and the Si \cdots H contacts are 0.1 Å longer (2.143 Å and 2.113 Å) than those typical of complexes with IHI. All these facts suggest that IHI are significantly reduced in this complex. The insufficiency of Si \cdots H interactions could be due to the low electron density of the Nb–H bond having its origin in a number of electron-withdrawing chlorine atoms at silicon. For the same reason the Nb–Si bonds are extremely short (Bent’s rule¹³⁴) as if the normal IHI were present.

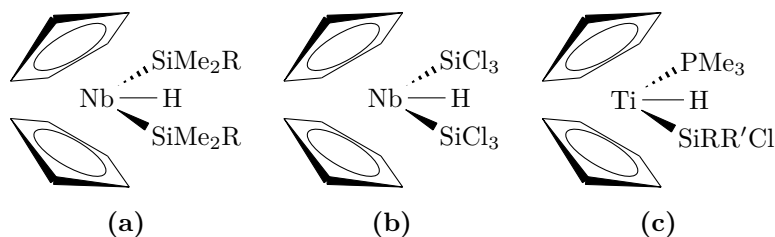


Figure 1.16: Niobium and titanium complexes with IHI. (a) SiMe₂R = SiMe₂Br (**Nb1**); SiMe₂I (**Nb2**); SiMe₂OMe (**Nb3**); (c) SiRR’Cl = SiMePhCl (**Ti1**); SiPh₂Cl (**Ti2**); SiMeCl₂ (**Ti3**); SiCl₃ (**Ti4**).

The IHI are present not only in niobium complexes but also were found, for instance, in titanium complexes such as titanocene silyl hydride complexes Cp₂Ti(PMe₃)(H)(SiRR’Cl)¹⁰³ (see Figure 1.16(c)). They were prepared and studied by NMR, IR, and X-ray diffraction. All structural and spectroscopic data confirmed the presence of IHI. The DFT calculations and structural data revealed that IHI weaken with increasing number of chlorine substituents. In contrast to Cp₂Nb(SiCl₃)₂H where Si–Cl distances are almost equal, for the titanium complexes the Si–Cl bonds are longer in the case of chlorine atoms that lie *trans* to the hydride. The longest Si–Cl bonds are 2.223 Å, 2.192 Å, and 2.161 Å for complexes **Ti1**, **Ti3**, and **Ti4** correspondingly. The other Si–Cl distances are significantly shorter.

The Si–H contacts in **Ti3** and **Ti4** complexes (1.749 Å and 1.75(3) Å respectively) point out the presence of interactions between hydride and silicon atoms. The Ti–H bonds are elongated and are 1.733 Å and 1.72(2) Å for these complexes. The direct Si···H interactions can be seen from the sign of $J(\text{Si–H})$ coupling constant which is negative for these two complexes (–22 Hz and –34 Hz respectively).

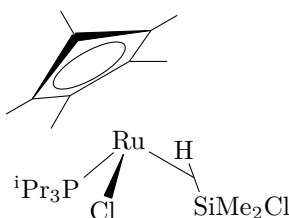


Figure 1.17: The first complex with simultaneous Si–H and RuCl···SiCl IHI.

$\text{Cp}^*(i\text{Pr}_3\text{P})\text{Ru}(\text{Cl})(\eta^2\text{-HSiClMe}_2)^{122}$ (see Figure 1.17) is an unusual example of a complex which is both a silane σ -complex and has simultaneous RuCl···SiCl IHI as it was shown by NMR and X-ray. The presence of Si–H σ -interaction was established by the ^1H NMR spectrum. The $J(\text{Si–H})$ coupling constant is 33.5 Hz pointing out to a σ -interaction. The X-ray structure of the complex showed a short Ru–Si bond of 2.398 Å, which is shorter than that in a classical complex $\text{Cp}^*(\text{PyI}_3\text{P})\text{RuH}_2(\text{SiPhMe}_2)^{135}$ (2.421 Å). The Si···H contact is short as well (2.05(3) Å). The Si–Cl distance is elongated (2.155 Å) compared to R_3SiCl ,¹³⁰ which is typical of IHI. The most remarkable feature of this complex is that the IHI occur between Cl instead of H and Si–Cl. A short Si···Cl contact of 3.014 Å between silyl and chloride ligand from Ru–Cl bond was revealed. Here two Cl atoms are in *trans*-position to each other. This geometric configuration favors a donation from a lone pair of the chlorine bound to ruthenium to the

$\sigma^*(\text{Si}-\text{Cl})$ antibonding orbital, leading to the interligand hypervalent interaction.

1.2.3 Complexes with additional Si...H interactions

Bis(hydrido)-silyl complexes

Among hydrido-silyl complexes special interest is drawn by the bis(hydrido)-silyl complexes $\text{L}_n\text{M}(\text{H})_2(\text{SiR}_3)$ due to their unusual bonding nature and fluxional behavior. The $\text{M}(\eta^3\text{-H}_2\text{SiR}_3)$ motif was firstly suggested for rhenium complex $\text{Re}(\text{PPh}_3)_2\text{H}_6(\text{SiPh}_3)$ ¹³⁶ in 1990 by Luo *et al.* Although the positions of two hydride atoms were not defined by X-ray crystallography, close contacts between silicon and two hydrides were suggested (1.76 Å and 1.92 Å), which imply an H...Si...H interaction.

The first experimental evidence where silyl group interacts with two hydride ligands simultaneously and has a structure with H...Si...H bonding were obtained by Gutsulyak *et al.*¹³⁷ in 2008 and is shown in Figure 1.18. Two of these complexes, **Fe5** and **Fe6**, were studied by NMR spectroscopy and X-ray analysis. The experimental $J(\text{Si}-\text{H})$ coupling constants are around 19.2 Hz and 18.9 Hz, respectively. In the case of complex **Fe6**, using only NMR data, it is impossible to conclude whether there is a fast exchange between two forms of a silane-hydride complex or it is a static structure with double Si...H interactions without any hydride exchange. According to the X-ray structures for complexes **Fe5** and **Fe6** there are double Si...H interactions. This conclusion is based on the following data. The Fe–Si distance in **Fe5** is short (2.194 Å), while in **Fe6** is remarkably short (2.168 Å), compared to that in classical complexes and is very close to the value for the double Fe=Si bond. The Fe–H distances are 1.37(2) Å and 1.43(2) Å in **Fe5** complex. In complex **Fe6** the Fe–H distance is 1.35(3) Å. The Si–H distances for both complexes are longer than

those in a free silane, and are within the range 1.88(3) – 1.91(2) Å. DFT calculations on model complexes $\text{Cp}(\text{Me}_3\text{P})\text{Fe}(\text{H})_2(\text{SiMe}_{3-n}\text{Cl}_n)$ support the idea of two simultaneous $\text{Si}\cdots\text{H}$ interactions as well. Calculated Fe–Si and Si–H distances for $\text{Cp}(\text{Me}_3\text{P})\text{Fe}(\text{H})_2(\text{SiMeCl}_2)$ and $\text{Cp}(\text{Me}_3\text{P})\text{Fe}(\text{H})_2(\text{SiCl}_3)$ complexes are in good agreement with corresponding experimental results. The calculated Fe–H distances are about 0.2 Å longer than experimental values due to the well-known problem of locating H atoms by X-ray. Si–H Mayer bond orders of 0.17 are also indicative of interactions between silicon and hydrogen.

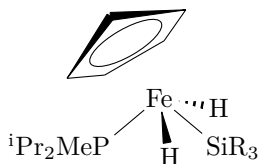


Figure 1.18: The first complexes with simultaneous $\text{H}\cdots\text{Si}\cdots\text{H}$ interactions. $\text{SiR}_3 = \text{SiMe}_2\text{Ph}$ (**Fe1**); SiHMePh (**Fe2**); SiH_2Ph (**Fe3**); SiMe_2Cl (**Fe4**); SiMeCl_2 (**Fe5**); SiCl_3 (**Fe6**).

The effect described above was discovered later in the tungsten complex **W1**¹³⁸ as well (see Figure 1.19). The ^1H NMR shows that this complex has fluxional behavior in which two hydrides rapidly exchange their positions. The measured $J(\text{Si}-\text{H})$ coupling constant is 15.9 Hz, which is lower than the limit of 20 Hz which is used to distinguish between classical and non-classical complexes. However, according to the recent studies, there are more complexes with double $\text{H}\cdots\text{Si}\cdots\text{H}$ interactions where measured $J(\text{Si}-\text{H})$ smaller than 20 Hz. One example is $\text{Cp}(\text{}^i\text{Pr}_2\text{MeP})\text{Fe}(\text{H})_2(\text{SiCl}_3)$ with $J(\text{Si}-\text{H})$ of 18.9 Hz¹³⁷ and another is $\text{Cp}^*(\text{CO})_2\text{W}(\text{H})_2(\text{SiPh}_2\text{Cl})$ with $J(\text{Si}-\text{H})$ equals to 18.3 Hz.¹³⁹ They are suggested to have double $\text{Si}\cdots\text{H}$ interactions based on the X-ray structures. Since, according to Nikonov *et al.*,^{112,137} the observed $J(\text{Si}-\text{H})$ is a sum of negative $^1J(\text{Si}-\text{H})$ and

positive $^2J(\text{Si}-\text{H})$, if the observed $J(\text{Si}-\text{H})$ is small it would be misleading and insufficient to take into account only this constant to categorize complex to one of the two types (see page 20). Although X-ray could not determine the position of two hydride atoms, W–Si distance is in a good agreement with the calculated one in model complex $\text{Cp}(\text{CO})_2\text{W}(\text{H})_2\text{SiH}(\text{OMe})(\text{C}(\text{SiH}_3)_3)$ (2.620 Å *vs* 2.606 Å). The calculated W–H distances in model complex are 1.750 Å and 1.757 Å, and the Wiberg bond indices are 0.501 and 0.474 still considerably large. The Si–H distances are about 25% longer than the normal covalent Si–H bond (1.913 Å and 1.860 Å respectively). The bond indices for them are 0.241 and 0.281 which is about 35% of the Si–H bond index in SiH_4 . All these data along with MO analyses support the idea about two weak $\text{Si}\cdots\text{H}$ bond interactions.

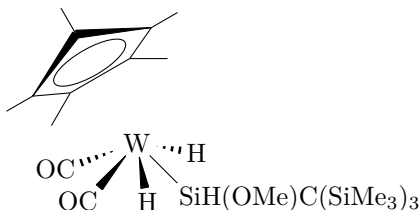


Figure 1.19: The structure of tungsten complex $\text{Cp}^*(\text{CO})_2\text{W}(\text{H})_2\text{SiH}(\text{OMe})(\text{C}(\text{SiMe}_3)_3)$ (**W1**).

Ruthenium complexes $\text{TpRu}(\text{PPh}_3)(\text{H})_2(\text{SiR}_3)^{140}$ (see Figure 1.20) were also shown to have weak $\text{Si}\cdots\text{H}$ interactions. Based on NMR and DFT studies, these complexes were originally formulated as σ -silane-hydride complexes with fast equilibrium between two forms.¹⁴¹ However, according to X-ray study it is more appropriate to describe these complexes as static structures with almost symmetrical $\text{H}\cdots\text{Si}\cdots\text{H}$ bonding. $J(\text{Si}-\text{H})$ experimental values are 28.4 Hz, 25.0 Hz, and 19.2 Hz for **Ru1**, **Ru2**, and **Ru3**, correspondingly, indicating the presence

of non-classical interactions. It must be noted that each of two hydride atoms were located and refined in each structure. The common feature of these complexes is almost symmetrical interaction of silicon with two hydride atoms. In the series of complexes **Ru1–Ru2–Ru3** the Si–H¹ and Si–H² distances are 2.016 Å *vs* 1.928 Å, 1.903 Å *vs* 1.955 Å, and 1.94(2) Å *vs* 1.965 Å respectively. As one can see, all of them are elongated. The Ru–H bond lengths (1.491–1.568 Å) are within the normal range typical of classical ruthenium complexes.

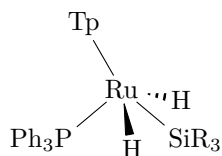


Figure 1.20: The structure of ruthenium complexes. SiR₃ = SiPh₃ (**Ru1**); SiPh₂Me (**Ru2**); SiPhMe₂ (**Ru3**).

It is worth noting that some indication of an H···Si···H motif in a ruthenium complex had been presented as early as in 1999.¹⁰⁰ The distances between silicon and two hydride atoms are almost symmetrical in the complex Ru(H)₂(H₂)(HSiPh₃)(PCy₃)₂ as X-ray study shows. Their values 1.72(3) Å and 1.83(3) Å allow further Si···H interactions. However, the complex was formulated as that rather containing σ-silane moiety than H···Si···H motif.

Hydrido-bis(silyl) complexes

The interactions similar to those in H···Si···H systems occur in hydrido-bis(silyl) complexes. As an example, some iron complexes can be consistent with this description (see Figure 1.21). According to the X-ray data, for **Fe7**¹⁴² the Si–H distance was found to be 2.06(7) Å, which is indicative of a Si–H contact. It was shown that Si–Fe–Si bond

angle is small ($113.9(1)^\circ$). Another hydrido-bis(silyl) iron complex is **Fe8**.^{121,143} The X-ray data are available for it as well although the position of a hydride was not determined. In this complex the Si–Fe–Si bond angle of $115.3(1)^\circ$ is very close to that in **Fe7**. There is no large difference in Fe–Si bond distances – 2.252 \AA vs 2.249 \AA for **Fe7** and **Fe8** complexes respectively. This suggests that similar Si–H contact may exist in the latter. Taking these short Si–H distances into account one can conclude the presence of weak Si \cdots H interactions and so the presence of entire $\text{R}_3\text{Si}\cdots\text{H}\cdots\text{SiR}_3$ ligand. Complex **Fe8** exhibits $J(\text{Si–H})$, determined from Si satellites,¹⁴⁴ of 20 Hz.

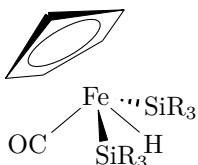


Figure 1.21: Iron complexes with suggested simultaneous Si \cdots H \cdots Si interactions. $\text{SiR}_3 = \text{SiF}_2\text{Me}$ (**Fe7**); SiCl_3 (**Fe8**).

Complexes with Si \cdots H \cdots Si pattern can exhibit fluxional behavior as well. Two examples of such complexes with fluxionality are $[\text{Cp}^*\text{Rh}(\text{PMe}_3)(\text{SiR}_3)(\text{HSiR}_3)]\text{BAr}_4$ ¹¹⁷ (see Figure 1.22) where R = Me or Et and Ar = 3,5- $\text{C}_6\text{H}_3(\text{CF}_3)_2$. For both complexes hydride resonance shows ^{29}Si satellites in ^1H NMR spectra and the $J(\text{Si–H})$ coupling constants are 28.5 Hz and 27.8 Hz, respectively, which supports the assignment of these complexes as silyl- η^2 -silane complexes. A single resonance for the SiMe_3 groups in ^1H NMR spectra is in agreement with its fluxional nature.

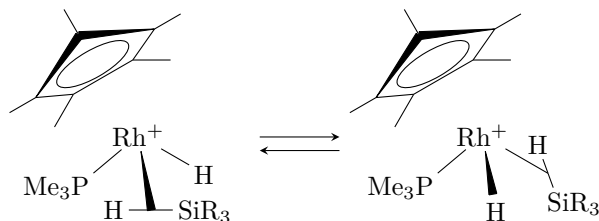


Figure 1.22: Hydrogen fluxionality in a rhodium hydrido-bis(silyl) complexes. $\text{SiR}_3 = \text{SiMe}_3$ (**Rh1**); SiEt_3 (**Rh2**).

1.2.4 Potential energy surface in organometallic complexes with two silyl and one hydride ligands

When an Si–H interaction is possible, two silicons can compete for it, giving rise to a silyl-silane complex, in which case interconversion between two forms can take place (Figure 1.23b) and the PES for hydrogen transfer has two minima. In this case the vibrational wavefunction can have either one or two maxima (Figure 1.6b). If the barrier is low enough to ensure an interconversion rapid on the NMR timescale, the situation is referred to as hydrogen fluxionality. The rhodium complexes $[\text{Cp}^* \text{Rh}(\text{PMe}_3)(\text{SiR}_3)(\text{HSiR}_3)]\text{BAr}_4$ ¹¹⁷ ($\text{R} = \text{Me}$ or Et , $\text{Ar} = 3,5\text{-C}_6\text{H}_3(\text{CF}_3)_2$) are examples of such fluxionality. For both complexes hydride resonance shows ²⁹Si satellites in ¹H NMR spectra and the $J(\text{Si-H})$ coupling constants are 28.5 Hz and 27.8 Hz respectively, which supports the assignment of these complexes as $\eta^1\text{-silyl-}\eta^2\text{-silane}$ complexes. The observation in ¹H NMR spectra of a single resonance for the SiMe_3 groups is in agreement with this fluxional nature of the complex. On the other hand, the hydrogen can interact with both silicon atoms *simultaneously* but be located closer to one of them (Figure 1.23c), with the entire $\text{R}_3\text{Si}\cdots\text{H}\cdots\text{SiR}'_3$ moiety behaving

as a single ligand.^{114,121,122} The PES is of double-well character as well, with a small barrier (Figure 1.6c). In this case the vibrational wavefunction has a single maximum above transition state. In the extreme case, the barrier may vanish at all, giving rise to a single-well PES and a vibrational wavefunction with a single maximum (Figure 1.6a). The experimentally found structure of certain iron complexes such as $\text{CpFe}(\text{CO})(\text{SiF}_2\text{Me})_2(\text{H})$ ¹⁴² and $\text{CpFe}(\text{CO})(\text{SiCl}_3)_2(\text{H})$ ¹⁴³ is consistent with this description. A more recent computational study¹²¹ by Vyboishchikov and Nikonov also supports the symmetric configuration of $\text{CpFe}(\text{CO})(\text{SiR}_3)_2(\text{H})$ complexes with weak $\text{Si}\cdots\text{H}\cdots\text{Si}$ interactions.

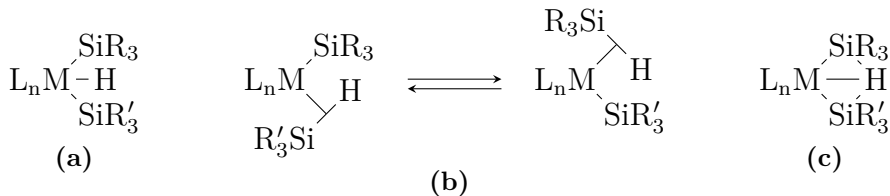


Figure 1.23: Bonding patterns in transition metal complexes with two silyl and one hydride ligands. a) Pure bis(silyl)-hydride complex. c) Dynamic equilibrium in a silyl-silane complex. b) Complex with simultaneous $\text{Si}\cdots\text{H}\cdots\text{Si}$ interactions.

In general, it is not always easy to distinguish between the fluctational behavior and the simultaneous triple $\text{Si}\cdots\text{H}\cdots\text{Si}$ interactions. Therefore, a static description of such complexes may be inadequate and quantum-chemical calculations are necessary to shed light on the situation.

1.3 Organocobalt(V) complexes

Organometallic complexes of transition metals in high oxidation states are of interest since they could play role as intermediates in vari-

ous cross-coupling, alkane oxidation, and alkene hydrosilylation reactions.¹⁴⁵⁻¹⁴⁸ A high oxidation state can be more readily achieved for *4d* and *5d* transition metal complexes.^{108,149,150} Quite a few rhodium(V)^{116,151-153} and iridium(V)¹⁵⁴⁻¹⁵⁷ complexes were reported, while organocobalt complexes in high oxidation states were unknown until Bower and Tennent obtained the first cobalt(IV) complex.¹⁵⁸ Several cobalt(IV) complexes were obtained since.¹⁵⁹⁻¹⁶⁴ Later, Byrne and Theopold reported the isolation of a cobalt(V) complex.^{159,160} For *3d* transition metals, high oxidation states were considered to play a role as intermediates in olefin hydrosilylation and cyclometallation reactions,¹⁶⁵⁻¹⁶⁷ but isolated examples are still rare.¹⁶⁸⁻¹⁷⁰ The principal difficulty is that only a small variety of organic ligands can bind to a strongly electron-withdrawing metal center in a high oxidation state. The compatibility depends mainly on the ligand ability to alleviate a large positive charge of the metal.¹⁶² Alkyl ligands are known to be among the strongest σ -donors and can stabilize a high oxidation state of a metal, e.g. in $\text{Co}(1\text{-norbornyl})_4$,^{159,160} $[\text{Co}(1\text{-norbornyl})_4]\text{BF}_4$,^{159,160} Cp^*IrMe_4 .^{155,171} Hydride and silyl complexes in high oxidation states are also known. Examples among *4d* and *5d* transition metal complexes are $(\text{C}_6\text{Me}_6)\text{Ru}(\text{H})_2(\text{SiMe}_3)_2$,¹⁷² $\text{Cp}^*\text{Ir}(\text{H})_2(\text{SiR}_3)_2$,¹⁵⁶ $\text{Cp}^*\text{Rh}(\text{H})_2(\text{SiR}_3)_2$,¹⁵³ $\text{Cp}^*\text{Ir}(\text{H})_3(\text{SiR}_3)$ ¹⁷³ as well as $\text{Cp}^*\text{Ir}(\text{H})_4$.¹⁵⁴ Although *3d* transition metals are less inclined to form complexes in high oxidation states, some examples such as iron hydride-silyl complex $(\eta^6\text{-PhMe})\text{Fe}(\text{H})_2(\text{SiHCl}_2)_2$ ¹⁷⁴ and those of cobalt $\text{Cp}^*\text{Co}(\text{H})_2(\text{SiPh}_2\text{H})_2$ ¹⁶⁸ were reported.

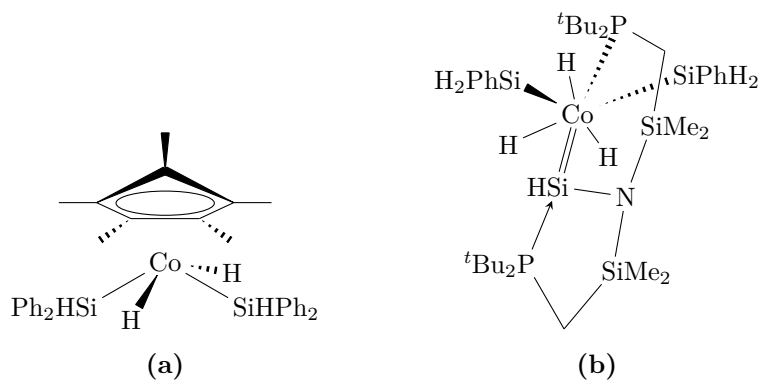


Figure 1.24: Rare examples of organocobalt(V) complexes.

Chapter 2

Methods

Since advent of modern quantum chemistry till now there has been a giant leap in theoretical methods. At present, electron structure theory can treat not only small molecules with a very high accuracy, but also large molecules with an adequate accuracy. The motion of nuclei is also of importance. This fact led to development of various methods of solving vibrational problem.

Various of the electronic structure theory methods, such as DFT, MP2, and CCSD, were used in this thesis. Since these methods have been developed by other workers and essentially are employed by us as they are, they will not be discussed in details.

In this thesis we deal with vibrational methods and are more interested in systems that characterized by anharmonic vibrational motion. Thus, in this Chapter we give an overview of existing methods for solving the vibrational problem. The methods developed by us will be given in the Results and Discussion section (Chapter 4).

This chapter overviews, firstly, ways of representation of one- and N -dimensional PES which is important for solving the vibrational problem. Then, an overview of key vibrational methods is given. Subsequently, the Numerov method, which also used to solve Schrödinger

equation, is given. Finally, a widely used one-dimensional distributed Gaussians method, is explained.

2.1 Potential energy surface representation

Usually, the PES is obtained point by point by a series of quantum-chemical calculations. Nevertheless, in many cases it is possible to approximate it by a simple analytical formula.

2.1.1 Model potential for one-dimensional hydrogen transfer

The simplest description for hydrogen transfer is a one-dimensional model of a potential, and the simplest polynomial for symmetric double-well potential is given by a square-quadratic expression:¹⁷⁵

$$V^{(1)}(X) = -\frac{1}{2}aX^2 + \frac{1}{4}cX^4. \quad (2.1)$$

This equation contains only a *large*-amplitude (A–H) hydrogen bond coordinate X . Two minima are determined by the constants a and c as $X_{min} = \pm\sqrt{\frac{a}{c}}$ and the barrier height is $\Delta E = \frac{a^2}{4c}$. There is a saddle point, i.e. a transition state at $X = 0$. If one needs to model the *small*-amplitude (A \cdots B) vibration along the mass-weighted normal coordinate Q , a harmonic oscillator PES is used with Ω being the frequency of oscillator:

$$V^{(1)}(Q) = \frac{1}{2}\Omega^2Q^2. \quad (2.2)$$

2.1.2 Model potential for two-dimensional hydrogen transfer

Of course, a better description is possible if a coupling between large-amplitude and small-amplitude vibrations is taken into account. If this is considered, the hydrogen motion dynamics is described by the following Hamiltonian:¹⁷⁵

$$\hat{H} = \frac{P_X^2}{2} + \frac{P_Q^2}{2} + V(X, Q), \quad (2.3)$$

where the PES is represented as follows:

$$V(X, Q) = V^{(1)}(X) + V^{(1)}(Q) + V^{(2)}(X, Q). \quad (2.4)$$

Here the $V^{(2)}(X, Q)$ term represents the coupling between. The large-amplitude coordinate X is symmetric but the small amplitude coordinate Q can be either symmetric or anti-symmetric. Consequently, if there is a minimum at (X_0, Q_0) there must be an equivalent minimum at either $(-X_0, Q_0)$ or at $(-X_0, -Q_0)$.

Usually one can distinguish among three cases: *symmetric mode coupling*, *asymmetric mode coupling*, and *squeezed coupling*. It depends on the expression for the coupling term $V^{(2)}(X, Q)$.

The *Symmetric mode coupling*^{175,176} is characterized by the coupling term of the form:

$$V^{(2)}(X, Q) = \lambda X^2 Q. \quad (2.5)$$

In this equation λ is the coupling constant and Q is an even function of X . The symmetric mode coupling potential V_{SMC} can be written as:

$$V_{SMC} = -\frac{1}{2}aX^2 + \frac{1}{4}\tilde{c}X^4 + \frac{1}{2}\Omega^2 \left(Q + \frac{\lambda}{\Omega^2} X^2 \right)^2, \quad (2.6)$$

where

$$\tilde{c} = c - 2\lambda \text{ is a new constant,} \quad (2.7)$$

$$Q^{(0)} = -\frac{\lambda}{\Omega^2} X^2 \text{ is oscillator displacement.} \quad (2.8)$$

The saddle point has coordinates $(0, 0)$ and the two minima are at $(\pm\sqrt{\frac{a}{\tilde{c}}}, -\frac{\lambda a}{\tilde{c}\Omega^2})$, then the barrier height is $\Delta E = \frac{a^2}{4\tilde{c}}$. As one can see, the symmetric mode coupling Hamiltonian depends on four parameters a, c, Ω, λ . The set of these parameters can be reduced without loss of generality. To do this, dimensionless positions (\tilde{x}, \tilde{q}) have to be introduced:^{175,176}

$$X = x_m \tilde{x}, \quad (2.9)$$

$$Q = x_m \tilde{q}, \quad (2.10)$$

where x_m is the minimum position of x , i.e. $\pm\sqrt{\frac{a}{\tilde{c}}}$. The new symmetric mode coupling Hamiltonian \tilde{H}_{SMC} can be obtained by dividing the old one by $\frac{2a^2}{\tilde{c}}$:

$$\begin{aligned} \tilde{H}_{SMC} = & -\frac{g^2}{2} \left(\frac{\partial^2}{\partial \tilde{x}^2} + \frac{\partial^2}{\partial \tilde{q}^2} \right) + \frac{1}{8} (\tilde{x} + 1)^2 (\tilde{x} - 1)^2 + \\ & + \frac{\omega^2}{2} \left(\tilde{q} + \frac{\gamma}{\omega^2} (\tilde{x}^2 - 1) \right)^2, \end{aligned} \quad (2.11)$$

Now our new parameters are as follows:

$$g = \frac{\hbar \tilde{c}}{a\sqrt{2a}} = \frac{\hbar \Omega_x}{8\Delta E}, \quad (2.12)$$

$$\omega = \frac{\Omega}{\sqrt{2a}} = \frac{\Omega}{\Omega_x}, \quad (2.13)$$

$$\gamma = \frac{\lambda}{2\sqrt{a\tilde{c}}}, \quad (2.14)$$

where Ω_x is the harmonic frequency corresponding to the minima of the original symmetric mode coupling Hamiltonian. As one can see, now the new Hamiltonian depends on three parameters.

In the case of the *asymmetric mode coupling*^{175,176} the coupling term $V^{(2)}(X, Q)$ is represented by an odd function with respect to the X coordinate:

$$V^{(2)}(X, Q) = \lambda X Q. \quad (2.15)$$

The saddle point in has coordinates $(0, 0)$ and the two minima are at $\left(\pm\sqrt{\frac{a}{c} + \frac{\lambda^2}{c\Omega^2}}, -\frac{\lambda X_{min}}{\Omega^2}\right)$.

The case of *squeezed coupling*^{175,176} can be expressed by the following equation for the coupling term:

$$V^{(2)}(X, Q) = \lambda X^2 Q^2. \quad (2.16)$$

The coordinates of the saddle point and of the two minima are $(0, 0)$ and $(\pm\sqrt{\frac{a}{c}}, 0)$, respectively. In this case the PES can be expressed as an oscillator where the frequency depends on X :

$$V_{SQZ} = -\frac{1}{2}aX^2 + \frac{1}{4}cX^4 + \frac{1}{2}\omega^2(X)Q^2, \quad (2.17)$$

$$\omega(X) = \sqrt{\Omega^2 + 2\lambda X^2}. \quad (2.18)$$

If the $\lambda > 0$ the mode is weakened upon approaching the saddle point. This type of coupling occurs in out-of-plane modes.¹⁷⁷

Other model potentials capable of describing coupling were proposed in literature.¹⁷⁸⁻¹⁸⁰

2.1.3 Model potential for N -dimensional hydrogen transfer

The computational effort to calculate the full PES increases rapidly with increasing number of degree of freedoms. Since any function can

be divided into uncorrelated and correlated parts, to reduce the PES it is possible to expand it with respect of such correlations^{175,181} up to some level (n -mode coupling representation of the PES):

$$V(\mathbf{Q}) = \sum_{i=1}^N V^{(1)}(Q_i) + \sum_{i<j}^N V^{(2)}(Q_i, Q_j) + \sum_{i<j<k}^N V^{(3)}(Q_i, Q_j, Q_k) + \dots, \quad (2.19)$$

where $N = 3N_{at} - 6$ is the number of degrees of freedom, N_{at} is the number of atoms in a system, Q_i are vibrational normal modes, $V^{(n)}$ are n -mode correlation potentials which describe n -mode coupling, $\mathbf{Q} = (Q_1, \dots, Q_N)$ is the vector of normal coordinates.

The above expression (see Equation 2.19) can be rewritten as Taylor expansion about the equilibrium structure:

$$V(\mathbf{Q}) = V_0 + \frac{1}{2!} \sum_{i=1}^N h_i Q_i^2 + \frac{1}{3!} \sum_{i,j,k}^N t_{ijk} Q_i Q_j Q_k + \frac{1}{4!} \sum_{i,j,k,l}^N u_{ijkl} Q_i Q_j Q_k Q_l + \dots \quad (2.20)$$

Here V_0 , h_i , t_{ij} , u_{ijk} are potential energy at minimum, its second, third, and fourth derivatives respectively in terms of normal coordinates. The explicit expressions for the third and the fourth terms are:

$$\sum_{i,j,k}^N t_{ijk} Q_i Q_j Q_k = \sum_{i=1}^N t_{iii} Q_i^3 + \sum_{i \neq j}^N t_{iij} Q_i^2 Q_j + \sum_{i<j<k}^N t_{ijk} Q_i Q_j Q_k, \quad (2.21)$$

$$\begin{aligned} \sum_{i,j,k,l}^N u_{ijkl} Q_i Q_j Q_k Q_l &= \sum_{i=1}^N u_{iiii} Q_i^4 + \sum_{i \neq j}^N u_{iiij} Q_i^3 Q_j + \sum_{i \neq j < k}^N u_{iijk} Q_i^2 Q_j Q_k + \\ &+ \sum_{i < j < k < l}^N u_{ijkl} Q_i Q_j Q_k Q_l + \sum_{i < j}^N u_{iijj} Q_i^2 Q_j^2. \end{aligned} \quad (2.22)$$

These terms now can be regrouped into such with one mode, two different modes, three different modes, etc. Upon regrouping one obtains:

$$V^{1MR} = V_0 + \sum_{i=1}^N \left(\frac{1}{2!} h_i Q_i^2 + \frac{1}{3!} t_{iii} Q_i^3 + \frac{1}{4!} u_{iiii} Q_i^4 \right), \quad (2.23)$$

$$V^{2MR} = \sum_{i \neq j}^N \left(\frac{1}{3!} t_{ijj} Q_i^2 Q_j + \frac{1}{4!} u_{ijjj} Q_i^3 Q_j \right) + \frac{1}{4!} \sum_{i < j}^N u_{ijjj} Q_i^2 Q_j^2, \quad (2.24)$$

$$V^{3MR} = \frac{1}{3!} \sum_{i < j < k}^N t_{ijk} Q_i Q_j Q_k + \frac{1}{4!} \sum_{i \neq j < k}^N u_{ijjk} Q_i^2 Q_j Q_k, \quad (2.25)$$

$$V^{4MR} = \frac{1}{4!} \sum_{i < j < k < l}^N u_{ijkl} Q_i Q_j Q_k Q_l. \quad (2.26)$$

Here V^{1MR} , V^{2MR} , V^{3MR} , and V^{4MR} are one-, two-, three-, and four-mode representations of potential. If we consider our potential as Taylor polynomial of degree not higher than four (neglecting of higher-order terms), the representation of the PES will be as follows:

$$V(\mathbf{Q}) \approx V(Q_1, \dots, Q_4) = V^{1MR} + V^{2MR} + V^{3MR} + V^{4MR}. \quad (2.27)$$

This representation of the PES is called *quartic force field*. Its three-mode representation, i.e. without V^{4MR} term, referred to as 3MR-QFF is very promising.^{182–185}

Another possibility is to use *modified Shepard interpolation*.^{186–188} The following equation defines a configuration \mathbf{Q} of an N_{at} -atom molecule in a normal coordinate representation:

$$\mathbf{X} = \mathbf{X}_{\text{eq}} + \sum_{i=1}^N Q_i \mathbf{L}_i, \quad (2.28)$$

where \mathbf{X} and \mathbf{X}_{eq} are $3N_{at}$ mass-weighted Cartesian coordinates for current and equilibrium configurations respectively, and \mathbf{L}_i is the i th

normal mode vector. The potential energy V^{MSI} , in the terms of modified Shepard interpolation, can be expressed as:^{186,189,190}

$$V^{MSI}(\mathbf{Q}) = \sum_{m=1}^{N_R} W_m(\mathbf{Q}) V_m(\mathbf{Q}). \quad (2.29)$$

Here N_R is a number of reference points, $W_m(\mathbf{Q})$ is a normalized weight function for the m th reference point, and $V_m(\mathbf{Q})$ is a Taylor expansion of the potential about this point:

$$\begin{aligned} V^{(m)}(\mathbf{Q}) = & V_0^{(m)} + \sum_{i=1}^N g_i^{(m)} (Q_i - Q_i^{(m)}) + \\ & + \frac{1}{2} \sum_{i,j}^N h_{ij}^{(m)} (Q_i - Q_i^{(m)}) (Q_j - Q_j^{(m)}) + \dots \end{aligned} \quad (2.30)$$

The weight function has the form:

$$W_m(\mathbf{Q}) = \frac{w_m(\mathbf{Q})}{\sum_{k=1}^{N_R} w_k(\mathbf{Q})}, \quad (2.31)$$

$$w_m(\mathbf{Q}) = \left\{ \sum_{i=1}^N (Q_i - Q_i^{(m)})^2 \right\}^{-p}, \quad (2.32)$$

where $Q_i^{(m)}$ are coordinates of the m th reference point, and p is a parameter. It was shown that if the Taylor series $V_m(\mathbf{Q})$ extends to the n th order then the derivatives of $V^{MSI}(\mathbf{Q})$ at reference point are interpolated correctly if $p > n$.¹⁸⁶ According to the Equation 2.32, the closer reference point to the current configuration is, the larger weight is assigned to that reference point. Distant points contribute negligibly. If this reference point is placed at a minimum, the first-order energy derivatives $g_i^{(1)}$ are zero, and the second-order energy derivatives become $h_{ij}^{(1)} = h_{ij}^{(1)} \delta_{ij}$. Thus, only diagonal terms remain. In this case the MSI-PES coincides with QFF.

2.2 Vibrational SCF

The vibrational Hamiltonian for an N -mode non-rotating molecule in terms of normal coordinates is:¹⁹¹

$$\hat{H} = -\frac{1}{2} \sum_{i=1}^N \frac{\partial^2}{\partial Q_i^2} + \hat{V}(\mathbf{Q}). \quad (2.33)$$

In the VSCF theory the full vibrational wavefunction $\Psi_{\mathbf{p}}(\mathbf{Q})$ is represented as a product of one-mode wavefunctions *modals* $\phi_{p_i}^{(i)}(Q_i)$.¹⁹² Contrary to the electronic structure theory the antisymmetrization is unnecessary because the vibrational modes are distinguishable unlike the electrons:¹⁹³

$$\Psi_{\mathbf{p}}(\mathbf{Q}) = \prod_{i=1}^N \phi_{p_i}^{(i)}(Q_i), \quad (2.34)$$

where $\mathbf{p} = (p_1, \dots, p_f)$ specify vibrational state of a molecule. The modals can be obtained by solving the following VSCF equation:

$$\left[-\frac{1}{2} \frac{\partial^2}{\partial Q_i^2} + \bar{V}_i \right] \phi_{p_i}^{(i)} = \varepsilon_{p_i}^{(i)} \phi_{p_i}^{(i)}. \quad (2.35)$$

\bar{V}_i is an effective mean-field potential in which i th mode vibrates:

$$\bar{V}_i = \left\langle \prod_{j \neq i}^N \phi_{p_j}^{(j)} \right| \hat{V} \left| \prod_{j \neq i}^N \phi_{p_j}^{(j)} \right\rangle. \quad (2.36)$$

It can be obtained by integrating the PES over all modals except i th one. This pose a condition that Equation 2.35 has to be solved until self-consistency is achieved.

As an example let us consider a two-mode system to simplify the derivation. Within the VSCF method, the minimum of the energy functional $\langle \Psi_{l,m} | \hat{H} | \Psi_{l,m} \rangle$ is searched in the space of all possible Hartree products of single-coordinate functions:^{193,194}

$$\Psi_{l,m}(Q_1, Q_2) = \varphi_l(Q_1) \phi_m(Q_2), \quad (2.37)$$

where Q_1, Q_2 are the normal coordinates, and $\varphi_l(Q_1), \phi_m(Q_2)$ are the modal functions. Then, the Hamiltonian is:

$$\hat{H} = h_1 + h_2 + V_c(Q_1, Q_2), \quad (2.38)$$

h_i is a single-mode Hamiltonian:

$$h_i = T_i + V_i(Q_i) = -\frac{1}{2} \frac{\partial^2}{\partial Q_i^2} + V_i(Q_i). \quad (2.39)$$

The full potential is:

$$V(Q_1, Q_2) = V_1(Q_1) + V_2(Q_2) + V_c(Q_1, Q_2), \quad (2.40)$$

and $V_c(Q_1, Q_2)$ explicitly involves the coupling between modes. Modals satisfy equations from the variational procedure are as follows:

$$[h_1 + \langle \phi_m(Q_2) | V_c(Q_1, Q_2) | \phi_m(Q_2) \rangle_2 - \varepsilon_l] \varphi_l(Q_1) = 0, \quad (2.41)$$

$$[h_2 + \langle \varphi_l(Q_1) | V_c(Q_1, Q_2) | \varphi_l(Q_1) \rangle_1 - \varepsilon_m] \phi_m(Q_2) = 0. \quad (2.42)$$

In $\langle \phi_m(Q_2) | V_c(Q_1, Q_2) | \phi_m(Q_2) \rangle_2$ the integration is done over one coordinate Q_2 . Thus, determining so-called effective potentials:

$$V_m(Q_1) = V_1(Q_1) + \langle \phi_m(Q_2) | V_c(Q_1, Q_2) | \phi_m(Q_2) \rangle, \quad (2.43)$$

$$V_l(Q_2) = V_2(Q_2) + \langle \varphi_l(Q_1) | V_c(Q_1, Q_2) | \varphi_l(Q_1) \rangle, \quad (2.44)$$

and rewriting equations 2.43 and 2.44 in terms of these potentials one obtains next equations:

$$[T_1 + V_m(Q_1) - \varepsilon_l] \varphi_l(Q_1) = 0, \quad (2.45)$$

$$[T_2 + V_l(Q_2) - \varepsilon_m] \phi_m(Q_2) = 0. \quad (2.46)$$

Thus, Equations 2.45 and 2.46 are one-dimensional eigenvalue equations with corresponding energy eigenvalues ε_l , and ε_m . Nevertheless,

the effective potential for any of them is affected by the modal eigenfunction of the other eigenvalue equation. Hence, these equations are coupled and have to be solved using an iterative procedure.

To evaluate the effective potentials in Equations 2.45 and 2.46, a zero-order set of modal wavefunctions $\varphi_l^0(Q_1)$ and $\phi_m^0(Q_2)$ is used. The eigenvalue equations are solved, as a result new modal eigenfunctions and eigenvalues are obtained. These eigenfunctions are used to calculate new effective potentials. The latter are used to obtain new modal eigenfunctions and eigenvalues. Since this process is iterative, the iterations will continue until modal wavefunctions used to obtain the effective potentials are the same as the ones calculated by solving the eigenvalue equations using those potentials. In practice the zeroth-order modal wavefunctions $\varphi_l^0(Q_1)$ and $\phi_m^0(Q_2)$ are the eigenfunctions of Hamiltonians h_i or the normal-mode-harmonic-oscillator wavefunctions. Expanding the modals in a convenient basis:

$$\varphi_l^0(Q_1) = \sum_j \chi_j(Q_1) c_{jl}, \quad (2.47)$$

where χ_j are the normal mode eigenfunctions. To obtain the expansion coefficients one has to solve coupled equations which are similar to the Roothaan-Hall equations in the electronic structure theory.¹⁹⁵ The total VSCF energy for the $\Psi_{l,m}(Q_1, Q_2)$ state is expressed by the following equation:

$$\begin{aligned} E_{l,m} &= \left\langle \varphi_l(Q_1) \phi_m(Q_2) \left| \hat{H} \right| \varphi_l(Q_1) \phi_m(Q_2) \right\rangle = \\ &= \varepsilon_l + \varepsilon_m - \langle \varphi_l(Q_1) \phi_m(Q_2) | V_c(Q_1, Q_2) | \varphi_l(Q_1) \phi_m(Q_2) \rangle. \end{aligned} \quad (2.48)$$

For the N -dimensional case the total vibrational energy can be found by eigenvalues summation for each of single mode equations with subsequently subtracting terms that enter more than once into summation:¹⁹⁶

$$E = \sum_{i=1}^N \varepsilon_i - (N-1) \left\langle \prod_{i=1}^N \varphi_i(Q_i) | V_c(\mathbf{Q}) | \prod_{i=1}^N \varphi_i(Q_i) \right\rangle, \quad (2.49)$$

where N is the number of normal coordinates.

The VSCF method is applied to polyatomic systems to determine accurate IR transition energies.^{197,198} It is useful for studying large systems such as proteins¹⁹⁹ or monosaccharides,²⁰⁰ also useful to study weakly bound highly anharmonic systems where coupling between modes plays an important role, such as XeHe₂,²⁰¹ I₂He,²⁰¹ Ar₃,²⁰² Ar₁₃.²⁰³

Although VSCF gives a substantial improvement over the harmonic description and brings calculated frequencies into much closer agreement with experiment, further improvement can be reached by introducing correlation effects among modes that are not present in VSCF.

2.3 Vibrational MP2

For treating the correlations among modes, vibrational MP theory has been suggested.^{191,196,204}

As mentioned, the total VSCF energy is calculated according to the Equation 2.49. The perturbation can be defined as:

$$\Delta V = \hat{H} - \hat{H}_0, \quad (2.50)$$

or more explicit as a full Hamiltonian \hat{H} minus the sum of the single mode SCF Hamiltonians $h_i^{SCF}(Q_i)$ ^{197,198,203} (see Equation 2.39):

$$\begin{aligned} \Delta V(\mathbf{Q}) &= \hat{H} - \sum_{i=1}^N h_i^{SCF}(Q_i) = \\ &= V(\mathbf{Q}) - \sum_{i=1}^N \bar{V}_i(Q_i). \end{aligned} \quad (2.51)$$

Using Rayleigh-Schrödinger expressions for the first-, the second-, and

the third-order perturbation energy corrections one can obtain:¹⁹⁶

$$E_k^{(1)} = \langle \Psi_k | \Delta V | \Psi_k \rangle, \quad (2.52)$$

$$E_k^{(2)} = \sum_{n \neq k} \frac{|\langle \Psi_k | \Delta V | \Psi_n \rangle|^2}{E_k^{(0)} - E_n^{(0)}}, \quad (2.53)$$

$$E_k^{(3)} = \sum_{n \neq k} \left[\sum_{m \neq n \neq k} \frac{\langle \Psi_k | \Delta V | \Psi_n \rangle \langle \Psi_n | \Delta V | \Psi_m \rangle \langle \Psi_m | \Delta V | \Psi_k \rangle}{(E_k^{(0)} - E_n^{(0)})(E_k^{(0)} - E_m^{(0)})} \right] - E_k^{(1)} \sum_{n \neq k} \frac{|\langle \Psi_k | \Delta V | \Psi_n \rangle|^2}{(E_k^{(0)} - E_n^{(0)})^2}, \quad (2.54)$$

where Ψ_k , Ψ_n , and Ψ_m are entire product wavefunction, as defined by Equation 2.34, of the reference state and the excited states n , m . Corresponding energies $E_k^{(0)}$, $E_n^{(0)}$, and $E_m^{(0)}$ are the sums of the single mode energies in the reference state and the excited virtual states.

Like in the electronic structure theory, the zeroth-order energy is defined as:

$$E_k^{(0)} = \langle \Psi_k | \hat{H}_0 | \Psi_k \rangle. \quad (2.55)$$

The sum of the zeroth- and first-order energies gives the VSCF energy:

$$E_k^{(0)} + E_k^{(1)} = \langle \Psi_k | \hat{H}_0 + \Delta V | \Psi_k \rangle = E_k^{VSCF}. \quad (2.56)$$

Thus, the real correction to the VSCF energy happens starting from the second order:¹⁹²

$$E_k^{VSCF} + E_k^{(2)} = E_k^{VMP2}. \quad (2.57)$$

In some applications of VMP2 only coupling between pair of modes was included in a potential^{197,198,203,205} while neglecting interactions with direct three- or higher-mode coupling. With this approximation one needs only one-dimensional integrals to calculate effective mean-field potential (see Equation 2.36) and only two-dimensional integrals

for VSCF (see Equation 2.49) and correlation-corrected (see Equation 2.53) energies. This approximation, nevertheless, works with very good accuracy even in the case of highly anharmonic clusters such as $(\text{H}_2\text{O})_n$,²⁰⁵ $\text{Cl}^-(\text{H}_2\text{O})_n$,¹⁹⁸ $\text{H}_2\text{O}-\text{CH}_3\text{OH}$.¹⁹⁸

For low-lying non-degenerate vibrational states the perturbation theory exhibits rapid and effective convergence. The second-order method is highly accurate for low-lying vibrational states, but less so for highly-excited states.^{196,204}

2.4 Vibrational Coupled Clusters

Vibrational CC^{191,206} is an example of another method where correlation between vibrational modes are treated. The inherent feature of coupled clusters methods is the exponential wavefunction ansatz which in the case of VCC is:

$$|VCC\rangle = \exp(\hat{T}) |\Psi_{\mathbf{p}}\rangle, \quad (2.58)$$

where \hat{T} is the cluster operator, $\Psi_{\mathbf{p}}$ is the reference VSCF Hartree product for the state of interest, and $\mathbf{p} = (p_1, \dots, p_N)$ is a vector that specifies the excitation level of each mode.

Within the second-quantization formalism²⁰⁷ $\Psi_{\mathbf{p}}$ can be represented as follows:

$$|\Psi_{\mathbf{p}}\rangle = \prod_{i=1}^N a_{p_i}^{i\dagger} |vac\rangle, \quad (2.59)$$

where the creation operator $a_{p_i}^{i\dagger}$ creates an excitation in mode i . $|vac\rangle$ is the vacuum state.

The cluster operator \hat{T} contains the sum over excitations and in general can be represented as follows:

$$\hat{T} = \sum_{\mu} t_{\mu} \tau_{\mu}, \quad (2.60)$$

were t_μ are the cluster amplitudes, τ_μ are the excitation operators, corresponding to the μ th excitation. It can be rewritten in more detailed way as follows:²⁰⁶

$$\hat{T} = \hat{T}_1 + \hat{T}_2 + \hat{T}_3 + \cdots = \sum_{i=1}^N \sum_{\mu_i} t_{\mu_i} \tau_{\mu_i}, \quad (2.61)$$

where \hat{T}_1 contains all one-mode excitations, \hat{T}_2 contains all two-mode excitations and so on, i being the level of excitation. The cluster operator is usually truncated in order to limit the number of possible excitations.²⁰⁸

To obtain the VCC energy one has to insert Equation 2.58 into the time-independent Schrödinger equation and project it with reference state:

$$\begin{aligned} E_{VCC} &= \langle \Psi_{\mathbf{p}} | \exp(-\hat{T}) H \exp(\hat{T}) | \Psi_{\mathbf{p}} \rangle = \\ &= \langle \Psi_{\mathbf{p}} | H \exp(\hat{T}) | \Psi_{\mathbf{p}} \rangle. \end{aligned} \quad (2.62)$$

However, the most important task is to calculate the error vector e_μ which can be obtained in similar way by projecting with excited states instead of reference $|\mu\rangle = \tau_\mu |\Psi_{\mathbf{p}}\rangle$:

$$e_\mu = \langle \mu | \exp(-\hat{T}) H \exp(\hat{T}) | \Psi_{\mathbf{p}} \rangle = 0. \quad (2.63)$$

This set of equations has to be solved iteratively for amplitudes to be obtained. Iterations are based on the evaluation of the error vector. A new trial vector is generated until old one is less than a certain error norm threshold, and the difference in energy compared to the result of the previous iterations is less than a certain energy difference threshold.

The VCC method is very similar to the coupled-clusters method in the electronic structure theory.^{209,210} However, there are some differences due to Hamiltonian operator and due to distinguishable modes in contrast to indistinguishable electrons.

The energy expression obtained above corresponds to the so-called state-specific VCC. In this approach, equations for both ground and excited states must be solved. These states are calculated independently, whilst the so-called response VCC^{208,211} needs only a ground state to be calculated and excited states are obtained from a linear set of eigenvalue equations which is a simpler procedure. Using this method gives the potential of providing molecular properties in ground and excited states. Some calculations on small molecules show that the results of response VCC are almost identical or better to those of state-specific VCC, but, contrarily to the latter, there is no need to solve nonlinear equations for excited states.²⁰⁸ The VCC is a powerful method to obtain accurate vibrational spectra.^{212–214}

2.5 Numerov method

The Numerov method is a way to solve the second-order differential equations in which the first-order term is absent:

$$\frac{d^2y}{dx^2} = S(x) + Q(x)y(x), \quad (2.64)$$

where $S(x)$ and $Q(x)$ are continuous functions on a given domain.

For the Numerov method to be applied, the differential equations must satisfy two conditions, i.e. they must not contain first derivatives and the equations must be linear with respect to $y(x)$.²¹⁵

The time-independent one-dimensional Schrödinger equation is as the second-order ordinary differential equation:

$$\frac{d^2\psi(x)}{dx^2} = \frac{2m}{\hbar^2} (V(x) - E) \psi(x). \quad (2.65)$$

If one is requested to solve this Schrödinger equation, the solution has to be done with the following conditions:²¹⁶

1. $\psi(x) \rightarrow 0$ as $x \rightarrow \pm\infty$,
2. $\int_{-\infty}^{\infty} |\psi(x)|^2 dx = 1$,
3. $\psi(x)$ and $\psi'(x)$ are continuous if V is continuous, where $\psi'(x)$ is the first derivative of a wavefunction $\psi(x)$.

The first condition is a boundary condition, i. e. it specifies bounds $x \in (-\infty, \infty)$ while the second one is normalization condition. Thus, the Equation 2.65 will be solved as a boundary value problem. Firstly we need to discretize the interval with equally spaced points and step size h . Also, the Equation 2.65 can be rewritten in a more convenient form:

$$\frac{d^2\psi(x)}{dx^2} + k^2(x)\psi(x) = 0, \quad (2.66)$$

where

$$k^2(x) = \frac{2m}{\hbar^2} (E - V(x)) \psi(x). \quad (2.67)$$

A Taylor series for $\psi(x + h)$ is:

$$\begin{aligned} \psi(x + h) = & \psi(x) + h \frac{d\psi(x)}{dx} + \frac{h^2}{2!} \frac{d^2\psi(x)}{dx^2} + \frac{h^3}{3!} \frac{d^3\psi(x)}{dx^3} + \\ & + \frac{h^4}{4!} \frac{d^4\psi(x)}{dx^4} + \frac{h^5}{5!} \frac{d^5\psi(x)}{dx^5} + O(h^6). \end{aligned} \quad (2.68)$$

Similarly

$$\begin{aligned} \psi(x - h) = & \psi(x) - h \frac{d\psi(x)}{dx} + \frac{h^2}{2!} \frac{d^2\psi(x)}{dx^2} - \frac{h^3}{3!} \frac{d^3\psi(x)}{dx^3} + \\ & + \frac{h^4}{4!} \frac{d^4\psi(x)}{dx^4} - \frac{h^5}{5!} \frac{d^5\psi(x)}{dx^5} + O(h^6). \end{aligned} \quad (2.69)$$

After summing of these two equations the odd powers of h disappear:

$$\psi(x + h) + \psi(x - h) = 2\psi(x) + h^2 \frac{d^2\psi(x)}{dx^2} + \frac{h^4}{12} \frac{d^4\psi(x)}{dx^4} + O(h^6). \quad (2.70)$$

Thus, the second derivative which occurs in Schrödinger equation 2.66 can be expressed as:

$$\frac{d^2\psi(x)}{dx^2} = \frac{\psi(x+h) + \psi(x-h) - 2\psi(x)}{h^2} - \frac{h^2}{12} \frac{d^4\psi(x)}{dx^4} + O(h^4). \quad (2.71)$$

To evaluate $\frac{d^4\psi(x)}{dx^4}$ term one can use again Equation 2.66:

$$\frac{d^4\psi(x)}{dx^4} = -\frac{d^2}{dx^2} k^2(x)\psi(x). \quad (2.72)$$

If one substitutes the second and the fourth derivatives in Equation 2.71 for Equations 2.66 and 2.72 respectively, the expression can be rewritten as:

$$\begin{aligned} &\psi(x+h) + \psi(x-h) - 2\psi(x) + h^2 k^2(x)\psi(x) + \\ &+ \frac{h^4}{12} \frac{d^2}{dx^2} k^2(x)\psi(x) + O(h^6) = 0. \end{aligned} \quad (2.73)$$

Using central difference formula, the $\frac{d^2}{dx^2} k^2(x)\psi(x)$ term can be evaluated the following way:

$$\begin{aligned} \frac{d^2}{dx^2} k^2(x)\psi(x) &= \frac{1}{h^2} \left(k^2(x+h)\psi(x+h) + \right. \\ &\left. + k^2(x-h)\psi(x-h) - 2k^2(x)\psi(x) \right). \end{aligned} \quad (2.74)$$

After substituting the above equation into Equation 2.73 and rearranging the terms, the $\psi(x+h)$ is expressed as:

$$\begin{aligned} \psi(x+h) &= \frac{2(1 - \frac{5}{12}h^2 k^2(x))\psi(x)}{1 + \frac{1}{12}h^2 k^2(x+h)} - \\ &- \frac{(1 + \frac{1}{12}h^2 k^2(x-h))\psi(x-h)}{1 + \frac{1}{12}h^2 k^2(x+h)} + O(h^6). \end{aligned} \quad (2.75)$$

The final equation for one step can be written setting $x = x_0 + nh = x_n$ and $k_n = k(x_n)$:

$$\psi_{n+1} = \frac{2(1 - \frac{5}{12}h^2k_n^2)\psi_n - (1 + \frac{1}{12}h^2k_{n-1}^2)\psi_{n-1}}{1 + \frac{1}{12}h^2k_{n+1}^2} \quad (2.76)$$

It can be seen that it is a recurrence relation connecting ψ_n , ψ_{n+1} and ψ_{n-1} . To generate entire solution two initial values of ψ_n at successive points have to be known. They can be obtained using boundary conditions along with the asymptotic nature of the function if the latter is known.

The method is especially useful to solve ro-vibrational problem, e.g. for diatomic molecules when a spherical symmetry exists. In this case the three-dimensional Schrödinger equation, can be separated to a radial and angular parts. The former is subsequently solved as described above for the one-dimensional case.

Apart from one-dimensional case a generalization to two-dimensional case also exists.²¹⁷ The efficiency of this method was proven by applying it to the so-called non-spherically symmetric problems.^{218,219}

The Numerov method was employed to study the transitions of bound states into resonances,²²⁰ finding vibrational states of such molecules as water,²²¹ CS,²²² OF, OCl, OBr, OI,²²³ etc.

As one can see this method is not variational opposite to the previously described vibrational methods and following method which deals with distributed Gaussian functions. The Numerov method is a way to solve directly a second-order differential equation. Other non-variational methods which are used to solve Schrödinger equation are the simple finite difference matrices method²²⁴ and the trigonometric splines method.²²⁵

2.6 Distributed Gaussian functions method

The method of equally spaced real distributed Gaussians for one dimension as a basis in variational calculations of vibrational states was considered by Chesick²²⁶ and Shore.²²⁴ The generalization of this method to complex distributed Gaussians was done by Davis and Heller.²²⁷ Another generalization to unequally spaced Gaussians was done by Hamilton and Light.²²⁸ Their generalization provides more flexibility to basis set parameters and shows that sometimes generalization to complex Gaussians is unnecessary.

The Gaussian basis functions in one-dimensional case are expressed by the following equation:¹

$$\phi_i(x) = \exp\left(-A_i(x - x_i)^2\right), \quad (2.77)$$

where x_i is the center of i th Gaussian and A_i is an exponential parameter. The latter can be a constant or can depend on interior points as follows:

$$A_i = \frac{4c^2}{(x_{i+1} - x_{i-1})^2}. \quad (2.78)$$

c is a “free” parameter typically in the range 0.5–1.1.

If the Hamiltonian has the form:

$$\hat{H}(x) = -\frac{1}{2} \frac{d^2}{dx^2} + V(x), \quad (2.79)$$

and if the potential $V(x)$ is represented as the polynomial $\sum_{n=0}^M x^n$, the eigenvalues and eigenfunctions can be obtained as follows:

¹In the original paper of Hamilton and Light, normalized distributed Gaussians were employed. Here we give our own derivation using unnormalized Gaussians.

- Evaluate Hamiltonian \hat{H} and overlap matrix S in this basis:

$$V_{ij} = \int \phi_i V(x) \phi_j dx = \sum_{n=0}^M \int \phi_i x^n \phi_j dx, \quad (2.80)$$

$$V_{ij}^{(0)} = S_{ij} = \int \phi_i \phi_j dx = \sqrt{\frac{\pi}{2\zeta}} \exp\left(-\zeta \frac{(x_i - x_j)^2}{2}\right), \quad (2.81)$$

$$V_{ij}^{(1)} = \int \phi_i x \phi_j dx = \frac{x_i + x_j}{2} S_{ij}, \quad (2.82)$$

$$V_{ij}^{(n+2)} = \int \phi_i x^{n+2} \phi_j dx = \frac{n+1}{4\zeta} V_{ij}^{(n)} + \frac{x_i + x_j}{2} V_{ij}^{(n+1)}, \quad (2.83)$$

$$H_{ij} = T_{ij} + V_{ij}, \quad (2.84)$$

$$\begin{aligned} T_{ij} &= -\frac{1}{2} \int \phi_i \frac{d^2}{dx^2} \phi_j dx = \\ &= \zeta \left(\frac{1}{2} - \frac{\zeta}{2} (x_i - x_j)^2 \right) S_{ij}. \end{aligned} \quad (2.85)$$

Here S_{ij} , H_{ij} , T_{ij} , V_{ij} are overlap, Hamiltonian, kinetic- and potential-energy matrix elements respectively. A_i is a constant, $A_i = \zeta$

- Solve the generalized eigenvalue problem:

$$\mathbf{HC} = \mathbf{SCE}. \quad (2.86)$$

It was shown that even for highly anharmonic potentials this basis is flexible and efficient. There are several advantages of using real Gaussians, among them a reduction of basis set parameters and efficient evaluation of matrix elements. The latter can be very easy even for multidimensional systems. Also, the remarkable utilities are simplicity of choice of basis parameters, accuracy of results for given basis set sizes, stability of results with respect to variation of basis set

parameters and flexibility of basis to produce excellent results for arbitrary potentials.²²⁸ This method has a wide field of applications.^{229–232}

As an alternative to the distributed Gaussians one can use harmonic oscillator basis,²³³ cubic-spline basis²³⁴ or sine basis.²³⁵

Chapter 3

Objectives

The main objective of this thesis is to deeply understand the proton dynamics in proton sponge cations as well as hydride dynamics in organometallic complexes with Si \cdots H interactions by solving three-dimensional vibrational Schrödinger equation. Although many workers provided one- and two-dimensional solution of the vibrational Schrödinger equation for proton sponges and similar systems, there have been no studies giving a three-dimensional solution. Nor were there works on the dynamics of organometallic complexes with Si \cdots H interactions.

Since it is of importance to reproduce well N–H and Si–H distances in our systems, a careful choice of a method is required. *Thus, our first goal is to find a density functional with adequate performance for N–H as well as for Si–H distances.* To solve the three-dimensional vibrational Schrödinger equation for such systems, the corresponding model Hamiltonian must be derived. Subsequently, working formulae for the Hamiltonian matrix elements must be deduced and implemented into a computer program. Jacobi coordinates is a good choice to use for constructing kinetic and potential energy matrix elements. *Thus, the second goal is to derive Jacobi coordinates for our*

three-dimensional case.

To be able to solve the vibrational problem we need the potential energy surface. To have an analytic representation of it, we performed fitting using the linear least-squares method. *Hence, our third aim is to derive formulae for three-dimensional linear least-squares fitting, to build the three-dimensional PES and to perform a linear squares fitting.*

Distributed Gaussians will be used as a basis, since it allows an efficient evaluation of matrix elements. Subsequently, analytical formulae for kinetic and potential energy matrix elements of Hamiltonian have to be derived in this basis. *This is the fourth goal of the thesis.* Firstly, we solve the one-dimensional vibrational Schrödinger equation. Then, one-dimensional eigenfunctions, which are the solution of the one-dimensional problem, are used as a basis for the three-dimensional problem. *Those solutions are employed to analyze the vibrational frequencies, wavefunctions and to characterize the hydrogen motion in proton sponge cations and organometallic complexes. We also want to analyze an influence of vibrations on $J(\text{Si}-\text{H})$ spin-spin coupling constants.*

Another principal objective is to shed light on whether the $\text{Si}\cdots\text{H}$ interactions are present in bis(silyl)bis(hydride) $\text{Co}(\text{V})$ and $\text{Ir}(\text{V})$ complexes. Since $\text{Co}(\text{V})$ organometallic complexes are quite rare (only a few of them were obtained and isolated experimentally), it would be interesting to get insight into such complexes. *Our first aim is to find a density functional with appropriate performance for $\text{Si}-\text{H}$ distances, since it is also important to reproduce well $\text{Si}-\text{H}$ distances in bis(silyl)bis(hydride) complexes. The second aim is to analyze the presence of $\text{Si}\cdots\text{H}$ interactions based on calculated Wiberg bond indices and $J(\text{Si}-\text{H})$ spin-spin coupling constants.*

Chapter 4

Results and discussion

This Chapter deals with all necessary derivations for our method and with results obtained by it. The derivations are represented in the first four Sections. The one-dimensional Hamiltonian matrix elements are derived in Section 4.2, and that for three dimensions are given in Section 4.3. The derivation of the working equations for three-dimensional case of linear least-squares method is given in Section 4.4. The further three parts summarize the most important results obtained in this thesis. More details can be found in Appendices A, B, and C. The computational details are given in corresponding Appendices as well.

4.1 Jacobi coordinates for triatomic system

As the proton transfer in proton sponge cations is usually coupled to the N–N motion, a single proton transfer coordinate is not sufficient to adequately describe the system. Therefore, the N–N coordinate must be also taken into account. Further improvement can be achieved

by including the proton coordinate perpendicular to the N–N vector. One can expect that these three coordinates reasonably describe the hydrogen motion in proton sponge cations.

Similarly, the hydride transfer in organometallic complexes can be coupled to the Si–Si motion, and a single hydrogen transfer coordinate is not sufficient. Thus, the Si–Si and the M–H coordinates must be also taken into account. These three coordinates, as in the case with proton sponges, are expected to be a reasonable description of the hydrogen motion in organometallic complexes.

The choice of the coordinates for constructing the PES was dictated by the following considerations. The X and Y coordinates describe the deviation of the proton from the midpoint of the N–N vector. In particular, the X coordinate indicates the shift *along* the N–N vector, while the Y coordinate is *perpendicular* to the N–N vector. The N...N distance is adopted as Z coordinate. The advantages of this choice of the coordinate system become clear if we consider a fictitious triatomic system that consists of three particles 1, 2, and 3 with masses M , m , and M , correspondingly (see Figure 4.1). The kinetic energy operator

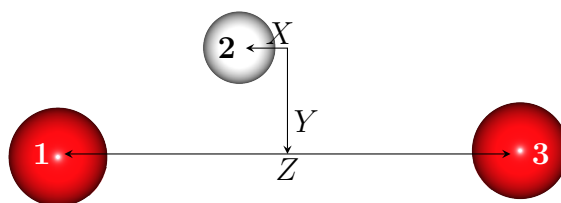


Figure 4.1: Three atomic coordinate system used to build Jacobi coordinates (see text for details).

for this system can be written in Cartesian coordinates as follows:

$$\hat{T} = -\frac{1}{2M}\nabla_1^2 - \frac{1}{2m}\nabla_2^2 - \frac{1}{2M}\nabla_3^2 = -\frac{1}{2M}\frac{\partial^2}{\partial x_1^2} - \frac{1}{2M}\frac{\partial^2}{\partial y_1^2} - \frac{1}{2M}\frac{\partial^2}{\partial z_1^2} - \frac{1}{2m}\frac{\partial^2}{\partial x_2^2} - \frac{1}{2m}\frac{\partial^2}{\partial y_2^2} - \frac{1}{2m}\frac{\partial^2}{\partial z_2^2} - \frac{1}{2M}\frac{\partial^2}{\partial x_3^2} - \frac{1}{2M}\frac{\partial^2}{\partial y_3^2} - \frac{1}{2M}\frac{\partial^2}{\partial z_3^2}. \quad (4.1)$$

The Jacobi coordinates for this system will contain the center-of-mass coordinates:

$$\mathbf{R}_{cm} = \frac{M\mathbf{r}_1 + m\mathbf{r}_2 + M\mathbf{r}_3}{2M + m}, \quad (4.2)$$

as well as the following coordinates (in vector notations):

$$\mathbf{R}_1 = \mathbf{r}_2 - \frac{1}{2}(\mathbf{r}_1 + \mathbf{r}_3), \quad (4.3)$$

$$\mathbf{R}_2 = \mathbf{r}_3 - \mathbf{r}_1. \quad (4.4)$$

If the particles 1 and 2 are only allowed to move along the x axis, and the particle 3 only along the x and y axes, the following three coordinates can be used:

$$X = x_2 - \frac{1}{2}(x_1 + x_3), \quad (4.5)$$

$$Y = y_2 - y_0 \quad \text{where} \quad y_0 = \frac{1}{2}(y_1 + y_3) \quad \text{is a constant}, \quad (4.6)$$

$$Z = x_3 - x_1. \quad (4.7)$$

If particles 1 and 3 are nitrogen atoms and particle 2 is a hydrogen atom, then the set of Jacobi coordinates for this system can be rewritten, excluding the coordinates of the center of mass, as follows:

$$X = x_H - \frac{1}{2}(x_{N^1} + x_{N^2}), \quad (4.8)$$

$$Y = y_H - \frac{1}{2}(y_{N^1} + y_{N^2}) = y_H - y_0, \quad (4.9)$$

$$Z = x_{N^1} - x_{N^2}. \quad (4.10)$$

The kinetic energy operator in the Jacobi coordinates is expressed as follows:

$$\hat{T} = -\frac{1}{2\mu_1} \frac{\partial^2}{\partial X^2} - \frac{1}{2\mu_2} \frac{\partial^2}{\partial Y^2} - \frac{1}{2\mu_3} \frac{\partial^2}{\partial Z^2}, \quad (4.11)$$

where the reduced masses μ_1 , μ_2 , μ_3 are:

$$\mu_1 = \mu_2 = \frac{2Mm}{2M + m}, \quad (4.12)$$

$$\mu_3 = M/2. \quad (4.13)$$

We take advantage of the fact that the proton sponge cations in question are symmetric and both nitrogen atoms can be assigned the same masses. As a consequence, the kinetic energy operator is diagonal; otherwise, the equations (4.8)–(4.10) would not have given Jacobi coordinates, and the kinetic energy expression would have contained cross terms (mixed derivatives). For our calculations, we used the values of the reduced masses obtained from harmonic analysis. The coordinate system used for the bis(silyl)hydride complexes is completely analogous.

4.2 One-dimensional Hamiltonian matrix elements

If we approximate the potential as a polynomial:

$$V(x) = \sum_{m=0}^M A_m x^m, \quad (4.14)$$

where A_m are coefficients, then the n -th order term of the ij -th potential matrix element in a basis of distributed Gaussian functions is as follows:

$$\begin{aligned} \langle i|x^n|j\rangle &= I_n(x_i, x_j, \zeta) = \int_{-\infty}^{\infty} x^n e^{-\zeta(x-x_i)^2} e^{-\zeta(x-x_j)^2} dx = \\ &= e^{-\zeta\frac{(x_i-x_j)^2}{2}} \int_{-\infty}^{\infty} x^n e^{-2\zeta\left(x-\frac{x_i+x_j}{2}\right)^2} dx, \end{aligned} \quad (4.15)$$

where ζ is a constant, x_i and x_j are centers of i th and j th Gaussians, respectively. Similarly:

$$\begin{aligned} I_{n+1}(x_i, x_j, \zeta) &= e^{-\zeta\frac{(x_i-x_j)^2}{2}} \int_{-\infty}^{\infty} x^{n+1} e^{-2\zeta\left(x-\frac{x_i+x_j}{2}\right)^2} dx, \\ I_{n+2}(x_i, x_j, \zeta) &= e^{-\zeta\frac{(x_i-x_j)^2}{2}} \int_{-\infty}^{\infty} x^{n+2} e^{-2\zeta\left(x-\frac{x_i+x_j}{2}\right)^2} dx. \end{aligned} \quad (4.16)$$

The value of integral I_n is:

$$\begin{aligned} I_n &= e^{-\zeta\frac{(x_i-x_j)^2}{2}} \int_{-\infty}^{\infty} x^n e^{-2\zeta\left(x-\frac{x_i+x_j}{2}\right)^2} dx = \\ &= \frac{e^{-\zeta\frac{(x_i-x_j)^2}{2}}}{n+1} \int_{-\infty}^{\infty} e^{-2\zeta\left(x-\frac{x_i+x_j}{2}\right)^2} d(x^{n+1}) = \end{aligned} \quad (4.17)$$

$$\begin{aligned}
&= \frac{4\zeta e^{-\zeta \frac{(x_i - x_j)^2}{2}}}{n+1} \int_{-\infty}^{\infty} x^{n+1} \left(x - \frac{x_i + x_j}{2}\right) e^{-2\zeta \left(x - \frac{x_i + x_j}{2}\right)^2} dx = \\
&= \frac{4\zeta e^{-\zeta \frac{(x_i - x_j)^2}{2}}}{n+1} \int_{-\infty}^{\infty} x^{n+2} e^{-2\zeta \left(x - \frac{x_i + x_j}{2}\right)^2} dx - \\
&\quad - \frac{2(x_i + x_j) \zeta e^{-\zeta \frac{(x_i - x_j)^2}{2}}}{n+1} \int_{-\infty}^{\infty} x^{n+1} e^{-2\zeta \left(x - \frac{x_i + x_j}{2}\right)^2} dx = \\
&= \frac{4\zeta}{n+1} I_{n+2} - \frac{2(x_i + x_j) \zeta}{n+1} I_{n+1}. \tag{4.18}
\end{aligned}$$

The integral I_{n+2} is expressed from Equation 4.18 as follows:

$$I_{n+2} = \frac{n+1}{4\zeta} I_n + \frac{x_i + x_j}{2} I_{n+1}. \tag{4.19}$$

Thus, $(n+2)$ th order term of the ij -th potential matrix element is calculated from I_n and I_{n+1} by a recurrence relation. To generate the solution two initial values have to be known. These initial values are:

$$I_0 = \sqrt{\frac{\pi}{2\zeta}} e^{-\zeta \frac{(x_i - x_j)^2}{2}}, \tag{4.20}$$

$$I_1 = \frac{1}{2} \sqrt{\frac{\pi}{2\zeta}} (x_i + x_j) e^{-\zeta \frac{(x_i - x_j)^2}{2}} = \frac{x_i + x_j}{2} I_0. \tag{4.21}$$

Obviously the zeroth order term I_0 is identical to the ij -th overlap matrix element.

Kinetic energy matrix elements are calculated as follows:

$$\begin{aligned}
T(x_i, x_j, \zeta) &= \int_{-\infty}^{\infty} e^{-\zeta(x-x_i)^2} \left(-\frac{1}{2} d^2/dx^2 \right) e^{-\zeta(x-x_j)^2} dx = \\
&= -\frac{1}{2} \int_{-\infty}^{\infty} e^{-\zeta(x-x_i)^2} \left(e^{-\zeta(x-x_j)^2} \right)'' dx = \\
&= -\zeta \int_{-\infty}^{\infty} e^{-\zeta(x-x_i)^2} \left(2\zeta(x-x_j)^2 - 1 \right) e^{-\zeta(x-x_j)^2} dx = \\
&= \zeta \left(\frac{1}{2} - \frac{\zeta}{2} (x_i - x_j)^2 \right) I_0. \tag{4.22}
\end{aligned}$$

Thus, kinetic energy matrix elements are calculated through the overlap matrix elements.

4.3 Three-dimensional Hamiltonian matrix elements

Let $\chi_\mu(x)$, $\kappa_\lambda(y)$, $\theta_\rho(z)$ be one-dimensional Gaussian basis functions centered at x_μ on the X axis, at y_λ on the Y axis, and at z_ρ on the Z axis, respectively:¹

$$\chi_\mu(x) = e^{-\zeta(x-x_\mu)^2}, \tag{4.23}$$

$$\kappa_\lambda(y) = e^{-\zeta(y-y_\lambda)^2}, \tag{4.24}$$

$$\theta_\rho(z) = e^{-\zeta(z-z_\rho)^2}. \tag{4.25}$$

¹The derivation for three-dimensional case is based on two-dimensional equations derived by Dr. S. F. Vyboishchikov.

In our case the three-dimensional Hamiltonian can be written as follows:

$$\begin{aligned} \hat{H} = \hat{T}_x + \hat{T}_y + \hat{T}_z + V(x, y, z) = & -\frac{1}{2\mu_1} \frac{\partial^2}{\partial x^2} - \frac{1}{2\mu_2} \frac{\partial^2}{\partial y^2} - \\ & - \frac{1}{2\mu_3} \frac{\partial^2}{\partial z^2} + \sum_{i=0}^I \sum_{j=0}^J \sum_{k=0}^K A_{ijk} x^i y^j z^k. \end{aligned} \quad (4.26)$$

Here the first three terms correspond to the one-dimensional kinetic energy operators and μ_i are the corresponding reduced masses. We partition this Hamiltonian as follows:

$$\begin{aligned} \hat{H} = \hat{T}_x + \hat{T}_y + \hat{T}_z + \sum_{i=0}^I \sum_{j=0}^J \sum_{k=0}^K A_{ijk} x^i y^j z^k = & \hat{T}_x + \hat{T}_y + \hat{T}_z + \sum_{i=0}^I A_{i00} x^i + \\ & + \sum_{j=1}^J A_{0j0} y^j + \sum_{k=1}^K A_{00k} z^k + \sum_{j=1}^J \sum_{i=1}^I A_{ij0} x^i y^j + \sum_{k=1}^K \sum_{j=1}^J A_{0jk} y^j z^k + \\ & + \sum_{k=1}^K \sum_{i=1}^I A_{i0k} x^i z^k + \sum_{k=1}^K \sum_{j=1}^J \sum_{i=1}^I A_{ijk} x^i y^j z^k = \left(\hat{T}_x + \sum_{i=0}^I A_{i00} x^i \right) + \\ & + \left(\hat{T}_y + \sum_{j=1}^J A_{0j0} y^j \right) + \left(\hat{T}_z + \sum_{k=1}^K A_{00k} z^k \right) + \sum_{j=1}^J \sum_{i=1}^I A_{ij0} x^i y^j + \\ & + \sum_{k=1}^K \sum_{j=1}^J A_{0jk} y^j z^k + \sum_{k=1}^K \sum_{i=1}^I A_{i0k} x^i z^k + \sum_{k=1}^K \sum_{j=1}^J \sum_{i=1}^I A_{ijk} x^i y^j z^k = \hat{H}_x + \\ & + \hat{H}_y + \hat{H}_z + V_{xy}(x, y) + V_{yz}(y, z) + V_{xz}(x, z) + V_{xyz}(x, y, z). \end{aligned} \quad (4.27)$$

Thus, the three-dimensional Hamiltonian is a sum of the one-dimensional Hamiltonians plus coupling terms $V_{xy}(x, y)$, $V_{yz}(y, z)$, $V_{xz}(x, z)$,

and $V_{xyz}(x, y, z)$:

$$\hat{H}_x = \left(\hat{T}_x + \sum_{i=0}^I A_{i00} x^i \right), \quad (4.28)$$

$$\hat{H}_y = \left(\hat{T}_y + \sum_{j=1}^J A_{0j0} y^j \right), \quad (4.29)$$

$$\hat{H}_z = \left(\hat{T}_z + \sum_{k=1}^K A_{00k} z^k \right), \quad (4.30)$$

$$V_{xy}(x, y) = \sum_{j=1}^J \sum_{i=1}^I A_{ij0} x^i y^j, \quad (4.31)$$

$$V_{yz}(y, z) = \sum_{k=1}^K \sum_{j=1}^J A_{0jk} y^j z^k, \quad (4.32)$$

$$V_{xz}(x, z) = \sum_{k=1}^K \sum_{i=1}^I A_{i0k} x^i z^k, \quad (4.33)$$

$$V_{xyz}(x, y, z) = \sum_{k=1}^K \sum_{j=1}^J \sum_{i=1}^I A_{ijk} x^i y^j z^k. \quad (4.34)$$

Now we determine the one-dimensional eigenfunctions of the operators \hat{H}_x , \hat{H}_y and \hat{H}_z in the basis $\{\chi_\mu(x)\}$, $\{\kappa_\lambda(y)\}$ and $\{\theta_\rho(z)\}$ correspondingly.

The eigenfunctions of \hat{H}_x are as follows:

$$F_i(x) = \sum_{\mu} C_{i\mu} \chi_{\mu}(x). \quad (4.35)$$

The corresponding energy eigenvalues are E_i^x .

Similarly for eigenfunctions of \hat{H}_y and \hat{H}_z :

$$G_j(y) = \sum_{\lambda} K_{j\lambda} \kappa_{\lambda}(y), \quad (4.36)$$

$$Q_u(z) = \sum_{\rho} P_{u\rho} \theta_{\rho}(z). \quad (4.37)$$

The corresponding energy eigenvalues are E_j^y and E_u^z .

We construct the basis set for the three-dimensional problem from all possible products of the lowest one-dimensional eigenfunctions $F_i(x)$, $G_j(y)$ and $Q_u(z)$:

$$F_i(x)G_j(y)Q_u(z) = \sum_{\mu}^{\mu_{\max}} \sum_{\lambda}^{\lambda_{\max}} \sum_{\rho}^{\rho_{\max}} C_{i\mu} K_{j\lambda} P_{u\rho} e^{-\zeta((x-x_{\mu})^2+(y-y_{\lambda})^2+(z-z_{\rho})^2)}. \quad (4.38)$$

The matrix elements between the new three-dimensional basis functions are evaluated as follows:

Overlap matrix will be unit matrix:

$$\begin{aligned} &\langle F_i(x)G_j(y)Q_u(z) | F_k(x)G_l(y)Q_s(z) \rangle = \\ &= \langle F_i(x) | F_k(x) \rangle \langle G_j(y) | G_l(y) \rangle \langle Q_u(z) | Q_s(z) \rangle = \delta_{ik} \delta_{jl} \delta_{us}, \end{aligned} \quad (4.39)$$

due to the orthogonality of one-dimensional eigenfunctions:

$$\langle F_i(x) | F_k(x) \rangle = \delta_{ik}, \quad (4.40)$$

$$\langle G_j(y) | G_l(y) \rangle = \delta_{jl}, \quad (4.41)$$

$$\langle Q_u(z) | Q_s(z) \rangle = \delta_{us}. \quad (4.42)$$

Hamiltonian matrix elements $\langle F_i(x)G_j(y)Q_u(z) | \hat{H} | F_k(x)G_l(y)Q_s(z) \rangle$:

$$\langle F_i(x) | \hat{H}_x | F_k(x) \rangle \langle G_j(y) | G_l(y) \rangle \langle Q_u(z) | Q_s(z) \rangle = \delta_{jl} \delta_{us} E_i^x \delta_{ik}, \quad (4.43)$$

$$\langle F_i(x) | F_k(x) \rangle \langle G_j(y) | \hat{H}_y | G_l(y) \rangle \langle Q_u(z) | Q_s(z) \rangle = \delta_{ik} \delta_{us} E_j^y \delta_{jl}, \quad (4.44)$$

$$\langle F_i(x) | F_k(x) \rangle \langle G_j(y) | G_l(y) \rangle \langle Q_u(z) | \hat{H}_z | Q_s(z) \rangle = \delta_{ik} \delta_{jl} E_u^z \delta_{us}. \quad (4.45)$$

The coupling terms are evaluated as follows:

$$\begin{aligned} & \langle F_i(x)G_j(y) | V_{xy}(x, y) | F_k(x)G_l(y) \rangle \langle Q_u(z) | Q_s(z) \rangle = \\ & = \delta_{us} \sum_{p=1}^P \sum_{n=1}^N A_{npo} \langle F_i(x) | x^n | F_k(x) \rangle \langle G_j(y) | y^p | G_l(y) \rangle \end{aligned} \quad (4.46)$$

$$\begin{aligned} & \langle G_j(y)Q_u(z) | V_{yz}(y, z) | G_l(y)Q_s(z) \rangle \langle F_i(x) | F_k(x) \rangle = \\ & = \delta_{ik} \sum_{r=1}^R \sum_{p=1}^P A_{0pr} \langle G_j(y) | y^p | G_l(y) \rangle \langle Q_u(z) | z^r | Q_s(z) \rangle \end{aligned} \quad (4.47)$$

$$\begin{aligned} & \langle F_i(x)Q_u(z) | V_{xz}(x, z) | F_k(x)Q_s(z) \rangle \langle G_j(y) | G_l(y) \rangle = \\ & = \delta_{jl} \sum_{r=1}^R \sum_{n=1}^N A_{n0r} \langle F_i(x) | x^n | F_k(x) \rangle \langle Q_u(z) | z^r | Q_s(z) \rangle \end{aligned} \quad (4.48)$$

$$\begin{aligned} & \langle F_i(x)G_j(y)Q_u(z) | V_{xyz}(x, y, z) | F_k(x)G_l(y)Q_s(z) \rangle = \\ & = \sum_{r=1}^R \sum_{p=1}^P \sum_{n=1}^N A_{npr} \langle F_i(x) | x^n | F_k(x) \rangle \langle G_j(y) | y^p | G_l(y) \rangle \langle Q_u(z) | z^r | Q_s(z) \rangle \end{aligned} \quad (4.49)$$

$\langle F_i(x) | x^n | F_k(x) \rangle$, $\langle G_j(y) | y^p | G_l(y) \rangle$ and $\langle Q_u(z) | z^r | Q_s(z) \rangle$ are the potential energy matrix elements – must be obtained previously by means of matrix transformations:

$$\langle F_i(x) | x^n | F_k(x) \rangle = \left(\mathbf{C}\mathbf{X}^{(n)}\mathbf{C}^+ \right)_{ik}, \quad (4.50)$$

$$\langle G_j(y) | y^p | G_l(y) \rangle = \left(\mathbf{K}\mathbf{Y}^{(p)}\mathbf{K}^+ \right)_{jl}, \quad (4.51)$$

$$\langle Q_u(z) | z^r | Q_s(z) \rangle = \left(\mathbf{P}\mathbf{Z}^{(r)}\mathbf{P}^+ \right)_{us}, \quad (4.52)$$

where \mathbf{C} , \mathbf{K} , \mathbf{P} are the matrices of coefficients, and $\mathbf{X}^{(n)}$, $\mathbf{Y}^{(p)}$, $\mathbf{Z}^{(r)}$ are the matrices that contain terms of one-dimensional potentials for x , y , and z at different powers n .

Within the method we used, first, three one-dimensional equations were separately solved with respect to each of the coordinates X , Y , Z .

Subsequently, all possible products of the lowest 12 one-dimensional eigenfunctions (i.e., a total of $12^3 = 1728$ three-dimensional functions) were used as a basis for the three-dimensional problem. All matrix elements were evaluated using analytical formulae given above. Consequently, a full Hamiltonian diagonalization using the standard Householder method was performed. Test calculations indicate that this approach yields a converged (i.e., nearly exact, within the given potential) solution of the three-dimensional Schrödinger equation.

4.4 Three-dimensional linear least-squares method

Although the potential energy surface is generated point by point, a representation by an analytical formula is preferential when used to solve the vibrational Schrödinger equation. The simplest and efficient way to do this is to use a polynomial function.

Usually, the higher order of polynomial is, the more exactly it describes the behavior of a real potential energy surface. Polynomial function through its cross-terms takes into account a coupling between various modes which is important for polyatomic molecules. It can be differentiated very easy and this plays significant role for fitting using for example linear least-squares method.

In spite of a large amount of a literature dedicated to the linear least-squares method, no explicit working formulae were found in the literature that would describe polynomial least-square fitting in several dimensions. Below we present our own derivation.

Let there be N energy points on a three-dimensional potential energy surface $E_n(X_n, Y_n, Z_n)$, $1 \leq n \leq N$. Our potential energy

surface is represented as polynomial:

$$V(X, Y, Z) = \sum_{i=0}^I \sum_{j=0}^J \sum_{k=0}^K A_{ijk} X^i Y^j Z^k, \quad (4.53)$$

where A_{ijk} are coefficients to be fitted.

The least squares method is based on the idea that the best-fit function is the one minimizing the (possibly weighted) sum of the squared deviations from a given set of data. Thus, the sum of weighted squared deviations is:

$$S(A_{ijk}) = \sum_{n=1}^N \omega_n (V(X_n, Y_n, Z_n) - E_n)^2, \quad (4.54)$$

or

$$S(A_{ijk}) = \sum_{n=1}^N \omega_n \left(\sum_{i=0}^I \sum_{j=0}^J \sum_{k=0}^K A_{ijk} X_n^i Y_n^j Z_n^k - E_n \right)^2, \quad (4.55)$$

where ω_n is the weighting factor of the n -th point. Then, the minimization of $S(A_{ijk}; X_n, Y_n, Z_n)$ with respect to the coefficients A_{ijk} :

$$\forall i, j, k \quad \frac{\partial S}{\partial A_{ijk}} = 0. \quad (4.56)$$

Evaluation of these derivatives yields:

$$\frac{\partial S}{\partial A_{abc}} = 2 \sum_{n=1}^M \omega_n (V(X_n, Y_n, Z_n) - E_n) \frac{\partial V(X_n, Y_n, Z_n)}{\partial A_{abc}}. \quad (4.57)$$

Using equation 4.53 and keeping in mind that the differentiation with respect to A_{abc} leaves only term where $i = a$, $j = b$, $k = c$, we express the derivative on the right-hand side of equation 4.57 as follows:

$$\frac{\partial V(X_n, Y_n, Z_n)}{\partial A_{abc}} = \frac{\partial}{\partial A_{abc}} \sum_{i=0}^I \sum_{j=0}^J \sum_{k=0}^K A_{ijk} X_n^i Y_n^j Z_n^k = X_n^a Y_n^b Z_n^c. \quad (4.58)$$

Inserting the equation 4.58 into the equation 4.57, we obtain:

$$\frac{\partial S}{\partial A_{abc}} = 2 \sum_{n=1}^M \omega_n \left(\sum_{i=0}^I \sum_{j=0}^J \sum_{k=0}^K A_{ijk} X_n^i Y_n^j Z_n^k - E_n \right) X_n^a Y_n^b Z_n^c, \quad (4.59)$$

and after simplification:

$$2 \sum_{n=1}^M \omega_n \left(\sum_{i=0}^I \sum_{j=0}^J \sum_{k=0}^K A_{ijk} X_n^{i+a} Y_n^{j+b} Z_n^{k+c} - E_n X_n^a Y_n^b Z_n^c \right) = 0, \quad (4.60)$$

or

$$\sum_{n=1}^N \omega_n \sum_{i=0}^I \sum_{j=0}^J \sum_{k=0}^K A_{ijk} X_n^{i+a} Y_n^{j+b} Z_n^{k+c} = \sum_{n=1}^N \omega_n E_n X_n^a Y_n^b Z_n^c. \quad (4.61)$$

Finally, the coefficients A_{ijk} were found by solving the resulting system of $(I+1)(J+1)(K+1)$ linear equations by the standard Gauss elimination method.

4.5 Hydrogen motion in proton sponge cations: A theoretical study

Our main purpose is to analyze the vibrational motion of proton in proton sponge cations by numerically solving the three-dimensional vibrational Schrödinger equation. To distinguish between three different vibrational patterns possible in proton sponges (see page 12), eight different proton sponge cations were analyzed (see Figure 4.2). These cations, with the exception of **PS7**, exhibit crystallographically symmetric NHN arrangement according to X-ray data of their salts. Four of them, **PS1**, **PS4**, **PS6**, and **PS7**, which represent variety of proton transfer barriers, were chosen for solving three-dimensional vibrational Schrödinger equation. The wavefunction will give us information about anharmonicity of the proton motion as well as about the coupling between the coordinates.

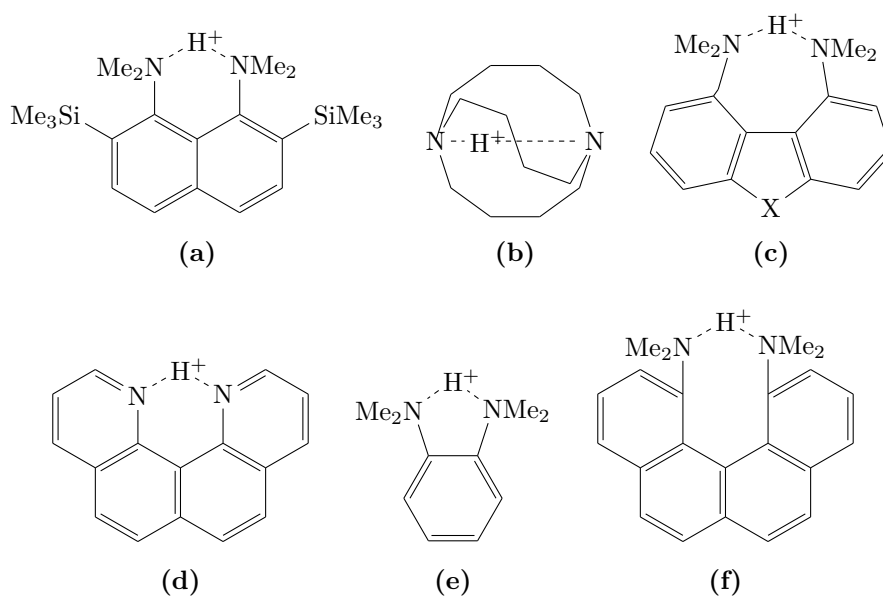


Figure 4.2: Proton sponges analyzed for possible vibrational patterns. (a) **PS1**; (b) **PS2**; (c) **PS3** (X=Se); **PS4** (X=S); **PS5** (X=CH₂); (d) **PS6**; (e) **PS7**; (f) **PS8**.

4.5.1 Three-dimensional vibrational frequencies

As a result of solving the three-dimensional vibrational Schrödinger equation anharmonic frequencies were obtained. The results are given in the penultimate column of Table 4.1. For a single-well potential of cation **PS1**, the anharmonic $\nu(H_x)$ is more than two times higher than the harmonic value. This result is valuable for us as it allows for a direct comparison with an experiment. Our result of 661 cm^{-1} is in fair agreement with the experimental value of 610 cm^{-1} ,²⁷ thus demonstrating that the approximations we made are reasonable. The calculated isotopic frequency ratio for **PS1**, $\nu(H_x)/\nu(D_x) = 1.54$, also agrees well with an experimental value of 1.60.²⁷ Values larger than $\sqrt{2}$ are typical of strong short hydrogen bonds with a barrier-free potential.^{236,237}

For cation **PS4**, which has a double-well potential with an extremely low barrier, the anharmonic $\nu(H_x)$ frequency is very close to that for **PS1**, although the corresponding harmonic frequencies differ dramatically. This is easily explicable by the fact that the width of the PES is rather similar for both systems. A tiny “bump” on the PES of **PS4** does not affect significantly the global proton motion, while the local potential curvature at the minimum is altered substantially. In the same manner, one can explain why the anharmonic frequency for **PS6** is almost an order of magnitude lower than the harmonic one. In this case, the barrier is already significant, which increases the potential curvature at the minima and thus the harmonic frequency, whereas the anharmonic proton motion is still substantially delocalized (*vide infra*) and determined by the global potential width. Cation **PS7** has the highest barrier among these four cations studied. The harmonic frequency is slightly lower than the anharmonic one.

For the proton motion perpendicular to the N–N vector ($\nu(H_y)$ values in Table 4.1), the deviation of harmonic values from the anharmonic ones is less pronounced than for the $\nu(H_x)$ frequencies, but is

up to 400 cm^{-1} for **PS6-PS7**. Finally, for the nitrogen motion (the $\nu(NN)$ rows in Table 4.1) the harmonic frequencies also deviate from the anharmonic ones, but exhibit the trend (**PS7**>**PS6**>**PS4**>**PS1**).

Comparison of the results obtained using the scaled PES for **PS6** with the corresponding unscaled ² one **PS6pbe** (see Figure 4.4) show that $\nu(H_x)$ frequency is quite close to that obtained for **PS6**, while $\nu(H_y)$ and $\nu(NN)$ are significantly affected by the scaling. This is a clear indication of a large coupling between the H and N–N vibrations.

Table 4.1 also includes the uncoupled frequency values (1D). They were obtained by solving the one-dimensional Schrödinger equation in the uncoupled part of the three-dimensional potential, which is a preliminary part of our computational algorithm. The comparison of the coupled (3D) and uncoupled (1D) values demonstrates a substantial difference between them in all cases. Particularly pronounced is the deviation in the case of $\nu(H_x)$ for **PS7**, where the uncoupled value is dramatically underestimated. This emphasizes the coupling between X and Z coordinates and the importance of the three-dimensional treatment for the systems under study.

4.5.2 Three-dimensional vibrational wavefunctions

The other result of solving the three-dimensional vibrational Schrödinger equation is the three-dimensional vibrational wavefunctions which provide the information regarding the hydrogen motion in the proton sponges. Since it is impractical to plot a three-dimensional wavefunction, two-dimensional probability densities $\rho(X, Z)$, defined by Equa-

²Test of various density functionals revealed that PBE reproduces well the PES obtained by MP2. However, it still yields some errors in the barrier height. To cope with this, we multiplied the fitted PES for PS6 and PS7 by a factor equal to the ratio of the MP2 barrier to the PBE barrier, $R = \Delta E(MP2)/\Delta E(PBE)$. The PBE surfaces modified in this way have barriers equal to those obtained at the MP2 level.

Table 4.1: Fundamental frequencies (in cm^{-1}) obtained by harmonic analysis, by solving the three-dimensional vibrational Schrödinger equation (3D), and by solving the one-dimensional Schrödinger equation for the one-dimensional part of the potential without taking into account the coupling (1D). $\nu(H_x)$, $\nu(H_y)$ are the vibrational frequencies of hydrogen; $\nu(NN)$ is the frequency of nitrogen-nitrogen vibrations. ΔE is the proton transfer barrier (in $\text{kcal}\cdot\text{mol}^{-1}$). $\angle\text{NHN}$ is the NHN angle in the equilibrium geometry(in $^\circ$).

Cation	Vibration	Harm. freq.	Anharm. freq.		ΔE	$\angle\text{NHN}$
			1D	3D		
PS1	$\nu(H_x)$	289	887	661	0	164.2
	$\nu(H_y)$	1763	1555	1435		
	$\nu(NN)$	719	983	885		
PS4	$\nu(H_x)$	1020	1277	880	0.09	175.9
	$\nu(H_y)$	1719	2061	1957		
	$\nu(NN)$	698	1365	1171		
PS6	$\nu(H_x)$	2540	789	308	2.38	149.0
	$\nu(H_y)$	1831	2047	2268		
	$\nu(NN)$	887	999	1356		
PS6pbe	$\nu(H_x)$	2540	745	337	1.59	149.0
	$\nu(H_y)$	1831	1637	1869		
	$\nu(NN)$	887	817	591		
PS7	$\nu(H_x)$	2612	575	1391, 2886*	3.37	139.5
	$\nu(H_y)$	1857	2061	2248		
	$\nu(NN)$	946	1323	1654		

*Two values due to tunneling splitting; see text.

tion 4.62, were plotted (see Figure 4.3) along with the PES contour plots. The $\rho(X, Z)$ value shows a probability to find the hydrogen at the coordinate $(X; Z)$ and *any* coordinate Y . The minimum energy path on the PES and the maximum wavefunction path are also shown.

$$\rho(X, Z) = \int \rho(X, Y, Z) dY = \int |\Psi(X, Y, Z)|^2 dY. \quad (4.62)$$

Cation **PS1** with a single-well PES has a single maximum of the probability density as well. The wavefunction maximum is located only 0.011 Å away from the PES minimum. The hydrogen is largely delocalized between both nitrogen atoms, and the wavefunction spatial extent (see Equation 4.63) along the X coordinate is ± 0.124 Å.

$$\bar{X} = \sqrt{\langle \Psi(X, Y, Z) | X^2 | \Psi(X, Y, Z) \rangle}. \quad (4.63)$$

For cation **PS4**, the PES has two shallow minima connected by a slightly curved minimum energy path, but the wavefunction still has a single maximum, located 0.014 Å from the transition state. Therefore, the likelihood of finding the proton is maximal at the symmetric configuration; the proton motion is completely delocalized and, actually, the proton does not “feel” the barrier. The spatial extent \bar{X} is ± 0.196 Å. Interestingly, the density maximum occurs at a positive value of the Z coordinate. Hence, in the most probable symmetric configuration the N–N distance is larger than in the transition state. The average N···H distance in the most probable configuration of 1.303 Å is significantly longer than the equilibrium N–H distance in the minimum of 1.190 Å.

For cation **PS6**, the PES has two minima separated by a non-negligible barrier. In this system, the wavefunction has two relatively weakly pronounced maxima. The probability density minimum value between two maxima is 90% of the value at the maximum, which points out to a large tunneling in this system. The wavefunction maxima are

distant from the respective PES minima by 0.183 Å, lying closer to the transition state than to the minima. The hydrogen motion is still delocalized in this case. A spatial extent \bar{X} of ± 0.199 Å manifests a higher degree of delocalization than in cations **PS1** and **PS4**, which is due to the fact that the potential in **PS6** is much broader than in **PS1** or **PS4**. The average N \cdots H separation, i.e., the observable N–H bond length, is 1.177 Å, which is markedly larger than the equilibrium N–H distance of 1.082 Å in the energy minimum. The maximum wavefunction path also lies away from the minimum energy path, being shorter and straighter than the latter. This manifests a smaller coupling between the X and Z coordinates in the wavefunction than the PES shape might suggest. Essentially, the proton transfer occurs largely by means of tunneling, and contracting the N \cdots N distance is not needed for an efficient transfer.

The wavefunction for the unscaled system **PS6pbe** has two very weakly pronounced maxima, which are 0.263 Å away from the PES minima. The $|\Psi|^2$ value on the maximum wavefunction path is 99% of the value at the maximum. The maximum wavefunction path is very short and straight, signifying that the tunneling is the principal mechanism of the hydrogen transfer. We conclude that **PS6pbe** is an intermediate case between proton sponges with a single-maximum wavefunction and those in which the wavefunction has two maxima.

For cation **PS7**, which has the largest barrier among these four cations, the wavefunction has two well separated maxima at a distance of 0.154 Å from the PES minima. The average N–H distance (1.137 Å) is larger than the equilibrium bond length (1.084 Å). The maximum wavefunction path between two wavefunction maxima does not coincide with the minimum energy path either, but there is a closer resemblance between both curves. Importantly, the maximum wavefunction path is significantly bent, manifesting a large coupling between the H motion (X coordinate) and N \cdots N contraction (Z coordinate). This corresponds to the classical mechanism of proton transfer,

which involves contraction of the N...N distance to facilitate the transfer. Nevertheless, the tunneling is considerable. The minimum value of probability density on the maximum wavefunction path is 47% of the value at the maximum indicating that the hydrogen is largely localized in the areas of the maxima.

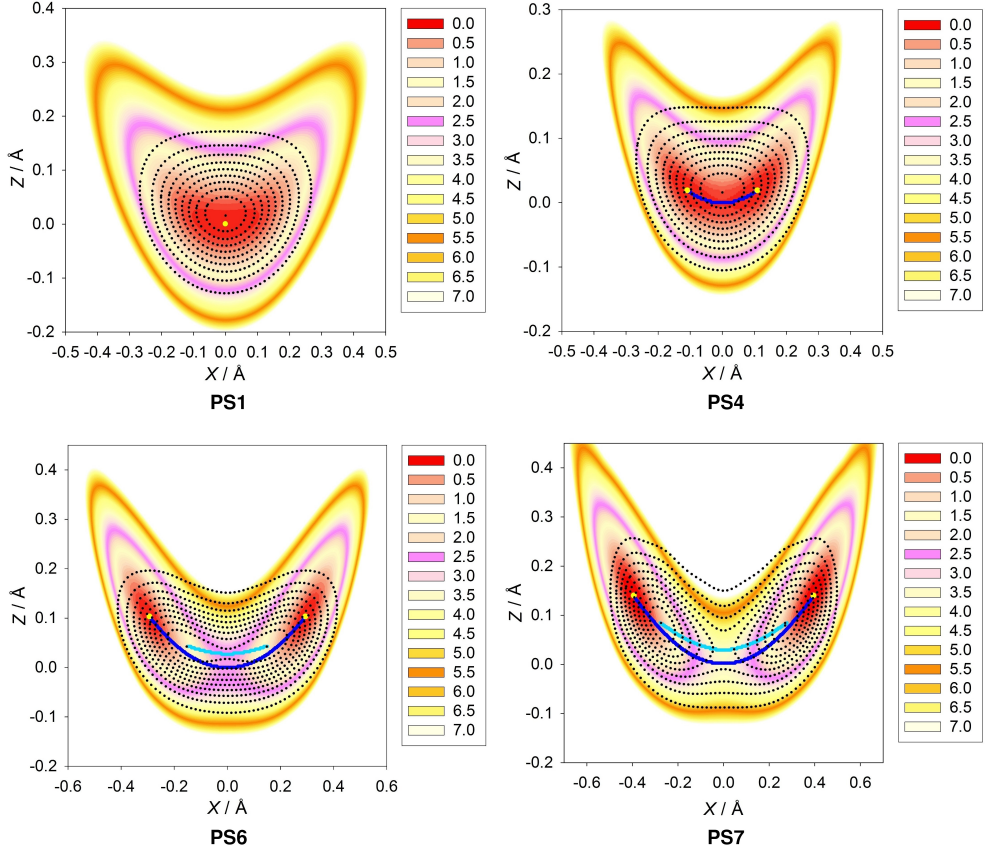


Figure 4.3: The PES and probability density contour plots for proton sponge cations **PS1**, **PS4**, **PS6** and **PS7** in the coordinates $X - Z$. The coordinates are shifted with respect to the symmetric configuration: $X = X_0 - X_e$, $Z = Z_0 - Z_e$, where $(X_e; Z_e)$ is symmetric equilibrium configuration; $(X_0; Z_0)$ is current values of coordinates. The levels of ground-state probability density, with values from $0.1\rho_{max}$ to $0.9\rho_{max}$, are given by black dotted lines. Yellow dots show the minima of the PES. Dark blue line is the MEP, and the light blue curve is the MWP between two maxima of the probability density.

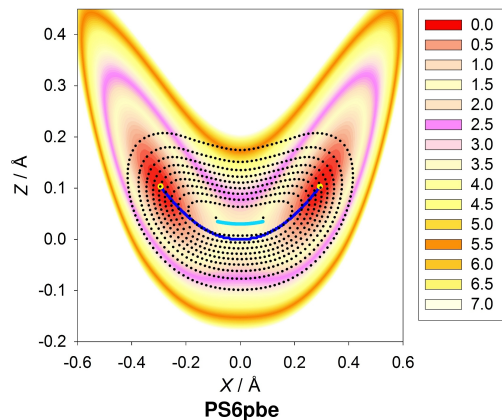


Figure 4.4: The PES and probability density contour plots for proton sponge cation **PS6pbe** in the coordinates $X - Z$. Notations are the same as in Figure 4.3

4.6 Dynamic behavior of hydrogen in transition metal bis(silyl)hydride complexes

In this Section our goal is to analyze the vibrational motion of hydride in organometallic complexes with Si \cdots H interactions by numerically solving the three-dimensional vibrational Schrödinger equation as well. The model complexes for our study (see Figures 4.5 and 4.6) were chosen in anticipation that the hydrogen transfer barriers in them could be quite different and, hence, they might exhibit diverse dynamic behavior (see page 35). In some cases, halogen substituents were placed on silyl in order to cause an IHI effect that could affect the PES. To solve three-dimensional vibrational Schrödinger equation **Tp1**, **Tp2**, **Tp3**, and **Cp9** were chosen since they represent a various hydride transfer barriers.

Moreover, since the vibrational motion of the hydride may affect the observed (i.e., averaged) Si–H spin-spin coupling constants, it is worth examining whether the effect of these vibrations on $J(\text{Si}-\text{H})$ is important.

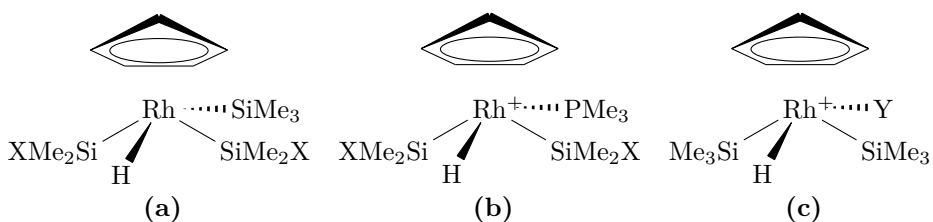


Figure 4.5: Cp bis(silyl)hydride complexes analyzed for possible vibrational patterns. (a) **Cp1** (X=H); **Cp2** (X=Cl); **Cp3** (X=Br); **Cp4** (X=I); (b) **Cp5** (X=H); **Cp6** (X= Cl); **Cp7** (X=Br); **Cp8** (X=I); (c) **Cp9** (Y=SiF₃); **Cp10** (Y=SiH₃).

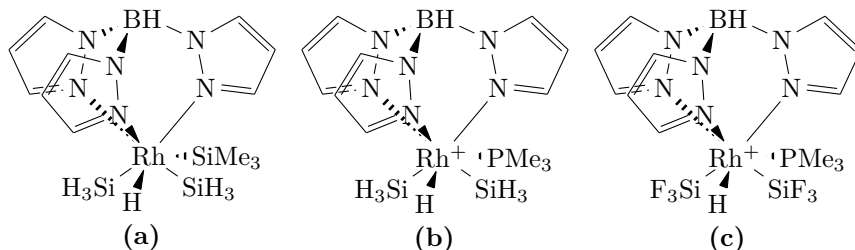


Figure 4.6: Tp bis(silyl)hydride complexes analyzed for possible vibrational patterns. (a) **Tp1**; (b) **Tp2**; (c) **Tp3**.

4.6.1 Three-dimensional vibrational frequencies

The anharmonic frequencies are given in the penultimate column of Table 4.2. In the case of complex **Tp1** (double-well potential with a low barrier), the anharmonic $\nu(H_x)$ frequency is more than 2.5 times lower than the harmonic one. Complex **Tp2** (double-well potential and a large barrier) shows tunneling splitting of 34 cm^{-1} , which originates from the double-well nature of the potential. For this reason, for complex **Tp2** two anharmonic frequency values are given in Table 4.2, both of which are lower than the harmonic frequency. Complex **Tp3** exhibits a significantly different harmonic and anharmonic frequencies. In this case the barrier is substantial, and the potential curvature at the minima is increased, as is the harmonic frequency. At the same time, the anharmonic hydrogen motion is still delocalized (*vide infra*) and determined by the global potential width. For complex **Cp9**, harmonic and anharmonic frequencies are very similar.

The frequencies for vibrations along the Y axis, which corresponds to the Rh–H stretching, can be compared with experimental IR spectra. The Rh–H stretching vibrations ($\nu(H_y)$ in Table 4.2), the anharmonic frequencies are close to the harmonic ones, and are within the re-

gion typical of experimental frequencies (1951–2090 cm^{-1}),^{85,153,238–241} except for **Tp2** where $\nu(H_y)$ is a bit lower. This gives us certainty that approximations incorporated in our computational models are reasonable. For the Si–Si vibrations, $\nu(\text{Si–Si})$ in Table 4.2, the anharmonic frequencies significantly deviate from the harmonic ones. The difference is most pronounced for complex **Cp9**, 65 cm^{-1} (harmonic) *vs* 350 cm^{-1} (anharmonic) and caused by coupling of hydrogen transfer with internal rotation of the Cp and SiMe₃ groups.

The frequencies obtained by solving the one-dimensional Schrödinger equation (1D) without taking into account the coupling between the X , Y , and Z coordinates are referred to in Table 4.2 as uncoupled frequencies. In the case of **Tp1**, **Tp3**, and **Cp9**, the coupled (3D) and uncoupled (1D) results are quite close, indicating the lack of coupling between hydrogen transfer and Si–Si vibrations. Hence, no coupling is present either. For **Tp2**, however, the difference between 1D and 3D parts is quite large, manifesting the coupling between X and Z coordinates. In mechanistic terms, the lack of coupling corresponds to a direct hydrogen transfer *without assistance of the Si–Si motion*, while when the coupling is present, the hydrogen transfer mainly occurs by way of Si–Si contraction.

4.6.2 Three-dimensional vibrational wavefunctions

Contour plots of the three-dimensional PES and those of the two-dimensional probability density in coordinates X , Z (see Equation 4.62) are presented in Figure 4.7. The minimum energy path on the PES as well as the maximum wavefunction path are shown.

For complex **Tp1**, having a double-well potential with an extremely low barrier ($\Delta E = 0.03 \text{ kcal}\cdot\text{mol}^{-1}$), the ground-state vibrational wavefunction has a single maximum corresponding to a symmetric structure, shifted by 0.156 Å away from the PES minimum. Consequently, the hydrogen is *delocalized* between two silicon atoms and the

Table 4.2: Fundamental frequencies (in cm^{-1}) obtained by harmonic analysis, by solving the three-dimensional vibrational Schrödinger equation (3D), and by solving the one-dimensional Schrödinger equation for the one-dimensional part of the potential without taking into account the coupling (1D). $\nu(H_x)$ and $\nu(H_y)$ are hydrogen vibrational frequencies; $\nu(Si - Si)$ is the frequency of silicon-silicon vibrations. ΔE is the hydride transfer barrier (in $\text{kcal}\cdot\text{mol}^{-1}$).

Complex	Vibration	Harmonic frequency	Anharmonic frequency		ΔE
			1D	3D	
Tp1	$\nu(H_x)$	789	358	288	0.03
	$\nu(H_y)$	2122	2032	1964	
	$\nu(Si - Si)$	341	315	310	
Tp2	$\nu(H_x)$	1244	95	473, 749*	1.13
	$\nu(H_y)$	1968	2032	1792	
	$\nu(Si - Si)$	137	337	287	
Tp3	$\nu(H_x)$	914	153	118	0.25
	$\nu(H_y)$	2122	2102	2029	
	$\nu(Si - Si)$	416	240	232	
Cp9	$\nu(H_x)$	571	666	537	0.64
	$\nu(H_y)$	2149	2136	2081	
	$\nu(Si - Si)$	65	333	350	

*Two values due to tunneling splitting; see text.

highest likelihood of finding it is in the symmetric configuration. The tiny barrier does not affect the hydrogen motion. The spatial extent (see Equation 4.63) along X coordinate, which is the average deviation of the hydrogen from the symmetric point, is ± 0.185 Å.

For complex **Tp2**, with a double-well potential and a relatively large barrier ($\Delta E = 1.13$ kcal·mol⁻¹), the vibrational wavefunction has two well separated maxima, which are shifted from the PES minima by some 0.05 Å. The maximum wavefunction path does not exactly coincide with the minimum energy path, the former being less bent. Therefore, the coupling between the H motion (X coordinate) and Si–Si motion (Z coordinate) is significant, but tunneling is also considerable in this system. It can be seen from the minimum value of probability density on the maximum wavefunction path, which is 24% of the value at the maximum. This indicates that the hydrogen is well *localized* in the areas of the potential minima.

For complex **Tp3** (a double-well potential and a low barrier of 0.25 kcal·mol⁻¹), the vibrational wavefunction has two weakly pronounced maxima separated by 0.133 Å from the respective PES minima, lying rather close to the TS. The maximum wavefunction path in this case is a virtually straight line that lies very close to the minimum energy path which is also scarcely bent. This shows that in this case no Si–Si motion is necessary to effect the hydrogen transfer. The minimum value of the probability density on the maximum wavefunction path is 98% of its value at the maximum. Thus, the predominant transfer mechanism is the *tunneling*. The hydrogen motion is delocalized and the spatial extent $\bar{X} = \pm 0.214$ Å is larger than that of **Tp1**, showing larger degree of delocalization. We conclude that **Tp3** is an intermediate case between one- and two-maxima wavefunctions.

For complex **Cp9** (a double-well potential and an intermediate barrier of 0.64 kcal·mol⁻¹) the vibrational wavefunction has a single maximum corresponding to a symmetric structure, similarly to complex **Tp1**. This maximum is located 0.283 Å from the PES minimum.

Despite a far larger barrier compared to complex **Tp1**, the hydrogen is delocalized, with a peak of probability density in the symmetric configuration. This can be accounted for by proximity of the two minima on the PES which are separated just by 0.28 Å. It can be rationalized in terms of the tunneling, which is known to depend exponentially on barrier width, as illustrated by a relatively small wavefunction spatial extent of ± 0.116 Å.

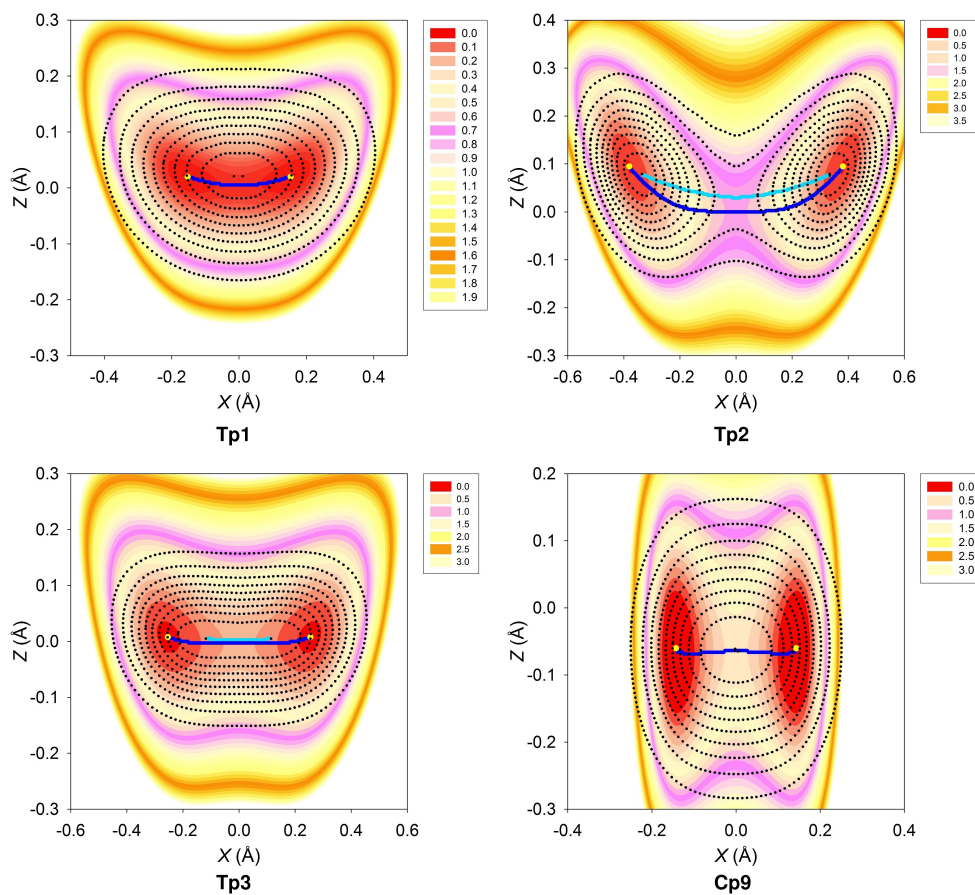


Figure 4.7: The PES and probability density contour plots for complexes **Tp1–Tp3** and **Cp9** in the coordinates $X - Z$. Notations are the same as in Figure 4.3.

4.6.3 $J(\text{Si-H})$ coupling constants

To estimate the influence of hydride vibrations on the $J(\text{Si-H})$ spin-spin coupling constant rigorously, the following integral has to be computed:

$$\langle J \rangle = \iiint |\Psi(X, Y, Z)|^2 J(X, Y, Z) dX dY dZ, \quad (4.64)$$

where $\langle J \rangle$ is the average spin-spin coupling constant, $J(X, Y, Z)$ is the spin-spin coupling constant corresponding to a particular geometrical configuration (X, Y, Z) , and $\Psi(X, Y, Z)$ is the ground-state vibrational wavefunction. At a finite temperature, excited-state wavefunctions would be needed as well. Since the integration itself would involve a prior calculation of $J(\text{Si-H})$ at very many molecular configurations, it is replaced by a finite summation over a limited number N of configurations (see Equation 4.65).

$$\langle J \rangle = \frac{\sum_{m=1}^N |\Psi(X_m, Y_m, Z_m)|^2 J(X_m, Y_m, Z_m)}{\sum_{m=1}^N |\Psi(X_m, Y_m, Z_m)|^2}. \quad (4.65)$$

Owing to this approximation, our results should be regarded as semi-quantitative. The results and their comparison with “static” $J(\text{Si}^1\text{-H})$ and $J(\text{Si}^2\text{-H})$ values in the minima are represented in Table 4.3. Two versions of averaged J are given: the first one corresponds to the local vibration around a minimum ($\langle J(\text{Si}^1\text{-H}) \rangle$ and $\langle J(\text{Si}^2\text{-H}) \rangle$), the second, denoted $\langle J \rangle$, to the delocalized motion or fluctuational behavior. The latter one is essentially an arithmetic mean of the former.

For complexes **Tp1**, and **Cp9**, both $J(\text{Si}^1\text{-H})$ and $J(\text{Si}^2\text{-H})$ are negative, thus corroborating the existence of the double $\text{Si}\cdots\text{H}\cdots\text{Si}$ interaction. The same is true even for complex **Tp3**, where the $\text{Si}^2\cdots\text{H}$ separation is more than 2.3 Å and the Mayer bond order is nearly

vanishing. However, for complex **Tp2**, $J(\text{Si}^2\text{-H})$ is slightly positive, meaning that the lack of the direct interaction, for the $\text{Si}\cdots\text{H}$ separation of 2.41 Å is very large in this case.

For complexes **Tp1**, **Tp2**, and **Cp9**, there is no large difference between spin-spin coupling constant J_{min} in the minimum and corresponding averaged values $\langle J(\text{Si}^1\text{-H}) \rangle$ and $\langle J(\text{Si}^2\text{-H}) \rangle$. However, for complex **Tp3** taking the vibrations into account results to a nearly double value of $J(\text{Si}^2\text{-H})$. This is accounted for by the fact that the vibrational wavefunction is quite large both near the minima and near the transition state. This increases the probability of finding the hydride at $\text{Si}^2\cdots\text{H}$ distances smaller than the equilibrium one, leading to a higher $\langle J(\text{Si}^2\text{-H}) \rangle$.

$\langle J \rangle$ turns out to be quite close to the arithmetic mean of the *local* spin-spin coupling constants $J(\text{Si}^1\text{-H})$ and $J(\text{Si}^2\text{-H})$ in minima. This provides a justification of the common procedure of computing coupling constants for fluctuational molecules as weighted average of the values calculated in PES minima.

Table 4.3: Averaged spin-spin coupling constants $\langle J \rangle$ (in Hertz) obtained taking into account vibrational motion, and static spin-spin coupling constants in the corresponding minima J_{min} .

	J_{min}		$J_{averaged}$		$\langle J \rangle$
	$J(\text{Si}^1\text{-H})$	$J(\text{Si}^2\text{-H})$	$\langle J(\text{Si}^1\text{-H}) \rangle$	$\langle J(\text{Si}^2\text{-H}) \rangle$	
Tp1	-55.01	-13.11	-54.29	-16.42	-35.32
Tp2	-73.64	+2.09	-76.18	+0.89	-37.66
Tp3	-136.28	-15.47	-123.93	-29.44	-76.67
Cp9	-17.87	-8.32	-19.35	-8.66	-13.96

4.7 Si...H interligand interactions in cobalt(V) and iridium(V) bis(silyl)bis(hydride) complexes

The principal question we address in this part is whether any kind of Si...H interactions exists in $\text{Cp}^*\text{M}(\text{H})_2(\text{SiR}_3)_2$ complexes of cobalt and iridium. No experimental evidence for Si...H interactions was reported¹⁶⁸ for the cobalt complex $\text{Cp}^*\text{Co}(\text{H})_2(\text{SiPh}_2\text{H})_2$. In the analogous rhodium $\text{Cp}^*\text{Rh}(\text{H})_2(\text{SiEt}_3)_2$ ¹⁵¹ and iridium $\text{Cp}^*\text{Ir}(\text{H})_2(\text{SiEt}_3)_2$ ¹⁵⁶ complexes weak Si-H coupling was detected, although it was through-bond Si-M-H coupling rather than a direct Si...H interaction. The $^2J(\text{Si-H})$ spin-spin coupling constant for the rhodium complex is 7.8 Hz. However, significant Si...H interactions are present in the related rhodium complex $\text{CpRh}(\text{H})_2(\text{SiMe}_3)_2$ ¹¹⁴ as it showed by quantum-chemical calculations. Similarly, $\text{Cp}(\text{CO})\text{Fe}(\text{H})(\text{SiR}_3)_2$ complexes, that used to be considered as classical, were eventually shown to have Si...H...Si interactions.¹²¹

In order to understand in depth the bonding situation in the bis(silyl)bis(hydride) complexes, we have performed quantum-chemical calculations of $\text{Cp}^*\text{M}(\text{H})_2(\text{SiR}_3)_2$ complexes ($\text{M} = \text{Co}$ or Ir) with various substituents R, including σ -donating ($\text{R} = \text{Me}$), π -donating σ -accepting ($\text{R} = \text{halogen}$) and σ -accepting ($\text{R} = \text{CF}_3$) ones (see Figure 4.8).

Apparently, the interatomic distances alone are not sufficient to detect or characterize a presence of a residual Si...H interactions, and, as indicators of a possible Si...H interactions, Wiberg bond indices²⁴² and NMR spin-spin coupling constants $J(\text{Si-H})$ were calculated.

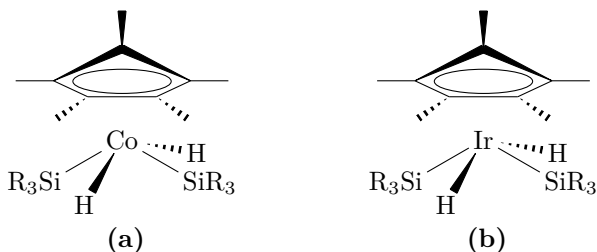


Figure 4.8: Cobalt and iridium candidates for Si–H interactions. (a) $\text{SiR}_3 = \text{SiPh}_2\text{H}$ (**Co1**); SiMe_3 (**Co2**); SiH_3 (**Co3**); SiF_3 (**Co4**); SiCl_3 (**Co5**); SiBr_3 (**Co6**); $\text{Si}(\text{CF}_3)_3$ (**Co7**); (b) $\text{SiR}_3 = \text{SiEt}_3$ (**Ir1**); SiMe_3 (**Ir2**); SiH_3 (**Ir3**); SiF_3 (**Ir4**); SiCl_3 (**Ir5**); SiBr_3 (**Ir6**); $\text{Si}(\text{CF}_3)_3$ (**Ir7**).

4.7.1 Wiberg bond indices and spin-spin coupling constants

Generally, calculated spin-spin coupling constants reflect the same bonding picture as the WBI, although some deviations do exist (see Table 4.4). In **Co2** and **Co5** both $J(\text{Si}^1-\text{H}^2)$ and $J(\text{Si}^2-\text{H}^2)$ are positive, suggesting no significant bonding. For complex **Co1**, $J(\text{Si}-\text{H})$ for Si^1-H^1 , Si^2-H^1 , and Si^2-H^2 exhibit negative values, confirming direct $\text{Si}\cdots\text{H}$ interactions, but Si^1-H^2 (the longest of the four) is slightly positive. Complex **Co4**, which has SiF_3 ligands, exhibit rather high negative $J(\text{Si}-\text{H})$, indicative of substantial direct $\text{Si}\cdots\text{H}$ interactions, although the corresponding WBI are relatively low. This remarkable increase in $J(\text{Si}-\text{H})$ can be accounted for by an increase in the s character of the residual $\text{Si}-\text{H}$ bond due to Bent’s rule. In the case of **Co6** and **Co7** strongly negative $J(\text{Si}^1-\text{H}^1)$ and $J(\text{Si}^1-\text{H}^2)$ spin-spin coupling constants undoubtedly manifest the corresponding residual interactions, while large positive $J(\text{Si}^2-\text{H}^1)$ and $J(\text{Si}^2-\text{H}^2)$ clearly show the absent of another two interactions.

Table 4.4: Si–H WBI and $J(\text{Si–H})$ spin-spin coupling constants (in Hz) for complexes **Co1–Co7**. Si–H distances are given in ångströms.

Complex		Distance	WBI	$J(\text{Si–H})$
Co1	Si ¹ –H ¹	2.210	0.109	-2.1
	Si ¹ –H ²	2.246	0.101	6.8
	Si ² –H ¹	2.080	0.136	-5.0
	Si ² –H ²	2.106	0.134	-13.4
Co2	Si ¹ –H ¹	2.110	0.126	-3.1
	Si ¹ –H ²	2.229	0.102	4.6
	Si ² –H ¹	2.110	0.126	-3.1
	Si ² –H ²	2.229	0.102	4.6
Co3	Si ¹ –H ¹	2.100	0.123	-3.5
	Si ¹ –H ²	2.128	0.115	-1.5
	Si ² –H ¹	2.100	0.123	-3.5
	Si ² –H ²	2.128	0.115	-1.5
Co4	Si ¹ –H ¹	2.067	0.102	-30.8
	Si ¹ –H ²	2.126	0.091	-24.3
	Si ² –H ¹	2.067	0.102	-30.8
	Si ² –H ²	2.126	0.091	-24.3
Co5	Si ¹ –H ¹	2.077	0.119	-9.5
	Si ¹ –H ²	2.229	0.094	1.5
	Si ² –H ¹	2.077	0.119	-9.5
	Si ² –H ²	2.229	0.094	1.5
Co6	Si ¹ –H ¹	1.921	0.177	-42.2
	Si ¹ –H ²	1.923	0.176	-42.2
	Si ² –H ¹	2.385	0.062	32.6
	Si ² –H ²	2.378	0.063	33.0
Co7	Si ¹ –H ¹	1.893	0.211	-46.0
	Si ¹ –H ²	1.904	0.210	-45.0
	Si ² –H ¹	2.466	0.059	22.0
	Si ² –H ²	2.495	0.059	21.5

In the case of iridium complexes, the WBI is significantly lower than for their cobalt counterparts, (0.09-0.12 for $\text{Si}^{1,2}-\text{H}^1$ distances, 0.10-0.08 for $\text{Si}^{1,2}-\text{H}^2$ distances (see Table 4.5). Albeit quite low, the WBI clearly correlates with Si-H distances within every given complex. The calculated spin-spin coupling constants (Table 4.5) for complexes **Ir1–Ir3** and **Ir7** are small and positive. Altogether, these data demonstrate nonexistence of direct $\text{Si}\cdots\text{H}$ interactions in the above complexes. In contrast, $J(\text{Si}-\text{H})$ in complexes **Ir5** and **Ir6** are slightly negative pointing out a remaining very weak $\text{Si}\cdots\text{H}$ interaction. Complex **Ir4**, having SiF_3 ligands, exhibits, similarly to **Co4**, substantially negative $J(\text{Si}-\text{H})$, in spite of low WBI and quite large interatomic separation, which suggest a presence of some $\text{Si}\cdots\text{H}$ interactions.

Table 4.5: Si–H WBI and $J(\text{Si–H})$ spin-spin coupling constants (in Hz) for complexes **Ir1–Ir7**. Si–H distances are given in ångströms.

Complex		Distance	WBI	$J(\text{Si–H})$
Ir1	Si ¹ –H ¹	2.297	0.115	1.4
	Si ¹ –H ²	2.384	0.100	3.0
	Si ² –H ¹	2.297	0.115	1.4
	Si ² –H ²	2.384	0.100	3.0
Ir2	Si ¹ –H ¹	2.282	0.112	1.6
	Si ¹ –H ²	2.375	0.096	3.6
	Si ² –H ¹	2.282	0.112	1.6
	Si ² –H ²	2.375	0.096	3.6
Ir3	Si ¹ –H ¹	2.285	0.111	2.3
	Si ¹ –H ²	2.304	0.104	3.1
	Si ² –H ¹	2.285	0.111	2.3
	Si ² –H ²	2.304	0.104	3.1
Ir4	Si ¹ –H ¹	2.258	0.089	-15.5
	Si ¹ –H ²	2.305	0.080	-11.3
	Si ² –H ¹	2.258	0.089	-15.5
	Si ² –H ²	2.305	0.080	-11.3
Ir5	Si ¹ –H ¹	2.265	0.107	-5.2
	Si ¹ –H ²	2.393	0.089	-0.5
	Si ² –H ¹	2.265	0.107	-5.2
	Si ² –H ²	2.393	0.089	-0.5
Ir6	Si ¹ –H ¹	2.263	0.110	-0.7
	Si ¹ –H ²	2.430	0.088	3.3
	Si ² –H ¹	2.263	0.110	-0.7
	Si ² –H ²	2.430	0.088	3.3
Ir7	Si ¹ –H ¹	2.344	0.103	0.5
	Si ¹ –H ²	2.425	0.093	2.5
	Si ² –H ¹	2.323	0.109	0.0
	Si ² –H ²	2.413	0.095	1.5

Chapter 5

Conclusions

Here the results obtained in previous chapters are summarized:

First: The first part of this work presents a study of intramolecular hydrogen bonds in proton sponge cations **PS1–PS8**. Three different situations were found at MP2 level: systems with a single-well potential (cations **PS1–PS2**), systems with a double-well potential and low barrier (cations **PS3–PS5**), and systems with double-well potential and high barrier (cations **PS6–PS8**). In general, short N...N distances and long N–H distances correspond to single-well or low-barrier potential.

A number of density functionals were tested and the results were compared with those obtained by MP2, which is considered as a reference method. These tests demonstrate that B3LYP, MPWB1K, and MPW1B95 functionals tend to underestimate the strength of the hydrogen bonds, consequently giving shorter N-H bonds and strongly overestimating the hydrogen transfer barrier. Moreover, in some cases these functionals incorrectly yield two-well potential. On the contrary, the PBEPBE functional both performs quite well for geometries and reasonably

reproduces the MP2 potential energy surface. Nevertheless, the PBEPBE somewhat underestimates the barrier.

For the further study of the proton dynamic behavior we selected one example with a single-well potential (cation **PS1**), one with a small barrier (cation **PS4**), and two with higher barriers (cations **PS6** and **PS7**). For these four cations the three-dimensional potential energy surfaces were constructed. The vibrational Schrödinger equation was solved in these potentials as well as for the model system **PS6pbe**. The PES is highly anharmonic in all these cases and the harmonic analysis yields incorrect frequencies.

The analysis of the ground-state wavefunction in these systems allows to classify the proton sponge cations according to the character of the hydrogen motion in them. Cations with a single-well potential (**PS1**) or a very low barrier (**PS4**) exhibit a single-maximum vibrational wave-function. In contrast, the wavefunction for a system with a higher barrier, such as cation **PS7** ($\Delta E_e = 3.4 \text{ kcal}\cdot\text{mol}^{-1}$) has two distinct maxima, manifesting localized proton motion. The borderline between proton sponges with a single-maximum wavefunction and those with a double maximum lies at ΔE_e barrier about $1.5 \text{ kcal}\cdot\text{mol}^{-1}$, as illustrated by cation **PS6pbe**, whose wavefunction has two very weakly pronounced maxima. Of course, this borderline is tentative, as the character of the wavefunction also depends upon the shape of the PES, in particular, upon the coupling with the N...N coordinate. To summarize, the proton motion in cations **PS1–PS5** should be deemed delocalized, in cation **PS7–PS8** localized, and in cation **PS6** partly localized.

The maximum-wavefunction path is rather straight and deviates strongly from the minimum-energy path for the cations with delocalized proton behavior, but is substantially curved for the

cations with localized proton, indicating strong coupling between the H and N \cdots N coordinates.

Second: This work demonstrates that rhodium bis(silyl)hydride complexes tend to form an asymmetric arrangement of silyl and hydride ligands with two different Si \cdots H distances. Nevertheless, in many cases the hydride ligand simultaneously interacts with both silyls. The hydride can be transferred from one silyl to the other, with energy barriers varying from 0 to 4 kcal \cdot mol $^{-1}$.

Various density functionals and the MP2 method yield substantially different geometries of the bis(silyl)hydride complexes. Hence, care must be exercised when choosing a method for production calculations. In some cases the M06L and M062X functionals underestimate the Si–H distances, while TPSSh sometimes tends to overestimate them. MP2, B3LYP, and BP86 overestimate them in nearly all cases, whereas B3LYP in some cases incorrectly yields an end-on η^1 -silyl coordination. By comparison with the single-point CCSD results we conclude that the TPSSh and M06L functionals usually perform better than the other methods.

For the complexes under study, the hydrogen transfer barrier varies between 0 and 3.4 kcal \cdot mol $^{-1}$. The Cp complexes typically have higher barriers than the Tp complexes. Among the complexes with a relatively low barrier (0–1.5 kcal \cdot mol $^{-1}$), somewhat smaller values are found for complexes with a shorter Si \cdots Si distance. However, for the entire set of Cp and Tp complexes, the hydrogen transfer barrier does not obviously correlate with geometry parameters.

To study the hydrogen dynamics in the Si \cdots H \cdots Si fragment, four complexes with relatively low hydrogen transfer barriers were selected. The three-dimensional PES were constructed and the

vibrational Schrödinger equation was solved in the resulting potentials. The PES turns out to be highly anharmonic for all these complexes, as demonstrated by much lower anharmonic vibrational frequencies compared to those computed within the harmonic approximation.

Based on the analysis of the ground-state vibrational wavefunctions in these systems, a classification of the complexes according to the character of the hydrogen motion can be proposed. A *single-maximum* vibrational wavefunction, corresponding to hydrogen *delocalization* between both silyls, is found in complexes with a single-well potential or with a very low barrier such as **Tp1** ($\Delta E = 0.03 \text{ kcal}\cdot\text{mol}^{-1}$). The delocalized hydride behavior can occur also in the case of a significant barrier, if both minima and the transition states are located on the PES in a close proximity to each other, as is the case for the complex **Cp9** ($\Delta E = 0.64 \text{ kcal}\cdot\text{mol}^{-1}$).

On the contrary, in the systems with a relatively high barrier, such as **Tp2** ($\Delta E = 1.13 \text{ kcal}\cdot\text{mol}^{-1}$), the hydride behaves as a classical particle, as manifested by a wavefunction with two well separated maxima localized near the PES minima. The hydrogen transfer is coupled with Si–Si motion in this case.

An intermediate situation between localized and delocalized hydride behavior is also possible, when the vibrational wavefunction has two weakly pronounced maxima. In this case there is virtually no coupling between the H and Si–Si motion, with tunneling accounting for a large part of the hydrogen transfer. The maximum-wavefunction path is a straight line showing that the hydrogen transfer is independent from the Si–Si distance contraction. The example is the complex **Tp3** ($\Delta E = 0.25 \text{ kcal}\cdot\text{mol}^{-1}$).

In the complexes **Tp1**, **Tp3**, and **Cp9** both spin-spin coupling constants $J(\text{Si}^1\text{-H})$ and $J(\text{Si}^2\text{-H})$ are negative, which is indicative of direct simultaneous $\text{Si}\cdots\text{H}\cdots\text{Si}$ interactions. Conversely, $J(\text{Si}^2\text{-H})$ for complex **Tp2** is slightly positive indicating the absence of a $\text{Si}^2\cdots\text{H}$ interaction. The vibrationally averaged spin-spin coupling constants are quite close to the arithmetic mean of $J(\text{Si}^1\text{-H})$ and $J(\text{Si}^2\text{-H})$, which justifies the widely used procedure of calculating $\langle J \rangle$ by averaging the corresponding values in the minima.

Third: This work demonstrates that $\text{Cp}^*\text{Co}(\text{H})_2(\text{SiR}_3)_2$ complexes tend to form a ligand arrangement with two equivalent relatively short Si-H distances ($\text{Si}^1\text{-H}^1$ and $\text{Si}^2\text{-H}^1$), and two other equivalent longer Si-H distances ($\text{Si}^1\text{-H}^2$ and $\text{Si}^2\text{-H}^2$). In other words, both silyls are located substantially closer to one and the same hydride.

Based on molecular structures as well as Wiberg bond indices and $J(\text{Si-H})$ spin-spin coupling constants, at least two residual $\text{Si}\cdots\text{H}$ interaction in **Co1**, **Co2**, **Co5**, **Co6**, **Co7** and all four $\text{Si}\cdots\text{H}$ interactions in **Co3** and **Co4** have been detected. The $\text{Si}\cdots\text{H}$ interaction in the SiBr_3 -containing complex **Co6** is quite strong and is of IHI nature, while **Co7** may be considered as complex with one silyl and one “silicate” ligand $[\text{H}\cdots\text{Si}(\text{CF}_3)_3\cdots\text{H}]^-$.

The analogous iridium complexes $\text{Cp}^*\text{Ir}(\text{H})_2(\text{SiR}_3)_2$, on the contrary, are classical iridium(V) bis(silyl)bis(hydride) complexes with only rudimentary $\text{Si}\cdots\text{H}$ interactions, if any. The SiF_3 -containing complex **Ir4** is an exception with noticeable (though still weak) $\text{Si}\cdots\text{H}$ interactions.

Appendix A

Hydrogen motion in proton sponge cations: A theoretical study

Y. Horbatenko, S. F. Vyboishchikov. "Hydrogen Motion in Proton Sponge Cations: A Theoretical Study". *Chem. Phys. Chem.* Vol. 12, issue 6 (April 2011) : 1118–1129. DOI: 10.1002/cphc.201000721

<http://dx.doi.org/10.1002/cphc.201000721>

<http://onlinelibrary.wiley.com/doi/10.1002/cphc.201000721/full>

Article first published online: 22 MAR 2011

Abstract

This work presents a study of intramolecular NHN hydrogen bonds in cations of the following proton sponges: 2,7-bis(trimethylsilyl)-1,8-bis(dimethylamino)naphthalene (1), 1,6-diazabicyclo[4.4.4.]tetradecane (2), 1,9-bis(dimethylamino)dibenzoselenophene (3), 1,9-bis(dimethylamino)dibenzothiophene (4), 4,5-bis(dimethylamino)fluorene (5), quino[7,8-h]quinoline (6) 1,2-bis(dimethylamino)benzene (7), and 1,12-bis(dimethylamino)benzo[c]phenantrene (8). Three different patterns were found for proton motion: systems with a single-well potential (cations 1–2), systems with a double-well potential and low proton transfer barrier, ΔE_e (cations 3–5), and those with a double-well potential and a high barrier (cations 6–8). Tests of several density functionals indicate that the PBEPBE functional reproduces the potential-energy surface (PES) obtained at the MP2 level well, whereas the B3LYP, MPWB1K, and MPW1B95 functionals overestimate the barrier. Three-dimensional PESs were constructed and the vibrational Schrödinger equation was solved for selected cases of cation 1 (with a single-well potential), cation 4 (with a ΔE_e value of 0.1 kcal mol⁻¹ at the MP2 level), and cations 6 ($\Delta E_e=2.4$ kcal mol⁻¹) and 7 ($\Delta E_e=3.4$ kcal mol⁻¹). The PES is highly anharmonic in all of these cases. The analysis of the three-dimensional ground-state vibrational wave function shows that the proton is delocalized in cations 1 and 4, but is rather localized around the energy minima for cation 7. Cation 6 is an intermediate case, with two weakly pronounced maxima and substantial tunneling. This allows for classification of proton sponge cations into those with localized and those with delocalized proton behavior, with the borderline between them at ΔE_e values of about 1.5 kcal mol⁻¹.

The excited vibrational states of proton sponge cations with a low barrier can be described within the framework of a simple particle-in-a-box model. Each cation can be assigned an effective box width.

Keywords

ab initio calculations; hydrogen bonding; potential-energy hypersurfaces; proton sponges; vibrational Schrödinger equation

Appendix B

Dynamic behavior of hydrogen in transition metal bis(silyl)hydride complexes

Y. Horbatenko, S. F. Vyboishchikov. "Dynamic Behavior of Hydrogen in Transition Metal Bis(silyl) Hydride Complexes". *Organometallics*. Vol. 32, issue 2 (2013) : 514–426. DOI: 10.1021/om300981y

<http://dx.doi.org/10.1021/om300981y>

<http://pubs.acs.org/doi/abs/10.1021/om300981y>

Received: October 19, 2012

Published: January 9, 2013

Abstract

A series of rhodium complexes $\text{CpRh}(\text{SiMe}_2\text{X})_2(\text{SiMe}_3)(\text{H})$ ($\text{X} = \text{Me, Cl, Br, I}$), Cp1–Cp4 , $\text{CpRh}(\text{SiMe}_2\text{X})_2(\text{PMe}_3)(\text{H})^+$ ($\text{X} = \text{Me, Cl, Br, I}$), Cp5–Cp8 , $\text{CpRh}(\text{SiMe}_3)_2(\text{SiF}_3)(\text{H})$, Cp9 , $\text{CpRh}(\text{SiMe}_3)_2(\text{SiH}_3)(\text{H})$, Cp10 , $\text{TpRh}(\text{SiH}_3)_2(\text{SiMe}_3)(\text{H})$, Tp1 , $\text{TpRh}(\text{SiH}_3)_2(\text{PMe}_3)(\text{H})^+$, Tp2 , and $\text{TpRh}(\text{SiF}_3)_2(\text{PMe}_3)(\text{H})^+$, Tp3 , were studied computationally to understand the hydrogen behavior in the $\text{Si}\cdots\text{H}\cdots\text{Si}$ moiety. The hydride ligand interacts with at least one of the silyls, and in many cases with both, but is located asymmetrically with regard to them, giving rise to a double-well potential energy surface (PES) for hydrogen motion. The hydrogen transfer barriers ΔE vary from 0.03 to 3 $\text{kcal}\cdot\text{mol}^{-1}$. For selected complexes Tp1 , Tp2 , Tp3 , and Cp9 the three-dimensional PESs were constructed and the vibrational Schrödinger equation was solved. The PES is highly anharmonic in all four cases. The hydrogen is delocalized between two silicons in complexes Tp1 , Tp3 , and Cp9 , but localized around the energy minima in complex Tp2 . Complex Tp3 is an intermediate case with a substantial tunneling. The delocalized behavior is pertinent to systems with $\Delta E < 0.25 \text{ kcal}\cdot\text{mol}^{-1}$. For complexes Tp1 , Tp2 , Tp3 , and Cp9 the $J(\text{Si–H})$ spin–spin coupling constants were calculated taking into account the vibrational motion of hydride. For Tp1 , Tp3 , and Cp9 both $J(\text{Si}^1\text{–H})$ and $J(\text{Si}^2\text{–H})$ are negative due to simultaneous $\text{Si}^1\cdots\text{H}\cdots\text{Si}^2$ interactions, while for Tp2 $J(\text{Si}^2\text{–H})$ is positive, indicating a single $\text{Si}\cdots\text{H}$ interaction only. Negative $J(\text{Si–H})$ values were obtained even for $\text{Si}\cdots\text{H}$ distances as large as 2.3 Å (complex Tp3). A possible effect of vibrations on the $J(\text{Si–H})$ values is also discussed.

Appendix C

**Si...H interligand
interactions in cobalt(V) and
iridium(V)
bis(silyl)bis(hydride)
complexes**

Y. Horbatenko, S. F. Vyboishchikov. "Si...H interligand interactions in cobalt(V) and iridium(V) bis(silyl)bis(hydride) complexes". ChemPlusChem. Vol. 78, issue 9 (September 2013) : 1073–1081. DOI: 10.1002/cplu.201300174

<http://dx.doi.org/10.1002/cplu.201300174>

<http://onlinelibrary.wiley.com/doi/10.1002/cplu.201300174/full>

Article first published online: 16 JUL 2013

Abstract

A series of bis(silyl)bis(hydride) cobalt complexes $[\text{Cp}^*\text{Co}(\text{H})_2(\text{SiR}_3)_2]$ (Cp^* =pentamethylcyclopentadienyl; $\text{SiR}_3=\text{SiPh}_2\text{H}$, SiMe_3 , SiH_3 , SiF_3 , SiCl_3 , SiBr_3 , $\text{Si}(\text{CF}_3)_3$; Co1–Co7) as well as the analogous iridium complexes $[\text{Cp}^*\text{Ir}(\text{H})_2(\text{SiR}_3)_2]$ ($\text{SiR}_3=\text{SiEt}_3$, SiMe_3 , SiH_3 , SiF_3 , SiCl_3 , SiBr_3 , $\text{Si}(\text{CF}_3)_3$; Ir1–Ir7) were studied to detect possible residual Si...H interactions. Tests of several density functionals by comparison with coupled-cluster results indicate that the TPSSh functional performs better than B3LYP, BP86, M06, M06L, and PBEPBE. Based on molecular structures, as well as Wiberg bond indices and $J(\text{Si},\text{H})$ spin–spin coupling constants as indicators of a possible Si...H interaction, at least two residual Si...H interactions in Co2, Co5, and all four possible Si...H interactions in Co3 and Co4 have been detected. Co6 and Co7 exhibit stronger Si...H bonding than the other complexes studied. On the contrary, the iridium complexes Ir1–Ir3 and Ir5–Ir7 are classical iridium(V) bis(silyl)bis(hydride) complexes with only rudimentary Si...H interactions, if any.

Keywords

ab initio calculations; cobalt; hydride ligands; iridium; silyl ligands

Bibliography

- [1] Alder, R. W.; Bowman, P. S.; Steele, W. R. S.; Winterman, D. R. *Chem. Commun.* **1968**, 723–724.
- [2] Alder, R. W. *Chem. Rev.* **1989**, *89*, 1215–1223.
- [3] Raab, V.; Kipke, J.; Gschwind, R. M.; Sundermeyer, J. *Chem. Eur. J.* **2002**, *8*, 1682–1693.
- [4] Raab, V.; Harms, K.; Sundermeyer, J.; Kovačević, B.; Maksić, Z. B. *The J. Org. Chem.* **2003**, *68*, 8790–8797.
- [5] Raab, V.; Gauchenova, E.; Merkoulov, A.; Harms, K.; Sundermeyer, J.; Kovačević, B.; Maksić, Z. B. *J. Am. Chem. Soc.* **2005**, *127*, 15738–15743.
- [6] Staab, H. A.; Kriege, C.; Hieber, G.; Oberdorf, K. *Angew. Chem. Int. Ed.* **1997**, *36*, 1884–1886.
- [7] Rodriguez, I.; Sastre, G.; Corma, A.; Iborra, S. *Journal of Catalysis* **1999**, *183*, 14–23.
- [8] Taggi, A. E.; Hafez, A. M.; Wack, H.; Young, B.; Ferraris, D.; Lectka, T. *J. Am. Chem. Soc.* **2002**, *124*, 6626–6635.

- [9] Hughes, R. P.; Kovacic, I.; Lindner, D. C.; Smith, J. M.; Willemsen, S.; Zhang, D.; Guzei, I. A.; Rheingold, A. L. *Organometallics* **2001**, *20*, 3190–3197.
- [10] Holub, J.; Wille, A. E.; Stibr, B.; Carroll, P. J.; Sneddon, L. G. *Inorg. Chem.* **1994**, *33*, 4920–4926.
- [11] Shedlow, A. M.; Carroll, P. J.; Sneddon, L. G. *Organometallics* **1995**, *14*, 4046–4047.
- [12] Wille, A. E.; Su, K.; Carroll, P. J.; Sneddon, L. G. *J. Am. Chem. Soc.* **1996**, *118*, 6407–6421.
- [13] Kakiuchi, K.; Nakamura, I.; Matsuo, F.; Nakata, M.; Ogura, M.; Tobe, Y.; Kurosawa, H. *J. Org. Chem.* **1995**, *60*, 3318–3333.
- [14] Gaines, D. F.; Bridges, A. N.; Hayashi, R. K. *Inorg. Chem.* **1994**, *33*, 1243–1244.
- [15] Charmant, J. P.; Lloyd-Jones, G. C.; Peakman, T. M.; Woodward, R. L. *Tetrahedron Lett.* **1998**, *39*, 4733–4736.
- [16] H. Charmant, J. P.; Lloyd-Jones, G. C.; Peakman, T. M.; Woodward, R. L. *Eur. J. Org. Chem.* **1999**, *1999*, 2501–2510.
- [17] Mazaleyrat, J.-P.; Wright, K. *Tetrahedron Lett.* **2008**, *49*, 4537–4541.
- [18] Pietrzak, M.; Try, A. C.; Andrioletti, B.; Sessler, J. L.; Anzenbacher, P.; Limbach, H.-H. *Angew. Chem. Int. Ed.* **2008**, *47*, 1123–1126.
- [19] Pietrzak, M.; Wehling, J. P.; Kong, S.; Tolstoy, P. M.; Shenderovich, I. G.; Lopez, C.; Claramunt, R. M.; Elguero, J.; Denisov, G. S.; Limbach, H.-H. *Chem. Eur. J.* **2010**, *16*, 1679–1690.

- [20] Perrin, C. L.; Ohta, B. K. *J. Am. Chem. Soc.* **2001**, *123*, 6520–6526.
- [21] Woźniak, K.; Krygowski, T. M.; Pawlak, D.; Kolodziejski, W.; Grech, E. *J. Phys. Org. Chem.* **1997**, *10*, 814–824.
- [22] Malarski, Z.; Sobczyk, L.; Grech, E. *J. Mol. Struct.* **1988**, *177*, 339–349.
- [23] Głowiak, T.; Malarski, Z.; Sobczyk, L.; Grech, E. *J. Mol. Struct.* **1992**, *270*, 441–447.
- [24] Głowiak, T.; Majerz, I.; Malarski, Z.; Sobczyk, L.; Pozharskii, A. F.; Ozeryanskii, V. A.; Grech, E. *J. Phys. Org. Chem.* **1999**, *12*, 895–900.
- [25] Bieńko, A. J.; Latajka, Z.; Sawka-Dobrowolska, W.; Sobczyk, L.; Ozeryanskii, V. A.; Pozharskii, A. F.; Grech, E.; Nowicka-Scheibe, J. *J. Chem. Phys.* **2003**, *119*, 4313–4319.
- [26] Ozeryanskii, V. A.; Pozharskii, A. F.; Bieńko, A. J.; Sawka-Dobrowolska, W.; Sobczyk, L. *J. Phys. Chem. A* **2005**, *109*, 1637–1642.
- [27] Degtyarev, A. V.; Ryabtsova, O. V.; Pozharskii, A. F.; Ozeryanskii, V. A.; Starikova, Z. A.; Sobczyk, L.; Filarowski, A. *Tetrahedron* **2008**, *64*, 6209–6214.
- [28] Vergeer, P.; Kooijman, H.; Schreurs, A. M. M.; Kroon, J.; Grech, E. *Acta Cryst. Sect. C* **1999**, *55*, 1822–1824.
- [29] Bouma, B.; Kooijman, H.; Kroon, J.; Grech, E.; Brzezinski, B. *Acta Cryst. Sect. C* **1999**, *55*, 1824–1826.

- [30] Woźniak, K.; Wilson, C. C.; Knight, K. S.; Jones, W.; Grech, E. *Acta Cryst. Sect. B* **1996**, *52*, 691–696.
- [31] Fox, M. A.; Goeta, A. E.; Howard, J. A. K.; Hughes, A. K.; Johnson, A. L.; Keen, D. A.; Wade, K.; Wilson, C. C. *Inorg. Chem.* **2001**, *40*, 173–175.
- [32] Roziere, J.; Belin, C.; Lehman, M. S. *J. Chem. Soc., Chem. Commun.* **1982**, *0*, 388–389.
- [33] Alder, R. W.; Orpen, A. G.; Sessions, R. B. *J. Chem. Soc., Chem. Commun.* **1983**, *0*, 999–1000.
- [34] Sawka-Dobrowolska, W.; Grech, E.; Brzeziński, B.; Malarski, Z.; Sobczyk, L. *J. Mol. Struct.* **1995**, *356*, 117–124.
- [35] Bartoszak-Adamska, E.; Jaskólski, M.; Brzezinski, B. *J. Mol. Struct.* **1998**, *446*, 229–234.
- [36] Bartoszak-Adamska, E.; Jaskólski, M.; Brzezinski, B. *J. Mol. Struct.* **1999**, *475*, 167–173.
- [37] Katrusiak, A.; Dolska, M.; Urjasz, H.; Grech, E.; Brzezinski, B. *J. Mol. Struct.* **2002**, *605*, 123–131.
- [38] Katrusiak, A.; Dolska, M.; Urjasz, H.; Grech, E.; Brzezinski, B. *J. Mol. Struct.* **2002**, *610*, 73–80.
- [39] Katrusiak, A.; Urjasz, H.; Grech, E.; Brzezinski, B. *J. Mol. Struct.* **2002**, *643*, 109–114.
- [40] Bartoszak-Adamska, E.; Jaskólski, M.; Brzezinski, B. *J. Mol. Struct.* **1998**, *448*, 57–62.
- [41] Bartoszak-Adamska, E.; Jaskólski, M.; Urjasz, H.; Brzezinski, B. *J. Mol. Struct.* **2005**, *738*, 271–274.

- [42] Grech, E.; Malarski, Z.; Sawka-Dobrowolska, W.; Sobczyk, L. *J. Phys. Org. Chem.* **1999**, *12*, 313–318.
- [43] Chmielewski, P.; Ozeryanskii, V. A.; Sobczyk, L.; Pozharskii, A. F. *J. Phys. Org. Chem.* **2007**, *20*, 643–648.
- [44] Pietrzak, M.; Wehling, J.; Limbach, H.-H.; Golubev, N. S.; López, C.; Claramunt, R. M.; Elguero, J. *J. Am. Chem. Soc.* **2001**, *123*, 4338–4339.
- [45] Klimkiewicz, J.; Koprowski, M.; Stefaniak, L.; Grech, E.; Webb, G. *J. Mol. Struct.* **1997**, *403*, 163–165.
- [46] Klimkiewicz, J.; Stefaniak, L.; Grech, E.; Webb, G. *J. Mol. Struct.* **1997**, *412*, 47–50.
- [47] Pietrzak, M.; Stefaniak, L.; Pozharskii, A. F.; Ozeryanskii, V. A.; Nowicka-Scheibe, J.; Grech, E.; Webb, G. *J. Phys. Org. Chem.* **2000**, *13*, 35–38.
- [48] Lloyd-Jones, G. C.; Harvey, J. N.; Hodgson, P.; Murray, M.; Woodward, R. L. *Chem. Eur. J.* **2003**, *9*, 4523–4535.
- [49] Bernatowicz, P.; Kowalewski, J.; Sandström, D. *J. Phys. Chem. A* **2005**, *109*, 57–63.
- [50] Nakano, T.; Masuda, Y. *J. Phys. Chem. A* **2012**, *116*, 8409–8418.
- [51] Masuda, Y.; Nakano, T.; Sugiyama, M. *J. Phys. Chem. A* **2012**, *116*, 4485–4494.
- [52] Yaghmaei, S.; Khodagholian, S.; Kaiser, J. M.; Tham, F. S.; Mueller, L. J.; Morton, T. H. *J. Am. Chem. Soc.* **2008**, *130*, 7836–7838.

- [53] Saunders, M.; Jaffe, M. H.; Vogel, P. *J. Am. Chem. Soc.* **1971**, *93*, 2558–2559.
- [54] Saunders, M.; Vogel, P. *J. Am. Chem. Soc.* **1971**, *93*, 2559–2561.
- [55] Saunders, M.; Vogel, P. *J. Am. Chem. Soc.* **1971**, *93*, 2561–2562.
- [56] Saunders, M.; Telkowski, L.; Kates, M. R. *J. Am. Chem. Soc.* **1977**, *99*, 8070–8071.
- [57] Perrin, C. L.; Ohta, B. K. *J. Mol. Struct.* **2003**, *644*, 1–12.
- [58] Howard, S. T. *J. Am. Chem. Soc.* **2000**, *122*, 8238–8244.
- [59] Llamas-Saiz, A.; Foces-Foces, C.; Elguero, J. *J. Mol. Struct.* **1994**, *328*, 297–323.
- [60] Kanters, J. A.; Ter Horst, E. H.; Kroon, J.; Grech, E. *Acta Cryst. Sect. C* **1992**, *48*, 328–332.
- [61] Perrin, C. L.; Karri, P.; Moore, C.; Rheingold, A. L. *J. Am. Chem. Soc.* **2012**, *134*, 7766–7772.
- [62] Głowiak, T.; Grech, E.; Malarski, Z.; Sobczyk, L. *J. Mol. Struct.* **1997**, *403*, 73–82.
- [63] Grech, E.; Malarski, Z.; Sawka-Dobrowolska, W.; Sobczyk, L. *J. Mol. Struct.* **1997**, *416*, 227–234.
- [64] Grech, E.; Malarski, Z.; Milart, P.; Sawka-Dobrowolska, W.; Sobczyk, L. *J. Mol. Struct.* **1997**, *436-437*, 81–89.
- [65] Basato, M.; Detomi, N.; Meneghetti, M.; Valle, G.; Veronese, A. C. *Inorg. Chim. Acta* **1999**, *285*, 18–24.

- [66] Pan, Y.; McAllister, M. A. *J. Am. Chem. Soc.* **1997**, *119*, 7561–7566.
- [67] Pan, Y.; McAllister, M. A. *J. Am. Chem. Soc.* **1998**, *120*, 166–169.
- [68] Chen, J.; McAllister, M. A.; Lee, J. K.; Houk, K. N. *J. Org. Chem.* **1998**, *63*, 4611–4619.
- [69] Głowiak, T.; Malarski, Z.; Sobczyk, L.; Grech, E. *J. Mol. Struct.* **1992**, *270*, 441–447.
- [70] Grech, E.; Malarski, Z.; Sawka-Dobrowolska, W.; Sobczyk, L. *J. Mol. Struct.* **1997**, *406*, 107–117.
- [71] Valdés-Martínez, J.; Del Rio-Ramirez, M.; Hernández-Ortega, S.; Aakeröy, C. B.; Helfrich, B. *Cryst. Growth Des.* **2001**, *1*, 485–489.
- [72] Koch, W.; Holthausen, M. C. *A Chemist's Guide to Density Functional Theory*; Wiley-VCH Verlag GmbH, 2001; pp 220–221.
- [73] Giese, K.; Petković, M.; Naundorf, H.; Kühn, O. *Phys. Rep.* **2006**, *430*, 211–276.
- [74] Sekiya, H.; Takesue, H.; Nishimura, Y.; Li, Z.-H.; Mori, A.; Takeshita, H. *J. Chem. Phys.* **1990**, *92*, 2790–2796.
- [75] Sekiya, H.; Nagashima, Y.; Nishimura, Y. *J. Chem. Phys.* **1990**, *92*, 5761–5769.
- [76] Madeja, F.; Havenith, M. *J. Chem. Phys.* **2002**, *117*, 7162–7168.
- [77] Tanaka, K.; Honjo, H.; Tanaka, T.; Kohguchi, H.; Ohshima, Y.; Endo, Y. *J. Chem. Phys.* **1999**, *110*, 1969–1978.

- [78] Baba, T.; Tanaka, T.; Morino, I.; Yamada, K. M. T.; Tanaka, K. *J. Chem. Phys.* **1999**, *110*, 4131–4133.
- [79] Somorjai, R. L.; Hornig, D. F. *J. Chem. Phys.* **1962**, *36*, 1980–1987.
- [80] Basilevsky, M. V.; Vener, M. V. *Russ. Chem. Rev.* **2003**, *72*, 1–33.
- [81] Manca, C.; Tanner, C.; Coussan, S.; Bach, A.; Leutwyler, S. *J. Chem. Phys.* **2004**, *121*, 2578–2590.
- [82] Tomioka, Y.; Ito, M.; Mikami, N. *J. Phys. Chem.* **1983**, *87*, 4401–4405.
- [83] Piper, T. S.; Lemal, D.; Wilkinson, G. *Naturwissenschaften* **1956**, *43*, 129.
- [84] Tilley, T. D. *Acc. Chem. Res.* **1993**, *26*, 22–29.
- [85] Sunada, Y.; Fujimura, Y.; Nagashima, H. *Organometallics* **2008**, *27*, 3502–3513.
- [86] Ezbiansky, K.; Djurovich, P. I.; LaForest, M.; Sinning, D. J.; Zayes, R.; Berry, D. H. *Organometallics* **1998**, *17*, 1455–1457.
- [87] Speier, J. L. *Adv. Organomet. Chem.* **1979**, *17*, 407–447.
- [88] Marciniak, B.; Guliński, J. *J. Organomet. Chem.* **1993**, *446*, 15–23.
- [89] Marciniak, B. *Silicon Chem.* **2002**, *1*, 155–174.
- [90] Corey, J. Y.; Braddock-Wilking, J. *Chem. Rev.* **1999**, *99*, 175–292.

- [91] Malisch, W.; Jehle, H.; Möller, S.; Thum, G.; Reising, J.; Gbureck, A.; Nagel, V.; Fickert, C.; Kiefer, W.; Nieger, M. *Eur. J. Inorg. Chem.* **1999**, 1999, 1597–1605.
- [92] Malisch, W.; Jehle, H.; Möller, S.; Saha-Möller, C.; Adam, W. *Eur. J. Inorg. Chem.* **1998**, 1998, 1585–1587.
- [93] Corey, J. Y. *Chem. Rev.* **2011**, 111, 863–1071.
- [94] (a) Nikonov, G. I.; Kuzmina, L. G.; Lemenovskii, D. A.; Kottov, V. V. *J. Am. Chem. Soc.* **1995**, 117, 10133–10134; (b) Nikonov, G. I.; Kuzmina, L. G.; Lemenovskii, D. A.; Kottov, V. V. *J. Am. Chem. Soc.* **1996**, 118, 6333–6333.
- [95] Nikonov, G. I.; Kuzmina, L. G.; Vyboishchikov, S. F.; Lemenovskii, D. A.; Howard, J. A. K. *Chem. Eur. J.* **1999**, 5, 2947–2964.
- [96] Crabtree, R. H. *Angew. Chem. Int. Ed.* **1993**, 32, 789–805.
- [97] Lin, Z. *Chem. Soc. Rev.* **2002**, 31, 239–245.
- [98] Nikonov, G. I. *J. Organomet. Chem.* **2001**, 635, 24–36.
- [99] Sabo-Etienne, S.; Chaudret, B. *Coord. Chem. Rev.* **1998**, 178–180, Part 1, 381–407.
- [100] Hussein, K.; J. Marsden, C.; Barthelat, J.-C.; Rodriguez, V.; Conejero, S.; Sabo-Etienne, S.; Donnadiou, B.; Chaudret, B. *Chem. Commun.* **1999**, 1315–1316.
- [101] Tanabe, M.; Ito, D.; Osakada, K. *Organometallics* **2007**, 26, 459–462.
- [102] Tanabe, M.; Ito, D.; Osakada, K. *Organometallics* **2008**, 27, 2258–2267.

- [103] Ignatov, S. K.; Rees, N. H.; Tyrrell, B. R.; Dubberley, S. R.; Razuvaev, A. G.; Mountford, P.; Nikonov, G. I. *Chem. Eur. J.* **2004**, *10*, 4991–4999.
- [104] Mork, B. V.; Tilley, T. D.; Schultz, A. J.; Cowan, J. A. *J. Am. Chem. Soc.* **2004**, *126*, 10428–10440.
- [105] Bakhmutov, V. I.; Howard, J. A. K.; Keen, D. A.; Kuzmina, L. G.; Leech, M. A.; Nikonov, G. I.; Vorontsov, E. V.; Wilson, C. C. *J. Chem. Soc., Dalton Trans.* **2000**, 1631–1635.
- [106] Dorogov, K. Y.; Dumont, E.; Ho, N.-N.; Churakov, A. V.; Kuzmina, L. G.; Poblet, J.-M.; Schultz, A. J.; Howard, J. A. K.; Bau, R.; Lledos, A.; Nikonov, G. I. *Organometallics* **2004**, *23*, 2845–2847.
- [107] Dorogov, K. Y.; Yousufuddin, M.; Ho, N.-N.; Churakov, A. V.; Kuzmina, L. G.; Schultz, A. J.; Mason, S. A.; Howard, J. A. K.; Lemenovskii, D. A.; Bau, R.; Nikonov, G. I. *Inorg. Chem.* **2007**, *46*, 147–160.
- [108] Tanaka, I.; Ohhara, T.; Niimura, N.; Ohashi, Y.; Jiang, Q.; H. Berry, D.; Bau, R. *J. Chem. Res. (S)* **1999**, 14–15.
- [109] Schubert, U.; Ackermann, K.; Woerle, B. *J. Am. Chem. Soc.* **1982**, *104*, 7378–7380.
- [110] Scherer, W.; Eickerling, G.; Tafipolsky, M.; McGrady, G. S.; Sirsch, P.; Chatterton, N. P. *Chem. Commun.* **2006**, 2986–2988.
- [111] Nikonov, G. I. *Angew. Chem. Int. Ed.* **2001**, *40*, 3353–3355.
- [112] Nikonov, G. I. In *Recent Advances in Nonclassical Interligand Si···H Interactions*; Robert West, A. F. H., Stone, F. G. A.,

- Eds.; Adv. Organomet. Chem.; Academic Press, 2005; Vol. 53; pp 217–309.
- [113] Lachaize, S.; Sabo-Etienne, S. *Eur. J. Inorg. Chem.* **2006**, 2006, 2115–2127.
- [114] Vyboishchikov, S. F.; Nikonov, G. I. *Organometallics* **2007**, 26, 4160–4169.
- [115] Schubert, U. *Adv. Organomet. Chem.* **1990**, 30, 151–187.
- [116] Duckett, S. B.; Haddleton, D. M.; Jackson, S. A.; Perutz, R. N.; Poliakoff, M.; Upmacis, R. K. *Organometallics* **1988**, 7, 1526–1532.
- [117] Taw, F. L.; Bergman, R. G.; Brookhart, M. *Organometallics* **2004**, 23, 886–890.
- [118] Peulecke, N.; Ohff, A.; Kosse, P.; Tillack, A.; Spannenberg, A.; Kempe, R.; Baumann, W.; Burlakov, V. V.; Rosenthal, U. *Chem. Eur. J.* **1998**, 4, 1852–1861.
- [119] Ignatov, S. K.; Rees, N. H.; Merkoulov, A. A.; Dubberley, S. R.; Razuvaev, A. G.; Mountford, P.; Nikonov, G. I. *Chem. Eur. J.* **2008**, 14, 296–310.
- [120] Dubberley, S. R.; Ignatov, S. K.; Rees, N. H.; Razuvaev, A. G.; Mountford, P.; Nikonov, G. I. *J. Am. Chem. Soc.* **2003**, 125, 642–643.
- [121] Vyboishchikov, S. F.; Nikonov, G. I. *Chem. Eur. J.* **2006**, 12, 8518–8533.
- [122] Osipov, A. L.; Vyboishchikov, S. F.; Dorogov, K. Y.; Kuzmina, L. G.; Howard, J. A. K.; Lemenovskii, D. A.; Nikonov, G. I. *Chem. Commun.* **2005**, 3349–3351.

- [123] Lichtenberger, D. L. *Organometallics* **2003**, *22*, 1599–1602.
- [124] Colomer, E.; Corriu, R. J. P.; Marzin, C.; Vioux, A. *Inorg. Chem.* **1982**, *21*, 368–373.
- [125] Luo, X.-L.; Kubas, G. J.; Bryan, J. C.; Burns, C. J.; Unkefer, C. J. *J. Am. Chem. Soc.* **1994**, *116*, 10312–10313.
- [126] Luo, X.-L.; Kubas, G. J.; Burns, C. J.; Bryan, J. C.; Unkefer, C. J. *J. Am. Chem. Soc.* **1995**, *117*, 1159–1160.
- [127] Delpech, F.; Sabo-Etienne, S.; Chaudret, B.; Daran, J.-C. *J. Am. Chem. Soc.* **1997**, *119*, 3167–3168.
- [128] Delpech, F.; Sabo-Etienne, S.; Daran, J.-C.; Chaudret, B.; Hussein, K.; Marsden, C. J.; Barthelat, J.-C. *J. Am. Chem. Soc.* **1999**, *121*, 6668–6682.
- [129] Hoyano, J.; Elder, M.; Graham, W. A. G. *J. Am. Chem. Soc.* **1969**, *91*, 4568–4569.
- [130] Nikonov, G. I.; Kuzmina, L. G.; Howard, J. A. K. *J. Chem. Soc., Dalton Trans.* **2002**, 3037–3046.
- [131] Esteruelas, M. A.; Lahoz, F. J.; Oñate, E.; Oro, L. A.; Rodríguez, L. *Organometallics* **1995**, *14*, 263–268.
- [132] Kobayashi, H.; Ueno, K.; Ogino, H. *Organometallics* **1995**, *14*, 5490–5492.
- [133] Dorogov, K. Y.; Churakov, A. V.; Kuzmina, L. G.; Howard, J. A. K.; Nikonov, G. I. *Eur. J. Inorg. Chem.* **2004**, 771–775.
- [134] Bent, H. A. *Chem. Rev.* **1961**, *61*, 275–311.

- [135] Rodriguez, V.; Donnadieu, B.; Sabo-Etienne, S.; Chaudret, B. *Organometallics* **1998**, *17*, 3809–3814.
- [136] Luo, X. L.; Baudry, D.; Boydell, P.; Charpin, P.; Nierlich, M.; Ephritikhine, M.; Crabtree, R. H. *Inorganic Chemistry* **1990**, *29*, 1511–1517.
- [137] Gutsulyak, D. V.; Kuzmina, L. G.; Howard, J. A. K.; Vyboishchikov, S. F.; Nikonov, G. I. *J. Am. Chem. Soc.* **2008**, *130*, 3732–3733.
- [138] Ray, M.; Nakao, Y.; Sato, H.; Sakaki, S.; Watanabe, T.; Hashimoto, H.; Tobita, H. *Organometallics* **2010**, *29*, 6267–6281.
- [139] Sakaba, H.; Hirata, T.; Kabuto, C.; Horino, H. *Chem. Lett.* **2001**, 1078–1079.
- [140] Lee, T. Y.; Dang, L.; Zhou, Z.; Yeung, C. H.; Lin, Z.; Lau, C. P. *Eur. J. Inorg. Chem.* **2010**, *2010*, 5675–5684.
- [141] Ng, S. M.; Lau, C. P.; Fan, M.-F.; Lin, Z. *Organometallics* **1999**, *18*, 2484–2490.
- [142] Smith, R. A.; Bennett, M. J. *Acta Crystallogr. Sect. B* **1977**, *33*, 1118–1122.
- [143] Manojlović-Muir, L.; Muir, K. W.; Ibers, J. A. *Inorg. Chem.* **1970**, *9*, 447–452.
- [144] Graham, W. A. G.; Jetz, W. *Inorg. Chem.* **1971**, *10*, 1159–1165.
- [145] Beller, M.; Fischer, H.; Herrmann, W. A.; Ofele, K.; Brossmer, C. *Angew. Chem. Int. Ed.* **1995**, *34*, 1848–1849.

- [146] Louie, J.; Hartwig, J. F. *Angew. Chem. Int. Ed.* **1996**, *35*, 2359–2361.
- [147] Stahl, S. S.; Labinger, J. A.; Bercaw, J. E. *Angew. Chem. Int. Ed.* **1998**, *37*, 2180–2192.
- [148] Duckett, S. B.; Perutz, R. N. *Organometallics* **1992**, *11*, 90–98.
- [149] Shortland, A. J.; Wilkinson, G. *J. Chem. Soc., Dalton Trans.* **1973**, 872–876.
- [150] Herrmann, W. A.; Okuda, J. *Angew. Chem. Int. Ed.* **1986**, *25*, 1092–1093.
- [151] Fernandez, M.-J.; Maitlis, P. M. *J. Chem. Soc., Chem. Commun.* **1982**, 310–311.
- [152] Duckett, S. B.; Perutz, R. N. *J. Chem. Soc., Chem. Commun.* **1991**, 28–31.
- [153] Fernandez, M.-J.; Bailey, P. M.; Bentz, P. O.; Ricci, J. S.; Koetzle, T. F.; Maitlis, P. M. *J. Am. Chem. Soc.* **1984**, *106*, 5458–5463.
- [154] Gilbert, T. M.; Bergman, R. G. *Organometallics* **1983**, *2*, 1458–1460.
- [155] Alaimo, P. J.; Bergman, R. G. *Organometallics* **1999**, *18*, 2707–2717.
- [156] Fernandez, M. J.; Maitlis, P. M. *Organometallics* **1983**, *2*, 164–165.
- [157] Heinekey, D. M.; Hinkle, A. S.; Close, J. D. *J. Am. Chem. Soc.* **1996**, *118*, 5353–5361.

- [158] Bower, B. K.; Tennent, H. G. *J. Am. Chem. Soc.* **1972**, *94*, 2512–2514.
- [159] Byrne, E. K.; Theopold, K. H. *J. Am. Chem. Soc.* **1987**, *109*, 1282–1283.
- [160] Byrne, E. K.; Theopold, K. H. *J. Am. Chem. Soc.* **1989**, *111*, 3887–3896.
- [161] Anson, F. C.; Collins, T. J.; Coots, R. J.; Gipson, S. L.; Richmond, T. G. *J. Am. Chem. Soc.* **1984**, *106*, 5037–5038.
- [162] Collins, T. J.; Powell, R. D.; Slebodnick, C.; Uffelman, E. S. *J. Am. Chem. Soc.* **1991**, *113*, 8419–8425.
- [163] Pfaff, F. F.; Kundu, S.; Risch, M.; Pandian, S.; Heims, F.; Pryjomska-Ray, I.; Haack, P.; Metzinger, R.; Bill, E.; Dau, H.; Comba, P.; Ray, K. *Angew. Chem. Int. Ed.* **2011**, *50*, 1711–1715.
- [164] Lewis, R. A.; George, S. P.; Chapovetsky, A.; Wu, G.; Figueroa, J. S.; Hayton, T. W. *Chem. Commun.* **2013**, *49*, 2888–2890.
- [165] Brookhart, M.; Grant, B. E. *J. Am. Chem. Soc.* **1993**, *115*, 2151–2156.
- [166] Doherty, M. D.; Grant, B.; White, P. S.; Brookhart, M. *Organometallics* **2007**, *26*, 5950–5960.
- [167] Beck, R.; Frey, M.; Camadanli, S.; Klein, H.-F. *Dalton Trans.* **2008**, 4981–4983.
- [168] Brookhart, M.; Grant, B. E.; Lenges, C. P.; Prosenc, M. H.; White, P. S. *Angew. Chem. Int. Ed.* **2000**, *39*, 1676–1679.

- [169] Ingleson, M.; Fan, H.; Pink, M.; Tomaszewski, J.; Caulton, K. G. *J. Am. Chem. Soc.* **2006**, *128*, 1804–1805.
- [170] Ingleson, M. J.; Pink, M.; Fan, H.; Caulton, K. G. *J. Am. Chem. Soc.* **2008**, *130*, 4262–4276.
- [171] Isobe, K.; Bailey, P. M.; Maitlis, P. M. *J. Chem. Soc., Chem. Commun.* **1981**, 808–809.
- [172] Djurovich, P. I.; Carroll, P. J.; Berry, D. H. *Organometallics* **1994**, *13*, 2551–2553.
- [173] Ruiz, J.; Mann, B. E.; Spencer, C. M.; Taylor, B. F.; Maitlis, P. M. *J. Chem. Soc., Dalton Trans.* **1987**, 1963–1966.
- [174] Yao, Z.; Klabunde, K. J.; Hupton, A. C. *Inorg. Chim. Acta* **1997**, *259*, 119–124.
- [175] Giese, K.; Petković, M.; Naundorf, H.; Kühn, O. *Physics Reports* **2006**, *430*, 211–276.
- [176] Takada, S.; Nakamura, H. *J. Chem. Phys.* **1994**, *100*, 98–113.
- [177] Wójcik, M. J.; Nakamura, H.; Iwata, S.; Tatara, W. *J. Chem. Phys.* **2000**, *112*, 6322–6328.
- [178] Benderskii, V.; Grebenschikov, S.; Mil'nikov, G.; Vetoshkin, E. *Chem. Phys.* **1994**, *188*, 19–31.
- [179] Benderskii, V.; Grebenschikov, S.; Mil'nikov, G. *Chem. Phys.* **1995**, *194*, 1–18.
- [180] Benderskii, V.; Grebenschikov, S.; Mil'nikov, G. *Chem. Phys.* **1995**, *198*, 281–295.

- [181] Carter, S.; Culik, S. J.; Bowman, J. M. *J. Chem. Phys.* **1997**, *107*, 10458–10469.
- [182] Yagi, K.; Taketsugu, T.; Hirao, K.; Gordon, M. S. *J. Chem. Phys.* **2000**, *113*, 1005–1017.
- [183] Burcl, R.; Carter, S.; Handy, N. C. *Chem. Phys. Lett.* **2003**, *373*, 357–365.
- [184] Yagi, K.; Hirao, K.; Taketsugu, T.; Schmidt, M. W.; Gordon, M. S. *J. Chem. Phys.* **2004**, *121*, 1383–1389.
- [185] Fujisaki, H.; Yagi, K.; Hirao, K.; Straub, J. E. *Chem. Phys. Lett.* **2007**, *443*, 6–11.
- [186] Ischtwan, J.; Collins, M. A. *J. Chem. Phys.* **1994**, *100*, 8080–8088.
- [187] Thompson, K. C.; Jordan, M. J. T.; Collins, M. A. *J. Chem. Phys.* **1998**, *108*, 564–578.
- [188] Thompson, K. C.; Jordan, M. J. T.; Collins, M. A. *J. Chem. Phys.* **1998**, *108*, 8302–8316.
- [189] Yagi, K.; Taketsugu, T.; Hirao, K. *J. Chem. Phys.* **2002**, *116*, 3963–3966.
- [190] Yagi, K.; Oyanagi, C.; Taketsugu, T.; Hirao, K. *J. Chem. Phys.* **2003**, *118*, 1653–1660.
- [191] Christiansen, O. *Phys. Chem. Chem. Phys.* **2007**, *9*, 2942–2953.
- [192] Yagi, K.; Hirata, S.; Hirao, K. *J. Chem. Phys.* **2007**, *127*, 034111.
- [193] Bowman, J. M. *Acc. Chem. Res.* **1986**, *19*, 202–208.

- [194] Bowman, J. M. *J. Chem. Phys.* **1978**, *68*, 608–610.
- [195] Roothaan, C. C. *J. Rev. Mod. Phys.* **1951**, *23*, 69–89.
- [196] Norris, L. S.; Ratner, M. A.; Roitberg, A. E.; Gerber, R. B. *J. Chem. Phys.* **1996**, *105*, 11261–11267.
- [197] Chaban, G. M.; Jung, J. O.; Gerber, R. B. *J. Chem. Phys.* **1999**, *111*, 1823–1829.
- [198] Chaban, G. M.; Jung, J. O.; Gerber, R. B. *J. Phys. Chem. A* **2000**, *104*, 2772–2779.
- [199] Gregurick, S. K.; Fredj, E.; Elber, R.; Gerber, R. B. *J. Phys. Chem. B* **1997**, *101*, 8595–8606.
- [200] Gregurick, S. K.; Liu, J. H.-Y.; Brant, D. A.; Gerber, R. B. *J. Phys. Chem. B* **1999**, *103*, 3476–3488.
- [201] Horn, T. R.; Gerber, R. B.; Ratner, M. A. *J. Chem. Phys.* **1989**, *91*, 1813–1823.
- [202] Horn, T. R.; Gerber, R. B.; Valentini, J. J.; Ratner, M. A. *J. Chem. Phys.* **1991**, *94*, 6728–6736.
- [203] Jung, J. O.; Gerber, R. B. *J. Chem. Phys.* **1996**, *105*, 10682–10690.
- [204] Christiansen, O. *J. Chem. Phys.* **2003**, *119*, 5773–5781.
- [205] Jung, J. O.; Gerber, R. B. *J. Chem. Phys.* **1996**, *105*, 10332–10348.
- [206] Christiansen, O. *J. Chem. Phys.* **2004**, *120*, 2149–2159.
- [207] Christiansen, O. *J. Chem. Phys.* **2004**, *120*, 2140–2148.

- [208] Seidler, P.; Christiansen, O. *J. Chem. Phys.* **2007**, *126*, 204101.
- [209] Helgaker, T.; Jørgensen, P.; Olsen, J. *Molecular Electronic-Structure Theory*; Wiley: Chichester, 2000.
- [210] Bishop, R. *Theor. Chim. Acta* **1991**, *80*, 95–148.
- [211] Seidler, P.; Matito, E.; Christiansen, O. *J. Chem. Phys.* **2009**, *131*, 034115.
- [212] Seidler, P.; Sparta, M.; Christiansen, O. *J. Chem. Phys.* **2011**, *134*, 054119.
- [213] Thomsen, B.; Hansen, M. B.; Seidler, P.; Christiansen, O. *J. Chem. Phys.* **2012**, *136*, 124101.
- [214] Zocante, A.; Seidler, P.; Hansen, M. B.; Christiansen, O. *J. Chem. Phys.* **2012**, *136*, 204118.
- [215] González, J. L. M. Q.; Thompson, D. *Comput. Phys.* **1997**, *11*, 514–515.
- [216] Johnson, B. R. *J. Chem. Phys.* **1977**, *67*, 4086–4093.
- [217] Avdelas, G.; Konguetsof, A.; Simos, T. *Comput. Chem.* **2000**, *24*, 577–584.
- [218] Hajj, F. *J. Phys. B: At., Mol. Opt. Phys.* **1982**, *15*, 683–692.
- [219] Hajj, F. *J. Phys. B: At., Mol. Opt. Phys.* **1999**, *18*, 1.
- [220] Broeckhove, J.; Kłosiewicz, P.; Vanroose, W. *J. Comp. Appl. Math.* **2010**, *234*, 1238–1248.
- [221] Bakker, H. J.; Nienhuys, H.-K. *Science* **2002**, *297*, 587–590.

- [222] Honjou, N. *Chem. Phys.* **2008**, *344*, 128–134.
- [223] Léonard, C.; Le Quéré, F.; Rosmus, P.; Puzzarini, C.; de Lara Castells, M. P. *Phys. Chem. Chem. Phys.* **2000**, *2*, 1117–1122.
- [224] Shore, B. W. *J. Chem. Phys.* **1973**, *59*, 6450–6463.
- [225] Gordon, R. G. *J. Chem. Phys.* **1969**, *51*, 14–25.
- [226] Chesick, J. P. *J. Chem. Phys.* **1968**, *49*, 3772–3774.
- [227] Davis, M. J.; Heller, E. J. *J. Chem. Phys.* **1979**, *71*, 3383–3395.
- [228] Hamilton, I. P.; Light, J. C. *J. Chem. Phys.* **1986**, *84*, 306–317.
- [229] Bosch, E.; Moreno, M.; Lluch, J. M.; Bertrán, J. *J. Chem. Phys.* **1990**, *93*, 5685–5692.
- [230] Paz, J. J.; Moreno, M.; Lluch, J. M. *J. Chem. Phys.* **1995**, *103*, 353–359.
- [231] Makri, N.; Miller, W. H. *J. Chem. Phys.* **1987**, *86*, 1451–1457.
- [232] Makri, N.; Miller, W. H. *J. Chem. Phys.* **1987**, *87*, 5781–5787.
- [233] Shiff, L. I. *Quantum Mechanics*, 2nd ed.; McGraw-Hill: New York, 1955; pp 60–69.
- [234] Shore, B. W. *J. Chem. Phys.* **1973**, *58*, 3855–3866.
- [235] Locker, D. J. *J. Phys. Chem.* **1971**, *75*, 1756–1757.
- [236] Grech, E.; Malarski, Z.; Sobczyk, L. *Chem. Phys. Lett.* **1986**, *128*, 259–263.

- [237] Sokolov, N.; Vener, M.; Savel'ev, V. *J. Mol. Struct.* **1988**, *177*, 93–110.
- [238] Osakada, K.; Hataya, K.; Yamamoto, T. *Inorg. Chim. Acta* **1997**, *259*, 203 – 211.
- [239] Calimano, E.; Tilley, T. D. *Dalton Trans.* **2010**, *39*, 9250–9263.
- [240] Karshtedt, D.; Bell, A. T.; Tilley, T. D. *Organometallics* **2006**, *25*, 4471–4482.
- [241] Esqueda, A. C.; Conejero, S.; Maya, C.; Carmona, E. *Organometallics* **2010**, *29*, 5481–5489.
- [242] Wiberg, K. *Tetrahedron* **1968**, *24*, 1083–1096.